Digital twin virtual entities for online improvements in food and renewable energy operations

by

Misagh Ebrahimpour

A thesis submitted in partial fulfilment of the requirements for the degree of

Doctor of Philosophy (PhD) in Chemical and Materials Engineering, the University of Auckland,

April 2022

Abstract

The digital twin (DT) is one of Industry 4's enabling technologies, aiming to improve the performance of physical entities through the use of a virtual counterpart. DT is a real-time representation of a system or physical entity that can adapt to operational changes in real time by using data and information gathered online to predict the physical twin's future. Despite all the advancements in both the industrial and academic sectors, there are still challenges for which DT adaptation requires more investigation. DT has been developed and used for three major purposes: service, design, and manufacturing for general industrial purposes. To develop DT to achieve all three major purposes is not realistic since different industries have different implementation orders of DT depending on their hardware/software level, and maturities of service, design and manufacturing. In this project, we will focus on DT virtual entity development purposes based on their own situations to implement. Therefore, this research will focus on developing virtual entities for the identified gaps in industry application.

Full implementation of 'proper' DT requires twinning between the virtual and physical entities. However, this is complicated by computational effort, limitation of online measurements, and process complexity. This work introduces new approaches for processes in which mechanistical methods alone are incapable of providing DT virtual entities. The processes addressed are cream cheese fermentation and PCM energy storage, in the dairy and renewable energy industries respectively. These processes pose distinct challenges, necessitating novel approaches that combine data-driven and mechanistical methods.

Process design has advanced significantly in dairy industry as a result of the high global demand for dairy products; however, process operations (manufacturing) require further improvements in order to increase product throughput while maintaining consistent quality. DT can become an important tool toward improving the online process operation in the dairy. However, proper virtual representations of systems using DT introduces a significant challenge in the dairy industry due to the complexity of mechanisms, raw material variations, and the limitations of online measurements. These factors reduce the fidelity of current industry and academic models.

Additionally, developing DT for new renewable energy technologies is one of the most critical gaps. Online solutions can help improve the economic viability of such technologies,

by improving energy management during operation. The DT application for improving online operations necessitates a real time solution. However, this is challenging due to the complexity and nonlinearity of the systems involved in renewable energy technologies.

Two DT virtual entity development directions for the aforementioned industries are investigated in this study. The results can aim in energy savings in New Zealand which is necessary for achieving Zero Carbon Act objectives. The first is in the dairy industry, which is vital to New Zealand's economy and consumes a significant amount of energy. A cream cheese production unit including fermentations vats is studied. DT virtual entity needs to optimize the energy while meeting the quality standards by providing online scheduling of the vats. The second process involves using energy storage and solar air collectors as renewable energy sources. This system is well suited to New Zealand's temperate climate. However, this system's economic viability must be improved while meeting energy demands. DT can optimise the economical design of solar collectors and energy storages. DT can also provide an optimal control solution, allowing the system to save even more energy and cost.

In the cream cheese fermentation unit, the batch duration variation is the main challenge of optimizing the vats scheduling since mechanistic modelling of the dynamics of the fermentation process is difficult and includes many time-varying parameters. The other case introduced a different challenge, the mechanistic model of the system is available for active phase change material (PCM) systems; however, its complexity makes the optimization using that model computationally infeasible. To provide solutions, combination of data-driven and mathematical modelling as well as optimization were applied. The detailed virtual entity developments for the two industries are introduced in the following paragraphs.

The first process investigated the scheduling of cream cheese fermentation vats. The scheduling of fermentation vats was complicated by batch duration variations and the limitations of online measurements. For the first time in this work, a DT virtual entity was developed to schedule the cream cheese fermentation vats. The scheduling framework was twined with the fermentation vats for filling and draining them using the information for predicting the batch durations required for reaching the quality. The pH predictive models were studied because pH is an important quality indicator. Novel grey and black box models were developed for pH prediction. It was possible to create grey and black box models that could use available online measurements to improve pH prediction. Only one fermentation had a large error of 34.09 %, and the average network percentage relative error was less than

14 %. However, the results showed that the pH prediction at the final point matches the experimental data in all the test fermentations.

The pH predictive models were applied in a scheduling framework. The scheduling challenge is due to the inability to predict batch durations from the fermentation start time. This causes batches interferences during draining, resulting in higher energy consumption and waste. The new DT virtual entity for scheduling presented a mathematical programming optimization that was formulated to solve this problem by assuming an initial default batch duration at the start time and updating the batch duration later based on the pH prediction model later when enough measurements were available. The 12 hours initial batch duration led to the best results in reducing idle time, energy consumption, and waste.

In the second process, an energy storage was coupled with a solar air collector for supplying heat to a hut in Auckland. The model of the entire system plays an important role for achieving DT virtual entity. The entire system's first principles models were developed and validated using experimental data for this purpose. The results confirmed the dynamics model's reliability, with an average mean square error of 4°C between measured and predicted hut temperatures over 11 days. The validated model was used for designing. For the first time in this research, economical designing of the system was carried out for various application scenarios in Auckland. The results showed that the optimum surface area of the solar collector was the same at 1 square meter for all the scenarios; however, the optimum amount of PCM mass for service, domestic, and office scenarios was 35 kg, 20 kg, and zero, respectively.

The model was also used for developing a virtual entity for optimal control of the system. The desired optimal control should provide online solutions despite the system complexity coming from the nonlinearity and existence of binary variables. A novel optimal control was developed using reinforcement learning (RL). For addressing the approach advantages, it was compared with a model predictive control (MPC), as a classical approach. RL as a data driven optimal control can be trained offline and provide real time solutions. A novel formulation was proposed that allowed for the adjustment of a reward to prioritise between thermal comfort and energy cost savings. By prioritizing the cost saving, 97% more cost was saved compared to prioritizing thermal comfort case, however, the offset from the desired temperature was 54% less. A balance between energy cost savings and thermal comfort was achieved by adjusting the reward.

Acknowledgement

I would like to thank my supervisors Dr. Wei Yu, Prof. Brent Young and Prof. Mohammed Farid for their supports. Great thanks to Dr. Bruno Santoro and Dr. Gohar Gholamibozanjani for their helpful assistance.

Thanks to my colleagues in I^2C^2 group for their company. I am also grateful to the Department of Chemical and Materials Engineering for their help. Special thanks to The University of Auckland for providing financial support during my PhD.

Finally, I need to thank my parents and partner for their endless warmth and kindness.

Preface

This thesis is comprised of an edited collection of papers which explore digital twin virtual entity developments for food and energy industries. The papers are as follows:

Chapter 2: Artificial neural network modelling for cream cheese fermentation pH prediction at lab and industrial scales, *Food and Bioproducts Processing*, 126, 81-89.

Chapter 3: Computer Aided Chemical Engineering. Vol. 49. Elsevier, 2022. 541-546.

Chapter 4: Economical design optimization of a phase change material active system equipped with a solar collector. *Applied Thermal Engineering*, 216 (2022): 119002.

Chapter 5: Optimal control for An Active Phase Change Material System Using Reinforcement Learning. *2022 IEEE International Symposium on Advanced Control of Industrial Processes (AdCONIP).* IEEE, 2022.

Table of Contents

Table of Figures

List of Tables

CHAPTER 1

Introduction

1.1. Background

1.1.1. Digital twin definition

Over the last few decades, digitalisation has resulted in significant advances in the industry. Technologies such as computers, simulation tools, and internet can be used to create virtual representations of physical objects. As a result, plans and operations have become more effective and efficient [1-4].

The integration and interaction of the physical and digital worlds have created numerous opportunities [5]. This can be achieved using digital twin (DT) models, which represent the properties of the actual process [6]. To connect the real system with its virtual representation, DT employs models, sensors, and data.

The evolution of Industry 4.0 [7], which enabled technologies such as machine learning, cloud service, and multi-physics simulation [8], has made it possible to synchronize physical and virtual objects. DT is defined as a three-part system: a physical space, a virtual representation of that space, and data flow from the physical to the virtual representation [9]. The information might also be passed to the real space. Twining refers to the data flow cycle that occurs between virtual and physical spaces. The virtual space can include subspaces for different applications such as modelling, optimization, etc.

Some virtual spaces are not connected to the physical space and require manual input, whereas others are entirely integrated into the physical space. DT classification was proposed in [10]. The authors' classification of DT based on the degree of integration between physical and virtual environments is shown Fig. 1.1.

According to their definition, the digital model has no automated data exchange with the plant. Models can be built using manual data, but changes in the state of the physical object have no direct impact on the digital entity and vice versa. There is an automated one-way data flow between the real and digital objects in the digital shadow. When the physical object changes, the digital object changes as well, but not the other way around.

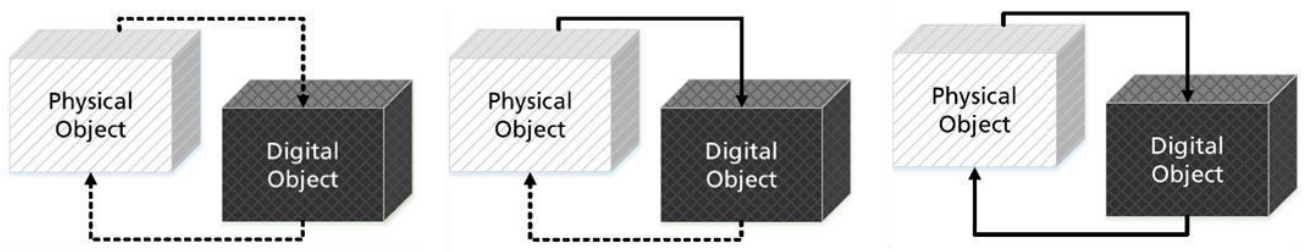

Fig. 1.1. From left to right: digital model, digital shadow and digital twin data flows. Dashed and solid lines represent the manual and automatic data flows respectively [7].

If the data flow between an existing physical object and a digital object is fully integrated into both directions, it is referred to as a Digital Twin. The digital object could also act as a controlling instance of the physical object in this scenario. Other physical and digital objects may also cause changes in the digital object's state. A change in the physical object's state causes a change in the digital object's state and vice versa.

Therefore, the main parts of a digital twin are [24]:

a) a model of the object
b) an evolving set of data relating to the object, and
c) a means of dynamically updating or adjusting the model in accordance with the data.

Parts b and c are the features of digital twin that makes it different from the traditional process models. Because the digital twin approach uses evolving data, one of its main advantages is that it accurately describes objects that change over time. A digital twin can extend the use of a validated model to timescales over which the object and its behaviour will change significantly. For instance, parameters in the model of the prototype would be updated using test data from the prototype, the updated model would be used to forecast performance in use, and finally the design would be updated. Furthermore, real-time operation can be improved using digital twin. For example, a digital twin of a machine tool would be able to simulate the mechanical and thermal processes involved in milling metal in real time and update knowledge about tool wear based on real-time measurements of part temperature and shape, enabling proactive and effective plant maintenance.

1.1.2. Digital twin applications

DT with various levels of integrity has been used in the industry. DT applications were identified at various stages of the lifecycle [11]. Design, manufacturing, and service were the three categories of DT's industrial applications. According to their findings, DT is currently

being used the most in production.

The majority of DT's production applications are process control and process optimisation. The process systems must run continuously with acceptable quality regardless of disturbances such as raw material composition changes. On the other hand, most control systems are designed at steady state regions [2] that ignore the system's dynamics in all the operating conditions. To improve the system's performance, DT combines a dynamic model of the system with real-time data from the actual system. Another advantage of DT is the ability to optimise processes in real time.

Although proper process design is critical, variations in operating conditions may be overlooked during the design phase [12]. Models that interact with the physical system can be used to optimise processes [13]. To achieve the best possible result, economic, safety, resource conditions, market demand, and other factors can all be considered.

DT concepts have been implemented partially in the industry before. Model predictive control, computer-integrated manufacturing, and virtual manufacturing systems are just a few examples [14]. Model predictive control (MPC) has been used exclusively in oil companies [15] and petrochemical plants [16] for a long time. The virtual model in MPC [17] uses measurements from the physical process to forecast future states of the process and control it properly. Scheduling and optimisation have also been developed with virtual models. RTO (real-time optimisation) is a process optimisation framework that includes process measurements [18]. The measurements solve model mismatch and disturbances [19], which can make implementing model-based optimal inputs impractical. Smart scheduling was also achieved by combining production scheduling with cyber-physical systems [20].

1.1.3. Digital twin challenges

Although different researchers [21] have defined different architectures for DT, DT's general and standard architecture includes a physical space, a virtual space, and the connection between them, as defined for the first time in [9].

The difficulties of employing DT have been discussed in some review publications. The following sections discuss these difficulties and challenges.

1.1.3.1. DT application contexts

DT should be able to incorporate with other digital twins and humans [22]. Standardisation and interoperability of virtual entities are essential for establishing communication between them to achieve this goal [15].

1.1.3.2. Data related challenges

In DT, data must be transformed in real-time or near real-time. On the other hand, the data often has a large volume, a high velocity, and a wide variety, making it difficult and expensive to send to DT via a cloud server. Data-related technologies such as data collection, mapping, processing, and data transmission are required to address these issues.

1.1.3.3. Technical implementation

The authors in [14] highlighted the high reliance of DT on existing technologies such as 5G, IoT, etc. On the other hand, these technologies were developed independently of the DT. Although using these technologies in DT saves money, the question of whether they are optimised for DT applications and industrial challenges remains.

1.1.3.4. Lifecycle

The DT lifecycle begins with the prototype phase and continues throughout the lifecycle [22]. There are, however, only a few DT applications that support the entire supply chain. Integrating DT from different phases, such as design, production, and service, is one of the most difficult tasks [14].

1.1.3.5. Perceived benefits

A lack of understanding about the benefits of DT was one of the challenges mentioned in the perceived benefits section. Considerations such as potential costs and infrastructure constraints should be investigated and compared to the expected return on investment before recommending DT to an industry.

1.1.3.6. Virtual entity requirements

According to the authors [14], the level of fidelity is one of the most important factors because the higher the fidelity, the better the virtual object can mimic the physical object.

Processing power limits and network speed, on the other hand, play a significant role in achieving a high-fidelity DT. The optimal level of accuracy is determined by taking into account these parameters and physical object dynamics to maximize benefits while reducing costs and implementation challenges. The models should correctly reflect reality, but, given the complexity of real-world systems, it is difficult to construct models for DTs using traditional methods such as mechanistic modelling [22]. New developments in machine learning have led to using data for building data-driven solutions such as grey box and black box models which provide solutions to the mentioned issues by using power of data for modelling [23].

In [11] model is mentioned as the core of DT. The physical object's complexity should be reflected in the simplified virtual models. According to the authors, a balance between computing effort and model correctness should be achieved for each component of the system, which is dependent on the impact of that component on the system's functionality. Simulation was mentioned as another important feature of DT. The virtual model can interact with the physical object in real-time through simulation. This sets DT apart from traditional simulations, which is possible thanks to the Internet of Things' real-time data collection and recording capabilities. However, the authors do point out that most existing research only flows data in one direction, from physical to virtual objects, and that more research is needed to develop models that can be used to run digital twin simulations. This was also discussed in [24], where the authors looked at the differences between a model and DT. The DT model should be able to update, or change based on the measured data. In addition, the model should be sufficiently quick to run and reach the decision considering the timescale of the system.

1.1.4. Virtual representation challenges in this thesis

As mentioned in Section 1.1.3.6, virtual entity development is one of the challenges of DT development. Despite significant advances in DT in both academic and industrial environments, more research is still needed in some industries. Full implementation of ‘proper’ DT requires twinning between the virtual and physical entities. However, this is complicated by computational effort, limitation of online measurements and process complexity. Therefore, this research will focus on the development of virtual representations for the identified gaps in industry application.

The food and renewable energy industries are two areas that require further investigation. DT virtual entity in food industry is required for improving the operating condition of the food production processes. Also, DT can aim in increasing the economic viability of new renewable energy technologies by enhancing their design and operation.

Difficulties of applying DT in the food industry were summarized in [39]. Using such technologies in the food industry is difficult, despite the fact that the food industry has a long history. This is due to the complexity and variability of raw materials, specialised equipment, processing rigidity, raw material and product shelf-life limitations, and the importance of quality. Developing a DT virtual entity necessitates the creation of models that can be used in real-time process equipment scheduling, which is extremely difficult.

The renewable energy industry has gotten a lot of attention in recent years as a result of international agreements like the Paris Agreement, which aim to reduce CO_2 emissions globally. The building sector has a lot of potential for implementing renewable energies since reducing energy consumption in this sector is one of the critical components for meeting the carbon reduction commitments. However, to achieve a reasonable payback time, moving to carbon low/zero alternatives necessitates proper design and operation of renewable solutions. DT has the potential to make a significant contribution to this goal. There are obstacles in the way of achieving this goal. For example, determining the best energy management control for a building can result in complex optimisation problems that can take a long time to solve which makes developing a DT virtual entity challenging.

1.2. Research objectives

The main objectives of this project are to develop DT virtual entities by combining data-driven and mechanistic approaches. DT tools require virtual representations that take advantage of online measurements to find real-time solutions. There are gaps in describing processes and obtaining real-time solutions for the industries studied in this project.

This work introduces new approaches for processes in which mechanistical methods either cannot represent the process or are costly for online computations. In the cream cheese fermentation unit, the batch duration variation is the main challenge of optimizing the vats scheduling since mechanistic modelling of the dynamics of the fermentation process is difficult and include many time-varying parameters. The other case introduced a different challenge,

the mechanistic model of the system is available for active PCM systems; however, its complexity makes the optimization using that model computationally infeasible. These processes pose distinct challenges, necessitating novel approaches that combine data-driven and mechanistical methods.

Novel research objectives were targeted that are listed below:

1. DT virtual entity for scheduling is achievable, which takes advantage of online measurements in data-driven approaches for determining the batch duration.

2. Data-driven approaches that are trained offline provide a feasible solution to the optimal control problem in real time which is necessary for DT virtual entity development.

1.3. Applications in food and renewable energy industries

New Zealand's gas emissions must be reduced by 30% below 2005 by 2030, according to the country's energy efficiency and conversion policy 2017-2022 [26]. Two of the four priority areas in New Zealand's energy strategy are the development of renewable energies and the efficient use of energy. In this thesis, these two areas were targeted by studying the digitalization opportunities in the dairy and energy storage industries.

Although digital twin tools in these two industries are new, their histories are vastly different. The dairy industry is a long-established industry that has evolved over many decades. Machine-assisted operations have replaced complete manual processes in this industry [27]. New sensors and measuring equipment have also improved product quality and operation control [28]. On the other hand, energy storage systems are a relatively new technology that has gotten a lot of attention in the last decade. Although there have been numerous academic studies, commercial implementations of such systems are still in the early stages. Such systems have been accelerated by global concerns about environmental issues such as climate change and global warming.

Dairy industries also include large plants with multiple units. The plant would benefit from strategies like DT but identifying these benefits and calculating the return on investment is difficult. These factors make decision-making difficult and time-consuming, necessitating agreement among managers at various levels. The technology is easier to implement in the case of energy storage, PCM for buildings. Energy storage systems can be used during the design and construction of buildings and as a retrofit to existing structures. Because the system scale

is smaller, the decision-making process would be more straightforward. However, other technologies on the market, such as heat pumps, compete with energy storage systems. This makes the optimum design and operation of such systems important.

In addition, the mechanisms at work in these two industries are vastly different. Dairy plants work with raw materials with a short shelf life and a diverse composition. Furthermore, the presence of bacteria increases the complexity of biochemical mechanisms in the processes. As a result, plants with batch and continuous operation units emerge, posing challenges in maintaining consistent throughput and quality. Although the system operates continuously in the energy storage case, finding the system's optimal operation presents a new challenge due to the system's rigorous mathematical models.

Finally, the dairy industry's online measurements are more limited than those available in the energy storage case. Lactate, for example, can be measured online during cream cheese fermentation, but lactose requires HPLC equipment, and biomass concentration measurements take more than a day. Aside from that, some critical final product quality parameters, such as sensory properties, are not automated. As a result, process modelling is a difficult task. Temperature and radiation measurements are easily obtained in the energy storage case, which would aid in the development of better mechanistic models.

1.3.1. Dairy industry

The dairy industry in New Zealand contributes significantly to the country's economy. Dairy exports have increased from NZ$2 billion per year to nearly $20 billion in the last 30 years [29]. In 2016, the dairy industry consumed 28.4 PJs of energy to generate process heat. In New Zealand, the 28.4 Petajoules (PJ) of fuel burned resulted in 2.1 million tonnes of CO_2 emissions [30]. Despite decades of research into the benefits of automation in the dairy industry [31], the food industry is not considered high-tech in general. New digitalisation and Industrial 4.0 breakthroughs may result in new industry movements [32].

Fermented dairy products are an important and widely consumed food around the world. In recent decades, the market for these products has been rapidly expanding [33]. To compete in the global market, products must have consistent quality and be reasonably priced. However,

achieving these objectives is difficult. This is due to the use of batch and semi-continuous processes in the dairy industry. Also, the procedures are extremely complicated. For example, biochemical mechanisms are involved in fermentation processes as a result of microorganisms, resulting in batch duration variation in the plant. This has an impact on product throughput and quality. Furthermore, the variability in the composition of milk as a raw material, as well as measurement limitations, add to the processes' complexity. The mentioned difficulties make dairy plants' modelling and scheduling complex tasks. The previous research for modelling and scheduling fermented production plants are reviewed in the following sections.

1.3.1.1. Modelling of fermentation

Milk fermentation is accomplished through the use of bacteria to produce lactic acid. Lactose is one of the substrates consumed by the bacteria. However, fermentation is not limited to the dairy industry; alcohol, amino acids, antibiotics, enzymes, single-cell protein (SCP),

citric and acetic acid, and beer [34] are all produced on a large scale around the world. As a result, models for the fermentation process in various industries have been developed. The models can be categorized into white box models (first-principles models), black box models and grey box models.

1.3.1.1.1. First principles models

There are two types of first principles models: structured and unstructured. Details of the involved mechanisms, such as cell structure and composition, are considered in the structured models [35, 36]. This complicates the mathematical models, making them unsuitable for use in DT online applications. For describing fermentation, the unstructured models use kinetic models. However, kinetic modelling is difficult due to the complexity of biochemical mechanisms. They contain a large number of variables that change during process runs and across different stages of the same experiment, demonstrating the difficulty of using these models in real time. For instance, in [37], authors studied the effect of pH on the flavor and specific growth rates of lactic acid fermentation by Lactococcus lactis ssp. lactis biovar. diacetylactis. They showed that the pH acts indirectly by changing the proportion of the non-dissociated lactic acid. Generalized models were presented in which the effect of pH was included.

1.3.1.1.2. Black box models

Data-driven models are derived from data and require less physical system knowledge [38]. Data-driven models take the place of first-principles models that cannot characterise complex systems due to a lack of engineering knowledge [39]. As a result of recent advances in cyber-physical systems, smart factories, and the industrial internet of things (IIoT), a large amount of process data is now available, making the application of more sophisticated data-driven approaches, such as machine learning, neural networks, and deep learning, in the industry viable [23]. As an alternative to first-principles models, researchers have used black box models. Applying data-driven models, however, comes with its own set of challenges and considerations. This was addressed in [40], which looked at two industrial cases. One of the case studies was the fermentation process in craft breweries. In this process, yeast is used to convert sugar to ethanol. The fermentation is complete when the desired ethanol concentration and flavour are achieved. In ideal conditions, the fermentation period should be consistent across all batches; however, batch duration varies due to ingredients and process temperature differences. Furthermore, alcohol measurements are not available online and are taken every

4-10 hours, resulting in overfermentation and a reduction in product quality. The amount of ethanol produced was predicted using ultrasonic and temperature measurements taken during the fermentation. Artificial neural networks were used to map the ethanol concentration prediction to the data (ANNs). The relationship between process variables was complex and nonlinear, which could be determined using data-driven methods. The most important factors to consider when designing a data-driven model for processes were discussed. It is critical to define the model's goal as well as the challenges that must be overcome. The application of the model determines the model's level of complexity. It will be more complicated than simply fitting the data if it is used to make predictions. The model's complexity is also influenced by the required model accuracy, which should be defined in light of the product specification, regulations, economic value, and safety criteria. When defining the boundaries of the process manufacturing system, manufacturers should take into account the availability and unpredictability of industrial data.

Other studies also looked at applying data-driven methods in fermentation. A static feedforward neural network was developed for modelling the continuous biodegradation of

phenol [41]. The continuous biodegradation of phenol was modelled using a static feedforward neural network [41]. In general, the authors came to the conclusion that the ANN outperformed a nonlinear Multiple Regression Analysis (MRA) model. Cui et al. [88] proposed a rolling-prediction approach based on ANN, in which training data was taken from historical batches as well as the batch of current interest. With different prediction horizons, the approach predicted the product formation process. For an 8-hour prediction, the average error of the product formation prediction from testing batches was 3.01 %. An ANN model for online optimisation was used to boost the productivity of a wheat beer fermentation [87]. As soon as 12 hours of process data were collected, the model was used to predict the fermentation course. The temperature trajectory of the process was optimised and fed to the controller using this information and the model, resulting in a 20% reduction in processing time. The authors of [90] proposed a static neural network for predicting the final time of the acidification step, followed by the addition of rennet. Because milk powder was used to make the milk in their study, the system inputs were the initial solid amounts, the starter culture addition ratio, and the pH at 0, 20, 40, and 60 minutes after inoculation. As the network's output, the final acidification process time was determined. The authors used industrial data to test their method, and they were able to make accurate predictions. For pH dynamics prediction, RNN models with lab-scale data were used.

1.3.1.1.3. Grey box models

Grey box models can also be created by combining first-principle and ANN models. This type of model benefits from the incorporation of prior knowledge from first-principle models into neural networks, reducing the neural networks' sole reliance on data.

A fed-batch fermentation of a foreign protein production unit was determined using grey box models [45]. For the five critical parameter functions of growth rate, glucose consumption rate, oxygen consumption rate, acetate production rate, and protein production rate, neural networks were discovered. The parameters were then used in the first principle equations of the conservation equations. The neural network parameters accurately predicted dynamic response data in simulations. The fermentation of ricotta cheese whey for the production of ethanol was investigated in [46]. Neural networks are combined with mass balance equations for lactose, ethanol, and biomass in the grey box model. The model predicted the biomass,

lactose, and ethanol concentration profiles with an average error percentage less than 10%. Black box and grey box models were developed for online estimation of the biomass concentration in a PHB fed-batch fermentation process [47]. The authors used a grey box model that included mass balance equations and either a feedforward or RFBN network. The grey box model performed better than the other approaches, according to the findings.

1.3.1.2. Scheduling

Unlike the chemical industry, the dairy sector uses batch and semi-continuous processes, making optimisation and scheduling of these operations difficult. Previous research focused on the dairy factories' plant-wide scheduling. The authors of [48] developed a scheduling algorithm for the filling line that fills the cups with yogurt, cream, and other items. By pre-empting production, scheduling helps clean the filling line between the filling of two items rather than at a specific time. The filling line's non-productive time was reduced as a result.

A combined optimization and constraint programming approach was used for optimal scheduling of a batch milk/yogurt powder process in [49]. The scheduling constraints were defined using a model that took into account the production process and available machines. The fermentation time of yogurt batches was assumed a constant value. The model was used in an optimization formulation with the objective of meeting the customers deadlines, while taking into account the efficiencies and costs of the available alternative machines.

A mixed-integer programming (MIP) algorithm was developed for scheduling an ice-cream manufacturing facility that produced eight different flavours [50]. The scheduling formula took into account all stages of processing, including the process line, aging vessels, and packing lines. The aging and cleaning durations, as well as the maximum shell life of materials, were included. The objective function minimized the makespan (the time point at which all product demands are met).

Optimal scheduling of the yogurt packaging lines was investigated in [51]. The yoghurt manufacturing unit produces a wide range of products with various characteristics. The problem of parallel machine scheduling with sequence-dependent setup times and costs arose as a result. A MILP model was used to solve the scheduling problem. The yoghurt fermentation batch time was assumed to be constant. The authors concluded that the method had a low computational cost and that its production decisions could significantly improve plant

operations by lowering setup and labour costs.

Batch and semi-batch production units are used in other process plants, such as those in the beverage and pharmaceutical industries. The scheduling of a penicillin bioprocess plant was studied in [102]. To solve the scheduling problem, forecasts of process productivity and completion times for the tertiary stages of industrial penicillin fermentations were combined with a genetic algorithm. The authors, on the other hand, ignored batch variation and used a nominal batch processing time in their scheduling formula. In [53], a scheduling solution for a beverage plant in the brewing industry was presented. The authors used a constant fermentation time that was significantly longer than the mean scheduling time. The variation in fermentation time, on the other hand, was not addressed. The throughput of the process was significantly reduced as a result of their schedule. The fermented liquid product could also be stored in tanks for several days.

The aforementioned studies did not take into account the batch duration variation in fermentation processes. It has a significant impact on the unit's operation. In dairy units, the process operation can change from batch to batch. This is because raw materials such as milk can vary from season to season and farm to farm. In addition, microorganisms are involved in the processes, which adds biochemical complexity to the system. These uncertainties result in varying batch durations in dairy operations, making scheduling difficult. Predicting batch duration applying models and using it to schedule fermentation vats can improve the unit operation.

1.3.1.1. Cream cheese plant

Cream cheese is a soft, fresh, acid-coagulated cheese. It is made from a mixture of milk and cream, cream, or skim milk [54]. Cream cheese is a dairy product with increasing economic importance in the food industry, with a projected global cheese market size of ~$8.3 billion USD by 2026 [55].

The cream cheese manufacturing process contains multiple continuous and batch units. Fig. 1.2 shows the discrete unit of a cream cheese plant owned by Fonterra. The upstream flow contains a mixture of homogenized milk and bacteria culture, which is passed to fill up the vats. During the fermentation process, bacteria consume lactose, and pH decreases. There are upper

and lower limits for curd pH at the end of fermentation which defines the desired bound. This process continues until the desired pH bound is reached. Then, the batch is drained to the continuous section. The curd is heated up in a cooker to kill the bacteria, which stops the acidification.

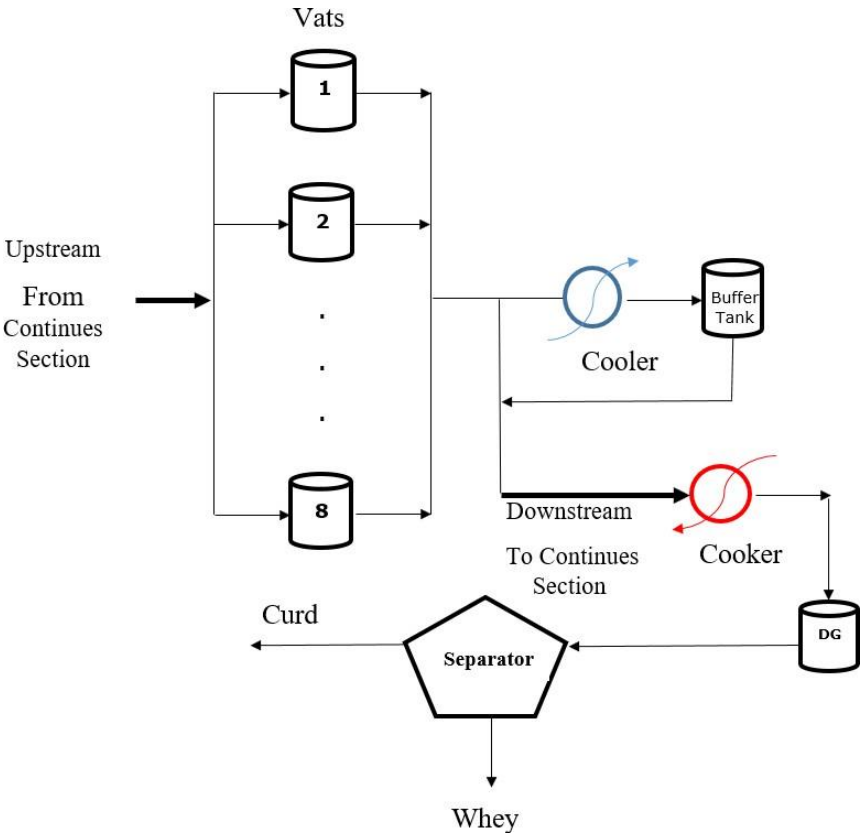

Fig. 1.2. Cream cheese production unit

It is essential to achieve consistency in the pH of batches since it strongly affects the quality [60]. However, achieving this consistency is difficult since the pH dynamics of batches and their durations vary in the plant. This causes variation between batch heating of the product curds, leading to over-acidification of some batches and, consequently, poor-quality product.

The continuous section has limited capacity. Therefore, in the event of batch drainage interference, the curd is bypassed to a cooler, where bacteria activity is reduced as a result of cooling. The cooled curd is then temporarily stored in the buffer tank before being transferred to the continuous section. The acidification process is not stopped by batch cooling, but it is slowed. Furthermore, if more than two batches reach the desired pH at the same time, one will be wasted. It's also worth noting that cooling consumes a lot of energy and should be avoided whenever possible.

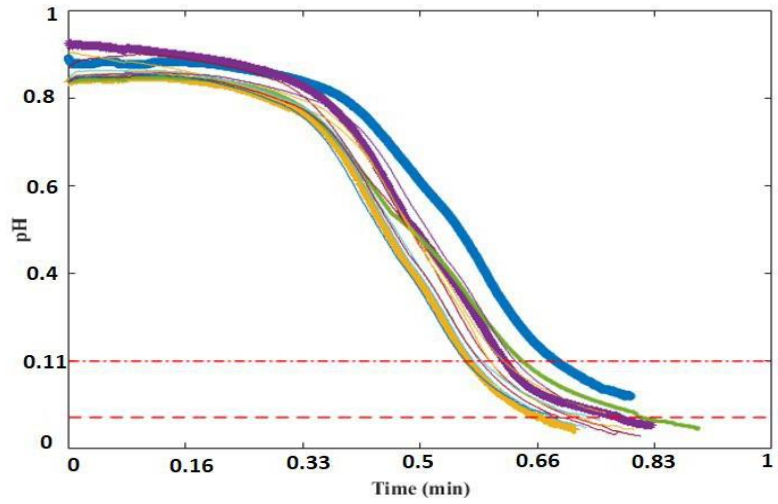

Fig. 1.3. Variation of batch duration in an industrial unit

Batch duration varies in the plant, as shown in Fig. 1.3. The lower and upper limits for curd pH are shown in red. The majority of batches exceed this limit, owing to poor batch filling scheduling, which causes interferences during drainage to the continuous section and draining delays. Another reason is the difficulty in determining the drainage start time, which should be chosen so that the batches reach the desired pH after 2 hours of draining.

More consistent curds can be produced by reducing batch interferences during draining. This can be achieved by improving the scheduling of fermentation vats. In this work, a digital twin entity was developed for online scheduling of the fermentation vats. Using data-driven approaches, pH prediction models were developed to predict the batch duration using the available measurements. The model predictions were then used to schedule the fermentation vats filling, draining and cleaning using optimisation programming.

1.3.2. Renewable industry

Renewable energy sources currently supply around 40% of the total energy demand in New Zealand [57]. Increasing this share is critical to meeting our international obligations and the Zero Carbon Act's 2050 net-zero target of reducing glasshouse gas emissions [58]. In recent years, this has increased the deployment of renewable energy sources.

Wind, hydro, solar, geothermal, biomass, and ocean energy are examples of renewable energy sources. The majority of these energy sources, on the other hand, are variable and partially unpredictable. For example, on days when there is little wind, and the sky is cloudy, renewable energy sources would be insufficient to meet the energy demand. Energy storage

systems increase renewable energy sources' reliability, affordability, and long-term viability. Governments have used dams to store water and use it as batteries on a national scale. This is a method of meeting varying power demands.

On the other hand, demand-side energy management is critical in the transition to 100 percent renewable energy. Energy storage improves energy management on the demand side, just as it does on a national scale. Solar energy, for example, is available when most members of the household are at work and energy demand is low. Solar power and heat are stored in energy storage systems during the day and then used at night. Furthermore, the less expensive energy generated during off-peak hours can be stored and used during the more expensive on-peak hours. Because of its moderate climate, this technology could be especially useful in New Zealand.

Buildings consume a huge amount of energy. This industry accounts for 30% of global glasshouse gas emissions and 40% of total energy consumption [59]. One of the technologies that have piqued the interest of many researchers is thermal energy storage (TES) [60]. Phase change materials (PCMs) are among the most applicable energy storage systems in buildings among the various TES approaches [61]. During their phase transition from liquid to solid and vice versa, PCMs absorb and release a large amount of energy. PCMs are simple to use, have a high energy storage density, and are durable and stable [62]. Buildings have been equipped with PCM for cooling, heating, or hybrid applications [63]. PCMs can be incorporated into buildings, either passively or actively [64]. In the passive approach, PCMs can be incorporated into the building envelope as an integrated material into building walls, roofs, floors, slabs, shading systems, fenestrations, insulation, and façades. Unlike the passive approach, active systems incorporate PCM as a storage medium in heat exchangers, tanks, etc.

Many researchers are interested in combining solar collectors with PCM storage. This is due to the fact that solar energy is intermittent, resulting in a mismatch between energy availability and actual demand. This problem could be solved by combining thermal energy storage (TES) with solar heat sources. However, the initial cost of such a system makes this technology economically unviable. DT can help improve the design and operation of such systems, resulting in greater energy and cost savings when PCM technology is used. The following section summarises previous research on modelling, design optimisation, and optimal control of systems that combine solar collectors and PCM storage.

1.3.2.1. Modelling

In [65], the authors numerically investigated a PCM-based cascaded energy storage unit with a solar air collector. Three paraffin-based materials (RT50, RT65, and RT80) were used as PCM for the energy storage unit. The thermal energy storage unit and the solar collector were modeled. The model was validated by the experimental data with high accuracy (R-squared was equal to 0.94).

In another research, simulation of net-zero energy (NZE) was first developed using TRNSYS [66]. The authors investigated the energy flexibility and performance of NZE houses using a solar-assisted heating, ventilation, and air conditioning (HVAC) system with thermal energy storage (TES), PVT collector, and demand-side management (DSM) strategies.

A simulation system of the NZE house was developed using TRNSYS to evaluate its performance under various conditions. The major components of the system, such as PVT collector and air-based PCM storage, were modeled and validated individually [67, 68]. In particular, the air-based PCM storage model was developed [67] to represent the thermal dynamics of the storage for cooling purposes in summer using the free ambient cooling at night to solidify PCM.

A novel solar thermal heater coupled with an active PCM heat storage wall was proposed in [69]. Hot water heated by the parabolic trough solar collectors flowed through the copper tube to discharge the cool load stored in the PCM wallboard. Also, the excess heat could be stored in the PCM wallboard to meet the indoor thermal demand when solar energy is insufficient. The transient model of the active PCM storage was combined with the TRNSYS model, which included the hut model. The indoor hut temperature was used to validate the accuracy of the model. The RSME during seven days of operation was 0.7^{o}C. Despite past studies on modeling solar collectors with PCM storage, it appears that a model that integrates the solar air collector, and PCM storage, and building models has not been previously reported.

1.3.2.2. Economical design optimization

Design optimization was investigated by applying optimization algorithms for obtaining the optimum design variables for the system coupling solar collectors and PCM units. In [70] a multi-objective optimization was carried out for TES systems, including PCMs for solar air systems in a lab-scale test rig. Thermal storage design variables such as the number of the air

channels and the number of PCM bricks were optimized. The optimum values increased the average heat transfer effectiveness and effective PCM charging time of the system.

In [71], a two-level model-based strategy was used to optimize a system including a Photovoltaic/thermal (PVT) collector with a centralized PCM thermal energy storage. The electrical and thermal performance of the system was increased by obtaining the optimum air flow rate, and optimum slope and orientation of the PVT collector. The design of a PVT with a passive PCM was optimized in [72]. PCMs were embedded into the building envelopes, while the heated air from the PVT collector was used for heating the building. The Taguchi-Fibonacci search method was used for the optimization. The optimized variables were PCM air flow rate, PCM type, PCM layer thickness, and additional wall insulation. The objective function maximized the signal-to-noise ratio of the coefficient of the thermal performance enhancement (CTPE) of the building simulated in TRNSYS.

In the above studies, the design optimization was focused only on improving the system's technical performance. However, ignoring the initial cost of solar collectors and PCM energy storage could lead to designing systems with long payback times, which could lead to unfeasible economical systems. For instance, in [73], parametric analysis was used for designing a solar heating air system, including an air vacuum tube solar collector and a concentric-tube latent heat thermal energy storage. The design of the energy storage system was optimized regarding the air outlet temperature of the storage and peak shift of the heat supply. The results showed that the optimal mass of PCM was 150-200 kg/m^2. This amount of PCM introduces a high initial cost that leads to a very long payback time.

The cost of implementing PCM is needed to be compared against the benefits of using such systems before making decisions [74]. The importance of economic factors was also mentioned in [75]. The optimal design of a solar collector integrating PCM thermal storage was carried out in this study. A front and back solar air collector (SAC) with a PCM-based absorber plate was considered. The objective function minimized the root mean square error between the solar air collector and the set temperature. The thickness of PCM in the absorber plate, the phase change temperature, and a parameter in the effective heat capacity curve were used as the optimization design variables. The objective function considered thermal performance parameters, but the authors concluded that the techno-economic constraints need to be added in future studies. The authors of [76] studied the optimal design of a renewable cooling and heating system that included a desiccant wheel, PVT, and a thermal storage unit was carried

out. The objective function was a twenty-year life cycle cost which included PVT price, PCM price, electricity purchase price, and electricity sale price. The results showed that the optimized design decreased the system's life cycle cost by 32.4% and 31.2% compared to two other design cases. It was found the electricity sale price had a significant influence on the optimization results. However, the results cannot be used in designing solar air collectors without PV panels, which only generate heat. Economical design optimization of systems including the coupling of solar air collectors and PCM energy storage, which minimize the system cost could facilitate increased deployment of such systems.

1.3.2.3. Optimal control

Optimal control strategies can help PCM technologies reach their full potential and, as a result, reduce payback time. In previous studies, researchers devised optimal control strategies.

MPC was applied for optimal control of a solar assisted HVAC system in [77]. A PVT collector and a PCM unit were integrated into a heat pump as part of the HVAC system. High and low-level controllers are used in the MPC formulation. For the high-level and low-level controllers, prediction horizons of 24 hours and 1 hour were considered, respectively. In the high-level controller, PCM was charged and discharged. At the lower level, the continuous air flow rate through the PCM storage and heat pump regulation were determined.

The MPC formulation's objective functions were defined as minimizing energy [78], minimizing energy cost [79], and maximizing PCM performance [80]. The authors of [79], for example, combined passive (on walls) and active PCM (PCM heat exchanger) systems with an HVAC system. A hierarchical, centralized energy management strategy was developed based on controlling active and passive PCM in the slow and fast time scales, respectively. The longer time horizon (up to 24 hours) associated with daily weather changes and energy price fluctuations contributed to the slow time scale. The short time horizon (a few minutes) associated with the occupancy and ambient conditions contributed to the fast time scale.

The MPC formulation leas to a mixed-integer non-linear problem which is due to the PCM heat capacity calculation. Solving this complex problem in real-time is challenging and needs specific solvers [81].

As an alternative, machine learning-based approaches such as Reinforcement Learning (RL) can be applied as an optimal control approach. Pre-computing the optimal solutions

through offline RL training overcomes the high online computational effort of MPC [82].

1.3.2.3.4. RL

Machine learning advancements have enabled not only modelling but also process control through reinforcement learning (RL) [83]. An agent learns to complete a task through repeated interactions with its surroundings in RL [84]. The repeated interactions are a trial-and-error search, leading to finding the optimal policy. Policy leads to mapping the states which describe the environment to the actions. Applying each action to the environment at each state has a reward signal which aims to learn the optimal policy. RL has some advantages over the classical optimal control methods such as model predictive control (MPC). The low cost of online computation is one of the key advantages of RL. In other words, the RL training process is done offline, which solves one of MPC's problems: high online computational requirements [85].

Furthermore, the system's uncertainties are unknown and non-stationary, whereas, for only some operational regions or scenarios in MPC, the uncertainty can be summarised by mean and variance [86]. RL finds the best strategy by accounting for system stochasticity, making it more practical for specific systems [87]. Additionally, RL can replace the combination of RTO and MPC. In [88], the combination of RTO and MPC was compared to RL, with RTO providing the best steady-state set point and MPC calculating the input trajectory to get to the set point. Economic MPC is similar to RL in that it combines RTO and MPC into a single framework.

RL has been used in a variety of cases and fields. In [88], RL was used to fine-tune the PI controller parameters. Traditional controllers have tuning parameters that must be adjusted based on the process conditions. Tuning, on the other hand, is a difficult and time-consuming task. Most industrial controllers are tuned using the Ziegler-Nichols technique; however, if the controllers are not re-tuned properly and on time, their performance will be less than ideal. For tuning traditional controllers, RL can provide an automatic and optimal solution. Parameters of a PI-controller were tuned dynamically using RL [89]. The controller controlled a stirred tank heater. RL was trained using a model and implemented on the tank. RL led to better performance compared to internal model control tuning methods by rejecting disturbances and tracking the set points. There are types of RL that can be useful for cases where accurate deriving models of a system is not possible. In another research, RL was applied to cool a data

centre [90]. As modelling of this process is very difficult, RL was used to find an optimal policy for controlling the system by interacting with it online. When compared to model-based methods, RL saved 22% more power. An adiabatic plug flow reactor was controlled using J-learning and Q-learning types of RL [91]. The reactor model was simulated and used as a virtual plant. RL showed the best control performance compared to two different PIDs and three different MPCs.

In a recent study [92], RL was used to determine the optimal operating condition of a hydrocracking unit. The operating condition was constantly changing due to changes in raw materials and production requirements. To achieve the highest efficiency in terms of both quality and cost, quick response optimisation methods were required. The optimisation process was optimised using actor-critical reinforcement learning instead of first-principles models, which has a high computational cost. RL was trained with a deep neural network model based on a mathematical model that had been validated. The proposed RL determined the optimal operating conditions of the process with a minimum accuracy of 95%.

1.3.2.1. Active PCM system for Auckland

Active systems incorporate PCM as a storage medium in heat exchangers, tanks, and solar-assisted PCM systems. Fig. 1.4 shows the active system implemented in Auckland. It shows that the air was flowed in different pathways by manipulating the ON/OFF valves and fans.

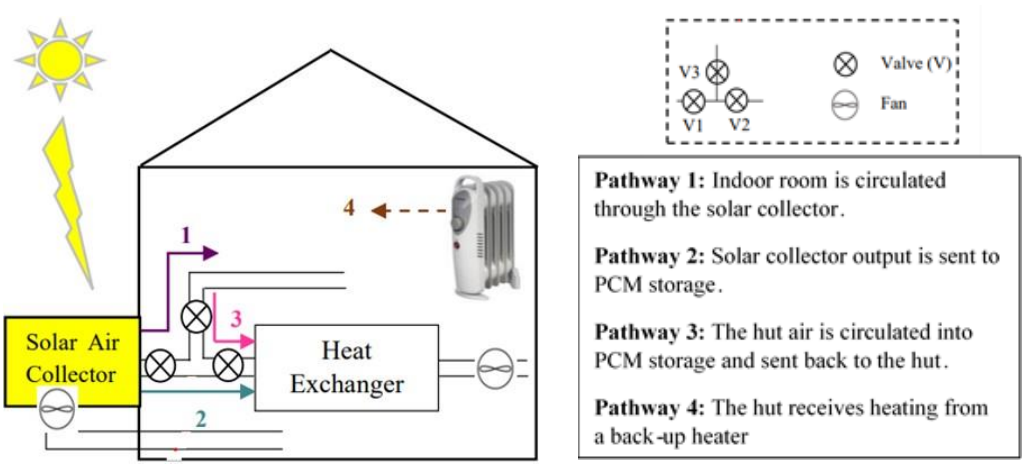

Fig. 1.4. The active PCM system set up in Auckland

Although better control and heat transfer performance is achievable using active systems [93], the capital cost of active systems is higher which makes them economically unviable.

Improving the economic design of such systems is carried out in this thesis for the first time. This is accomplished by developing a model representing the dynamics of the entire system which is obtained by interacting the system components.

Additionally, better performance of the active systems is due to better control comparing to the passive systems. This was shown in [93], where a comparison was made between passive and above active systems in the same situation in Auckland. Their results showed that active systems had greater energy-saving (22% less energy consumption) and more efficient peak load shifting (32% less electricity cost) compared to the passive approach. These conclusions were achieved by applying ON/OFF control for the above active system. Although the ON/OFF base controllers are cheaper and easily implemented, their algorithms do not consider the building dynamics. Dynamic behaviour is important for time-delayed processes like temperature dynamics in buildings [95]. Furthermore, because active systems require a higher initial investment, proper control is required to achieve the maximum potential for energy and cost savings [96]. Control performance can be improved by using optimal control strategies that include hut dynamics.

To improve the control performance, the application of MPC was investigated for the same active system numerically [97]. The objective was to minimize electrical energy consumption. The EnergyPlus model and system components such as the PCM heat exchanger were very nonlinear and rigorous, making the real-time computational cost expensive. EnergyPlus simulation determined the heating demand offline, and the values introduced to the optimization problem in MPC. However, for implementing such a control strategy, the real-time measurement from the building, as feedback, plays a very important role in reconciling the states and covering the mismatch between the model and the building. This is one of the advantages of DT. Besides that, the airflow rate was considered a continuous variable in the proposed MPC. However, the actual system includes ON/OFF valves that drive the air at a constant flow rate in the pathways. This leads to binary variables in the optimization problem, which makes the real-time implementation of MPC even harder.

DT virtual entity was developed for economical design optimization and optimal control of this system using dynamic models of the entire system. First, a validated dynamic model of the system was first obtained. Then, the model was used for economical design optimization.

It was also used for energy management by training a data-driven control approach, RL, which could deal with the complexity of finding an online solution for the system suitable for applying in DT.

1.4. Thesis framework

Fig. 1.5 shows a summary of the thesis framework. A literature review about DT has been given in the introduction chapter. Also, the two industries studied in this work have been introduced, and the challenges of developing DT tools have been addressed. Fig. 1.5 also shows the chapters allocated to each industry. Chapters 2 and 3 are about the cream cheese fermentation, and Chapters 4 and 5 present the energy storage research.

Each chapter begins with an introduction that covers the most recent and relevant works, followed by sections on study methods, results, discussion, and conclusion. An outline of each chapter published in this thesis is as follows:

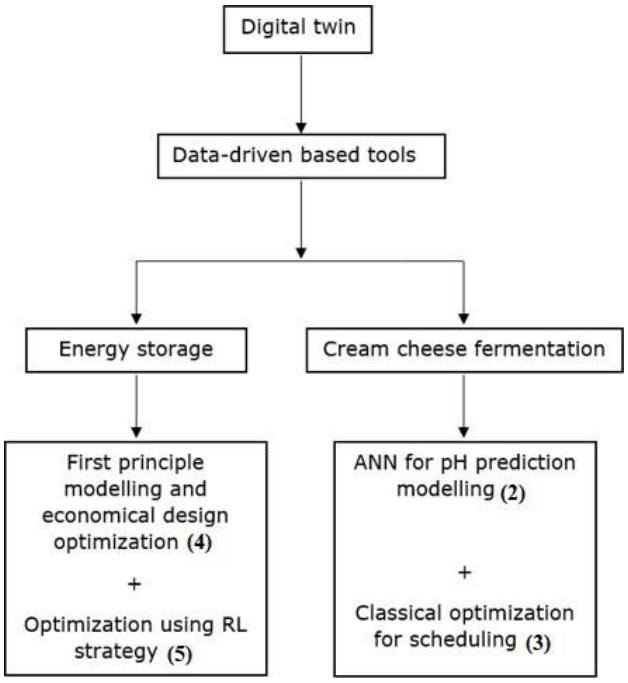

Fig. 1.5. Thesis structure

Chapter 2

The complexities of modelling the cream cheese fermentation process are discussed in this chapter. The literature was evaluated, and several types of fermentation model used in various

industries were summarised. Cream cheese fermentation dynamics were studied using white, grey, and black-box models. Each type of model was explored in terms of its benefits and drawbacks. The model's capability was assessed using data from laboratory fermentation. The performance of the model for pH dynamics prediction was tested using lab and industrial data, and a neural network model based on pH data was built. This research work has been published in the *Journal of Food and Bioprocess Products, 2021, Pages 81-89.*

Chapter 3

This chapter provides a cream cheese fermentation scheduling framework that combines mathematical programming optimisation with data-driven pH prediction. The scheduling formula took into account the constraints encountered during filling, draining, and cleaning in the actual Fonterra cream cheese unit. One of the most difficult aspects of scheduling the cream cheese unit is determining when to fill the vats so that there are no interferences while draining the batches. This is since the duration of the batches varies from batch to batch. The framework deals with this problem by updating the schedule using the pH model prediction information as soon as enough measurements for model prediction are available. In addition, an adaptive grey model was proposed, and the benefits of using measurements to improve prediction accuracy were demonstrated. This work has been published in *Computer Aided Chemical Engineering*, Vol. 49. Elsevier, 2022. 541-546.

Chapter 4

This chapter aims to develop a reliable model for an active PCM system that provides heat to a hut on Auckland's Ardmore campus. The system included a solar collector and a PCM heat exchanger, modelled in MATLAB. EnergyPlus was used to simulate the hut dynamics, and an interface was used to connect the entire system. The system model was validated using experimental data from winter 2020. The results showed the reliability of the model. The model was then used to optimally design the active system components for the same hut with different applications. The design was carried out while a proper control was applied to ensure using the full potential of the PCM heat exchanger, providing thermal comfort and minimizing system payback time. This work has been published in the *Journal of Applied Thermal Engineering*, 216 (2022): 119002.

Chapter 5

This chapter presents an optimal control strategy for the PCM active system of the previous chapter. Although a reliable mechanistic model was obtained, classical optimal approaches based on mathematical programming optimization were not suitable due to the model's complexity and the inclusion of binary variables. This was addressed by developing MPC for the system, and the obstacles of implementing it were addressed. Then reinforcement learning, a data-driven optimal control strategy, was adopted to the system. A novel reward formulation was proposed, prioritizing control based on achieving thermal comfort or increasing energy cost savings. A part of this work has been accepted in *the 7th International Symposium on Advanced Control of Industrial Processes*, Vancouver, Canada.

CHAPTER 2

Artificial neural network modelling for cream cheese fermentation pH prediction at lab and industrial scales

Foreword

The mechanism of cream cheese fermentation has a complex, which makes its modelling a challenging task. Researchers have proposed different approaches to modelling the fermentation process. The developed models can be categorized into white, grey, and black box models. In this paper, we studied these models and investigated their application by using lab and industrial scale data which were obtained in the presence of disturbances. The results showed that using the states of the white box model for predicting pH is challenging because of the complexity of the cream cheese compound. Although this problem was solved in the grey box model, there were difficulties in applying both white and grey box models mainly due to the lack of online measurements of states. Unlike white and grey box models, a black box model, an ANN model, was developed based on pH data, which are measured online. Using the experimental pH data, ANN model configurations with optimal feedback and time intervals were used to predict industrial fermentation pH dynamics. The ANN model provided reliable pH predictions at both lab and industrial scales. This chapter has been published in the *Journal of Food and Bioprocess Products* and has been included in the thesis.

1.5. Introduction

Fermented products such as alcohol, amino acids, antibiotics, enzymes, single- cell protein (SCP), citric and acetic acid, and beer [34] are produced globally on a large scale. These products should be produced to a consistently high quality with low costs to compete globally. In other words, products with high quality should be achieved along with reducing the processing time.

One product of such a process is cream cheese. Cream cheese is a soft, fresh, acid-coagulated cheese that is produced from a standardized, homogenized, and pasteurized mixture of milk and cream [98]. The cream cheese manufacturing process contains multiple continuous and batch units. The batch section of a cheese plant is dedicated to the fermentation of milk to curds using bacteria. As a result, lactic acid is produced, and acidity increases, which lowers the pH [99]. After reaching the desired pH, the bacteria are killed by heating the curd, consequently stopping the acidification process. It is essential to achieve consistency in the pH of batches since it strongly affects the quality [56]. However, achieving this consistency is challenging since the pH dynamics of batches, and consequently, their duration varies in the

plant due to the disturbances entering the system. For instance, the milk composition varies between species of cows, the cows' diet, the time of year for milking, and weather conditions.

The variation of batch duration causes variation between batch heating of the product curds, which leads to over-acidification of some batches and consequently, poor-quality products. Better scheduling of batches can decrease their variation by reducing possible interferences between batches due to variation of their duration. To achieve better batch control and therefore scheduling, models for predicting pH dynamics can play an important role.

Many first-principle models have been developed for the production of lactic acid from lactose and other substrates [35, 36, 100, 101, 37, 102, 103]. These models can be classified as structured and unstructured. Structured first-principle models consider some basic features of the cell structure, function, and composition [35, 36, 100]. However, these models are too far detailed for industrial use. Unstructured first-principle models consist of equations with physical sense and sufficient biological significance [101]. In unstructured first-principle models, kinetic parameters are used to describe the growth, substrate utilization, maintenance, and product formation, which are all intimately related. However, the complexity of the biochemical fermentation process makes kinetic modelling difficult. This complexity mainly comes from interactions between cells, lactose, and pH. To describe these interactions, the models include many parameters that change during process runs and even across different stages of the same experiment, shown in many studies. Cachon and Divines [37] studied the effect of pH on the flavor and specific growth rates of lactic acid fermentation by Lactococcus lactis ssp. lactis biovar. diacetylactis. They showed that the pH acts indirectly by changing the proportion of the non-dissociated lactic acid. Generalized models were presented in which the effect of pH was included. The effect of pH and substrate on the lactic acid fermentation by Lactobacillus plantarum was studied in [102]. In [103], the authors showed that pH affects the cell growth rate and lactic acid production. The death rate was also affected by pH and lactic acid, and it increases with increasing lactic acid concentration.

In addition to parameter variation in kinetic models, interesting process variables such as the biomass, substrate lactose, and the product lactic acid cannot be measured directly. The concentration of substrate lactose and lactic acid can be determined offline using High-Performance Liquid Chromatography (HPLC). The biomass measurements can be provided by cells two days after the sample has been taken. All these make the online estimation of parameters based on the measurements very challenging.

In summary, first-principle models can be used to describe many systems or processes based on prior knowledge and fundamental theories. However, the complexity of the biological raw materials, use of living organisms, lack of reliable online measurements, and complexity of first-principle models are the reasons for searching for alternative approaches for modelling fermentation quality [104]. Data-driven models such as artificial neural networks (ANN) are alternatives to first-principle models. Complex physical phenomena that are not fully understood can be represented by nonlinear data-driven models using data. ANN modelling has been proven to be a reliable, useful, and powerful tool in different areas of chemical engineering [105, 106, 107, 108, 109].

ANN has also been applied to the modelling of bioprocesses. ANN models have been developed for steady-state and dynamic modelling and optimization of different fermented processes. A static feedforward neural network was developed for modelling the continuous biodegradation of phenol [41]. In general, they concluded that the ANN's performance was far better than a nonlinear Multiple Regression Analysis (MRA) model. A moving window ANN was used for dynamic modelling and online estimation of unmeasurable state variables such as consumed sugar, cell mass, and product concentration in L-lysine fed-batch culture [110]. The authors concluded that with a certain degree of substrate variation, the estimator could give a satisfactory estimate of the critical fermentation variables. Online optimization was carried out using an ANN model in [43]. The productivity of a wheat beer fermentation was increased using an ANN model for online optimization. The model was used to predict the fermentation course as soon as 12 hours of process data was collected. Using this information and the model, the temperature trajectory of the process was optimized and fed to the controller, which led to a reduction of processing time of up to 20%.

For the aim of scheduling, Cui et al. [42] proposed a rolling-prediction approach based on ANN in which data from historical batches and the batch of the current interest was used as training data. The approach predicted the product formation process with different prediction horizons. The average error of the prediction of the product formation from testing batches was 3.01% for 8h ahead prediction. To schedule the lactic acid fermentation by lactose, a static neural network and a recurrent neural network for pH prediction were developed [111]. The static neural network was developed for pure culture and the recurrent neural network (RNN) for mixed cultures of lactic acid bacteria for yogurt production. The authors' results showed that this strategy predicts pH dynamics well. However, the experiments were carried out only

at different temperatures, and other variables were held constant, as the temperature was considered the main disturbance affecting the pH dynamics. In [44] authors proposed a static neural network to predict the final time of the acidification step, followed by rennet addition. In their study, milk powder was used to prepare milk, so the system inputs were the initial solid amounts, the addition ratio of the starter culture, and the pH at 0, 20, 40, and 60 min after inoculation. The final acidification process time was obtained as the output of the network. The authors applied the approach to industrial data, and successful predictions were achieved. RNN models with the lab-scale data were used for pH dynamics prediction.

The combination of first-principle and ANN models also can be applied as hybrid models. This type of models takes advantages of using prior knowledge of first-principle models into neural networks which reduces the dependency of neural networks only on the data. Some examples of hybrid models can be found in [112, 45, 46, 113, 47].

In this work, pH prediction of cream cheese fermentation was studied. Unlike the afore-mentioned works, the effect of significant disturbances on the pH profile was analysed by adding different initial concentrations of substrate, starter culture, and lactic acid to the fermentation. Furthermore, pH dynamics of industrial cream cheese fermentations were used in this work.

The objective of this investigation was to build a model that can predict the pH dynamics of cream cheese fermentation using online measurements and in the presence of disturbances. Such a model is necessary for scheduling purposes. In this content, three types of models; white, grey, and black box were studied. A first-principle model was applied as a white box model. For the grey box model, a hybrid model including a first-principle model and an ANN was considered. Then, the challenges of applying white and grey box models were investigated. Next, a black box model based on an autoregressive neural network with different configurations was studied, and its optimal configurations were obtained.

The paper is organized as follows. First, the lab experiment and disturbance details were described. Then, these experiments were used to calibrate the first principle models' parameters and training of the ANN model. Next, the results of the models were presented and discussed. Finally, the ANN model configurations obtained by using lab data were applied to predict the pH dynamics of an industrial cream cheese plant.

1.6. Materials and methods

1.6.1. Experiments

A mixture of 1.5 kg of milk (weight percentage of protein, carbohydrate, fat, and calcium are 3.32%, 4.76%, 3.40%, and 0.18%, respectively) and 0.5 kg of cream (weight percentage 1% protein and 37% fat) was prepared for cream cheese production. The mixture was added to a New Brunswick BioFlo 3000 fermenter in which both temperature and pH were measured. The mixture was heated up to 37 ^{o}C, while the stirring rate was set to 150 rpm. Next, the starter culture was added (Mesophilic Culture 72998 batch number 5693, which contains two main bacteria, *Lactococcus lactis subsp. cremoris and Lactococcus lactis subsp. Lactic*). Five minutes after adding the starter culture, which was enough for thorough mixing, a first sample was taken. Measurements were then taken every 1.5 hours for determining the biomass, lactose, and lactic acid concentrations. At the same time, temperature and pH measurements were recorded. The fermentation experiments were stopped as soon as pH reached 4.6 [114].

1.6.2. Models

Three types of models were applied for cream cheese pH prediction. The white box model, which is a first principle model, a grey model which is a hybrid model including a combination of a first principle model and an ANN model. Finally, a black box model was developed which is an ANN model based on the pH measurements.

1.6.2.1. White box model

An unstructured first-principle model was used in which biomass, lactose, and lactic acid concentrations are their states. After predicting the lactic acid concentration over time, the pH can be determined using these predictions. The model details are presented in the following.

This model structure was developed in [115], in which kinetics of the *Lacto-coccus lactis* strain on the M17 broth was studied. The model is based on the Luedeking-Piret equation, and the inhibiting effect of substrate, product, and high initial concentration of lactose is considered. Equations (2.1)-(2.3) describe the model:

$$\frac{dX}{dt} = \mu_{\max}\left(\frac{S}{K_{sx}+S}\right)\left(1-\frac{P-P_{ix}}{P_{mx}-P_{ix}}\right)\left(\frac{K_{ix}}{K_{ix}+S}\right)X \tag{2.1}$$

$$\frac{dS}{dt} = q_{s,\max}\left(\frac{S}{K_{ss}+S}\right)\left(\frac{P-P_{is}}{P_{ms}-P_{is}}\right)\left(\frac{K_{is}}{K_{is}+S}\right)X \tag{2.2}$$

$$\frac{dP}{dt} = \alpha\frac{dX}{dt} + q_{p,\max}\left(\frac{S}{K_{ssp}+S}\right)\left(1-\frac{P-P_{ip}}{P_{mp}-P_{ip}}\right)\left(\frac{K_{ip}}{K_{ip}+S}\right)X \tag{2.3}$$

Where, X, S, P are the concentrations of biomass, lactose and lactic acid (g L-1), respectively, μ_{max} is the maximum specific growth rate (h-1), $q_{p,max}$ is the maximum specific lactic acid production rate (g g-1 h-1), $q_{s,max}$ is the maximum specific lactose utilisation rate (g g-1 h-1), K_S is the Monod constant or substrate saturation constant (g L-1), P_i is the threshold lactic acid concentration (g/L), P_m is the maximum lactic acid concentration (g/L), K_i is the product inhibition constant (g/L) and α is the growth associated product form coefficient.

The model considers the limitation of the lactose in a non-competitive way, which is the same as the Monod equation. For the lactic acid's inhibiting effect, P_i is introduced as the initial value when the inhibiting effect occurs, and P_m is the maximum inhibitory value. The authors [88] tested the model on several batch fermentations with different initial lactose values. The correlation coefficient values (R^2) were all greater than 0.998, which shows an accurate representation of the model concerning the fermentation system.

1.6.2.1.1. Parameter estimation

To obtain a kinetic model based on the available experimental data, the parameters of both models should be estimated. A weighted least-squares minimization was used with an objective function as follows:

$$RSS = \sum W_x (X_{e,i} - X_{m,i})^2 + \sum W_p (P_{e,i} - P_{m,i})^2 + \sum W_S (S_{e,i} - S_{m,i})^2 \tag{2.4}$$

In the above objective function, RSS stands for the residual sum of squares, the subscript "*e*" represents the experiment, "*m*" represents the model calculated value, and "*i*" represents each experimental result. W_x, W_p and W_s represent the weights for biomass, lactic acid, and lactose respectively. The following values were used for weights: W_x and W_s were set equal to one, and was set to fifty. The different weight values used were chosen due to the greater

accuracy of W_p measuring lactic acid and lactose than biomass. Additionally, lactic acid concentration is important since it can be linked to thermal conductivity and pH. In industrial plants, pH measurement is used as an indication of fermentation proceeding. Using this approach, the parameters were estimated using MATLAB 2018. MATLAB's Ode45 function was applied for solving the differential equations. The objective function was minimized using the fmincon optimization function.

1.6.2.2. Grey box model

In this type of model, a combination of a white and black box models was applied for cream cheese pH prediction [116]. The black box model was used for correlating the states of the white box model to pH. This correlation is complex in cream cheese fermentation due to its complex compound. To predict the pH and the fermentation end-time consequently, a regressed white box model was used to generate biomass, lactose and lactic acid concentration over time. The state variables from the white box model were then used for predicting the pH.

Fig. 2.1 shows the structure of the hybrid model. The initial biomass, lactose and lactic acid concentration (X_0, P_0, S_0) were used as inputs to the kinetic model. The kinetic model predicted the dynamics of the states in the next hours (X_i, P_i, S_i). The predicted states were fed to a black box model (Long Short-Term Memory (LSTM) network) and pH values were obtained as the outputs. The white box model and LSTM are explained below. Please refer to the paper [116] for more details.

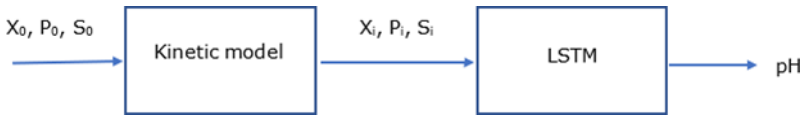

Fig. 2.1. Hybrid model structure.

1.6.2.2.1. Kinetic model

The white model explained in section 2.2.2.1 was used as the kinetic model. The parameters were estimated for different data sets detailed in section 0. The average values of the estimated parameters were considered in the model.

1.6.2.2.2. LSTM (long short-term memory network)

LSTM is a machine learning approach that was used for correlating the inputs and the outputs. It was chosen for its memory capacity and stability. At each time step, the inputs were the biomass, lactose, and lactic acid concentration, and the output was pH. LSTM aimed in correlating the states of the kinetic model to the pH without domain-specific information about the underlying biological-chemical process. To train the LSTM network, the data sets given in section 2.2.3, along with the measured pH data, were used. The number of hidden neurons was set to be 200. The solver chosen was Adam in MATLAB, with the initial learning rate set to 0.01 and the gradient threshold set to 1 by default.

1.6.2.3. Black box model

While the use of first-principle models is commonplace for chemical processes, such models' performance can be weak when applied to biochemical processes, as shown in the results section. Black box models can help with building models without detailed characteristics of the process. To achieve this in the cream cheese fermentation process, we applied a nonlinear autoregressive neural network, which was coded in MATLAB 2018. Fig. 2.2 shows the architecture of the network. The inputs to the system are a sequence of past pH measurements from time "t" to time "t − N" where "N" is called the feedback delay size. The hidden layer has "j" neurons with the sigmoid function as the response function to capture the nonlinearities of pH dynamics. The output layer uses a linear function to predict the pH at time "t + 1".

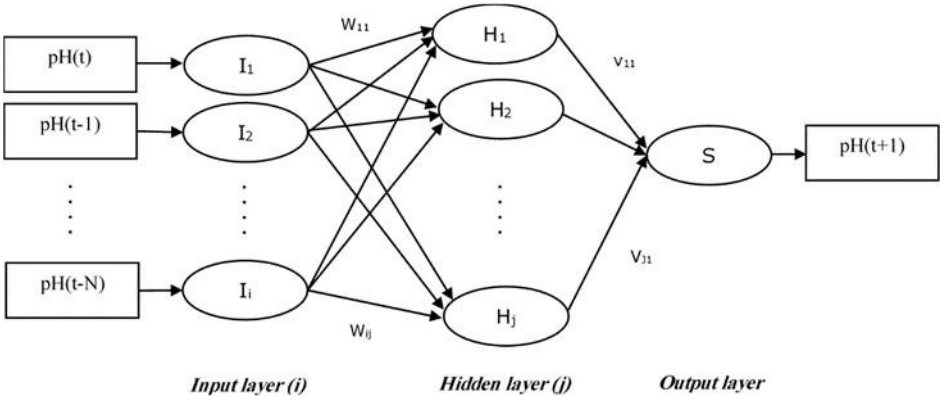

Fig. 2.2. Neural network architecture

The autoregressive model can predict the pH in future time steps based on the previous measurements or previous outputs of the network, by capturing the relationships between the

pH values in a time series. Unlike the first-principle models, which use biomass, lactose, and lactic acid as states to predict the pH, the neural network was de- signed to predict the pH dynamics using the past pH measurements directly. This was based on the assumption that all the effects of disturbances were embedded in the pH measurements. It should be noted that the fermentation pH measurements are available online and even manual measurements of pH are relatively straightforward and inexpensive, subject to the usual maintenance protocols around such measurements. However, the lactose and lactic acid measurements are measured offline by HPLC, and biomass measurement takes two days.

The network was trained using Levenberg-Marquardt optimization for fitting the weights of the network. To avoid overfitting during the training, the early stopping technique [117] was applied. In this technique, the training set is used to computing the gradient and update the network biases and weights, whereas the validation set is used to monitor the training progress. At the beginning of the training, both the validation and training set errors decrease; however, the validation error increases when overfitting occurs. The training is stopped, and the parameter values at the minimum validation error are considered the optimum values.

1.6.3. Data sets

Three different types of data sets were used in this study. Data sets including biomass, lactose and lactic acid concentration measurements were used for white and grey box models. For black box model data sets including lab and industrial pH data were applied.

1.6.3.1. Data sets of biomass, lactose and lactate

Cream cheese fermentation is affected by various disturbances. Milk composition is one of the significant disturbances which varies across different farms and seasons of the year. Additionally, bacteria's activity is an unpredictable and uncontrollable variable that affects the lactic acid production and, consequently, the pH dynamics. Seven experiments with different initial conditions were carried out in the lab. In the first four experiments, lactose, lactic acid, and biomass concentration were measured during the fermentation, which was used for parameter estimation and validation of first-principle models. These experiments represent the effect of the three major components on the cream cheese fermentation. Data set 1 is considered the normal initial condition, containing natural biomass, lactose, and lactic acid concentrations in the milk and cream mixture. In the data set, two double biomass is considered. High lactose concentration in data set 3 is provided by adding 100 ml of sterilized 125g/L α-lactose

monohydrate. 50ml of sterile 42.5g/L lactic acid was added to the natural amount of lactic acid to provide the high initial lactic acid concentration in data set 4. Table 2.1 shows the initial concentration of different components in g/L.

Table 2.1 Initial concentrations of components in the seven data sets. X, S, and P represent biomass, lactose and lactic acid respectively.

Component (g/L)	1 (2X,S,P)	2 (X,S,P)	3 (X,S,highP)	4 (X,high S,P)	5 (X,S,P)	6 (X,high S, highP)	7 (1.5X, S, P)
Biomass	0.123	0.035	0.053	0.038	0.034	0.042	0.060
Lactose	40.937	40.346	38.523	43.164	40.035	44.789	40.451
Lactic acid	0.024	0.012	0.472	0.026	0.027	0.450	0.072

1.6.3.2. Data sets for pH

To train and test the neural network, seven different experiments were carried out, and pH measurements were recorded as previously discussed in Section 2.2.3.1. The initial conditions of the experiments can be found in Table 2.2. Fig. 2.3 shows the pH dynamics of the experiments. It shows the modelling challenge of cream cheese fermentation. For instance, data sets 2, 4, 5 and 7 had different initial conditions; however, their pH dynamics during the first 2 hours were similar, making the fermentation duration prediction a difficult task.

Table 2.2 Data sets used for neural network training, validation and testing.

Case	data sets for training and validating	data set for testing
A	(2,3,4,5,6,7)	1
B	(1,3,4,5,6,7)	2
C	(1,2,4,5,6,7)	3
D	(1,2,3,5,6,7)	4
E	(1,2,3,4,6,7)	5
F	(1,2,3,4,5,7)	6
G	(1,2,3,4,5,6)	7

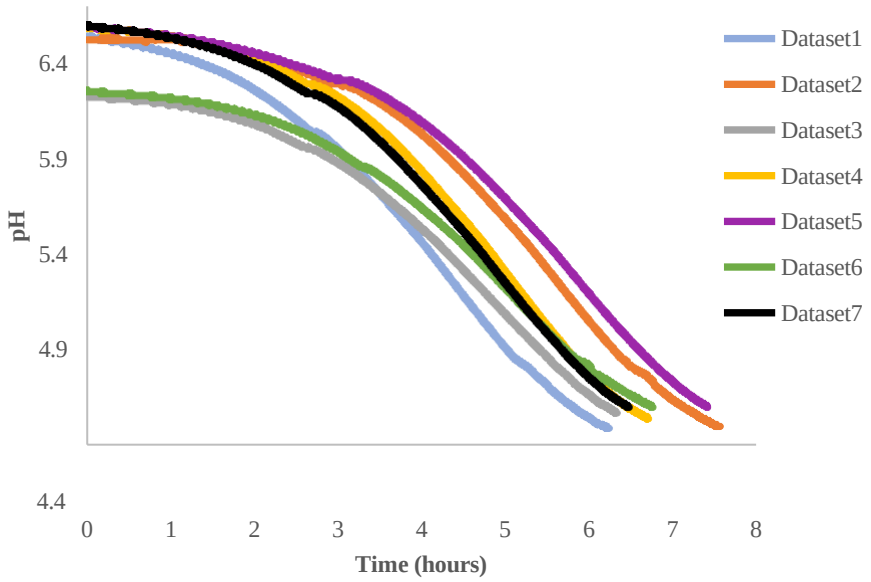

Fig. 2.3. pH dynamics for data sets

1.6.3.3. Industrial pH data

Industrial pH data of a cream cheese manufacturing unit from a Fonterra plant was also used in this work. In this process, a flow contains a mixture of homogenized milk and bacteria culture, which is used to fill up the fermentation vats. During the fermentation process, bacteria consume lactose, and the pH decreases. This process lasts until the desired pH is reached when the batch is drained to the continuous downstream processing. In order to avoid over-acidification, the curd is heated up in the cooker where bacteria are killed. A complete description of the process can be found in [118].

1.7. Results and discussion

1.7.1. White box model

The biomass, lactose, and lactic acid concentration for each data set were measured every 1.5 hours until the end of fermentation when pH reached around 4.6. The available data were separated into training and test groups. As mentioned in Section 2.2.3.1, biomass, lactose, and lactic acid concentration were measured in the first four data sets. Three sets of data were used for parameter estimation (training) and one of them for testing. Table 2.3 shows the A to D cases with estimation and test data sets. Table 2-4 summarizes the validation results via the averages of the relative errors for the different cases.

Table 2.3 Estimation and testing data sets for the four cases using the white box model.

Case	Data sets for estimation	Data set for testing
A	(1,2,3)	4
B	(1,2,4)	3
C	(1,3,4)	2
D	(2,3,4)	1

Table 2.4 White box model average percentage relative prediction errors of components.

Case	Biomass	Lactic acid	lactose
A	46.53	5.14	5.97
B	165.24	40.5	6.34
C	240	44.03	4.40
D	270.14	78.77	4.68

pH is used as an indication for stopping the fermentation in industry. Although pH is not a state of the white box model, it can be correlated to the model states, which are predicted over time. Lactic acid concentration can be used for pH calculation as showed in the following equation:

$$pH(t) = -\log_{10}\left(\left[H\right]^{+}\right) = -\log_{10}\left(\frac{p(t)}{112.8}\right) \tag{2.5}$$

The lowest error, 5.14, was obtained for case A. The concentrations of lactic acid for this case were used in Equation (2.5) to calculate the pH values. As Table 2.5 shows that pH cannot simply correlated to lactic acid concentration in cream cheese. pH measurement is complex during fermentation, as the process not only produces acid that lowers its value overtime, but also interacts with other compounds such as fats and proteins. At the same time, the undissociated lactic acid might also inhibit the fermentation. The difference between the calculated states using the white box model and the measured values (shown in Table 2.3) can also be explained.

Table 2.5 Calculated and measured pH values for case A along the fermentation.

Time	1.5 hrs	3 hrs	4.5 hrs	6 hrs
Model	2.29	2.11	1.82	1.53
Experiment	6.49	6.22	5.58	4.77

The bacteria of cream cheese fermentation is different from M17 broth, which were used to develop the model. The complex mixture of milk and cream, which happens in cream cheese

fermentation, is different from the case authors in [115] used for developing the model; hence some errors are expected.

Additionally, the model was developed in a fixed pH which is different from the cream cheese manufacturing where pH changes during the fermentation. The model includes many parameters that could change during process runs and even across different stages of the same experiment, shown for instance in [93] which considered the effect of pH on the cell growth for Lactic acid production from lactose by lactobacillus plantarum.

Moreover, it should be noted that there are many parameters involved in white box models, which usually makes the estimation problem a nonlinear optimization. The optimum points are the local minimums, which are highly dependent on the initial estimates and the constraints. Additionally, the measurements of states which are initial points for differential equations are not available online.

1.7.2. Grey box model

In [116] authors applied same data sets for evaluating the performance of their model. Their results showed that the hybrid model can give reasonable pH predictions. LSTM aimed in correlating the kinetic model states to the pH value, which is complex in cream cheese mixture. As explained in the previous section, because of the mixture complexity pH cannot be correlated to the states such as lactic acid concentration by simple correlations such as Equation (2.5).

Although this model could predict the pH value reliably, however there are many parameters involved in LSTM plus first-principle model combination. Training such a model requires big data of biomass, lactose and lactic acid concentrations along the fermentation which are difficult to be measured. Additionally, as kinetic model is used in the grey model, similar to first-principle model, providing initial measurement of states would be a challenge since they are not available online. Lactic acid and lactose measurements are available offline via HPLC and biomass measurements can be provided by cells two days after the sample has been taken.

1.7.3. Black box model

A neural network with one hidden layer and five neurons was chosen. The number of neurons was obtained after comparing the network performance using 3, 5, and 7 neurons. For example, Table 2.6 shows the summation of absolute mean error for all cases using different numbers of neurons and feedback delays. This was obtained from averaging several trials for each case. It shows that 5 neurons led to less prediction error when comparing to other numbers of neurons. Higher error of the network with 7 neurons could be due to overfitting the weights to the training and validating data sets which led to poor prediction of the testing data set consequently.

Table 2.6 Summation of pH prediction errors using different number of neurons in the hidden.

Feedback delay size	3 neurons	5 neurons	7 neurons
2	0.51	0.28	0.49
3	0.35	0.11	0.18

Fig. 2.4 represents a sample of the network training results, which shows a good fit between the neural network output and the experimental values for both training and validation cases. To achieve the best performance from the network, the effect of time step size, feedback delay size, and time series start time on the prediction by the network was studied.

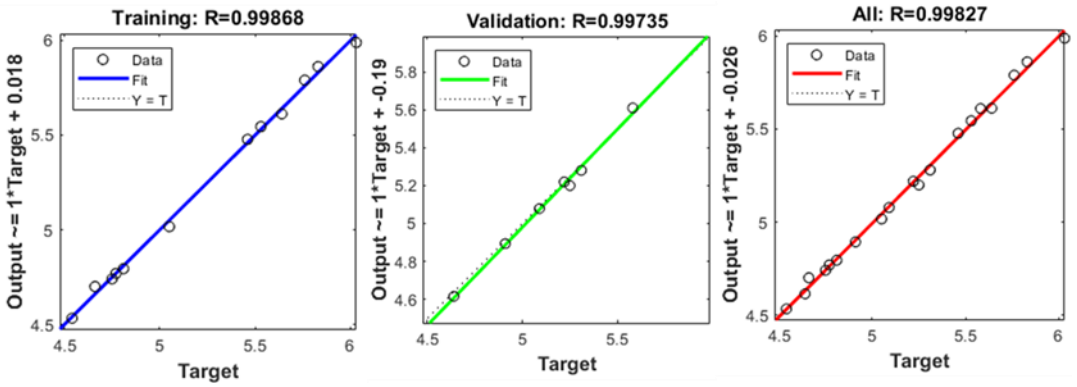

Fig. 2.4. A sample of the network training results. Output is the neural network prediction of pH, and Target is the experimental pH data.

1.7.3.1. Time step

The pH data was available every second. However, using all this data to train the network would increase the network size unduly. Additionally, this data would add more measurement error to the network and might overfit it. Three different time steps, 15, 30, and 60 minutes were chosen. To test the network performance, initial pH measurements should be provided. Measurements of the fermentation's first 60 minutes were specified. These measurements meant 5,3 and 2 data points for time series with time steps of 15, 30, and 60 minutes, respectively. Given the initial data points, the network predicted the pH dynamics until the end of fermentation. Table 2.7 shows the prediction error using different time steps. It presents the average of the absolute percentage relative error of sampling points for each case and the summation of them in total using different time steps. To have a consistent comparison, errors were calculated each hour from the second-hour data point until the end of fermentation. The total prediction error results show that the 60 minutes time step gives the best predictions in total. The network for this time step was further analysed in the following sections. It should be pointed out that higher time steps led to no improvement in the results. Additionally, high time steps could not capture the fermentation dynamics especially at the end of the fermentation which led to missing the desired pH.

Table 2.7 Percentage relative prediction errors using time steps of 15, 30 and 60 minutes.

Timestep (min)	case A	case B	case C	case D	case E	case F	case G	summation
15	5.84	3.01	2.96	5.16	3.73	2.6	1.91	25.25
30	1.93	1.58	2.26	1.4	3.7	3.36	0.37	14.60
60	1.67	2.8	1.52	0.51	4.75	1.38	0.47	13.12

1.7.3.2. Feedback delay

The feedback delay size is the number of past pH data points used to predict the next pH. These data points are the inputs to the network, as shown in Fig. 2.5 the pH (t-N) data point is the Nth past data point at time t, and N is the feedback delay size, which is also the number of inputs.

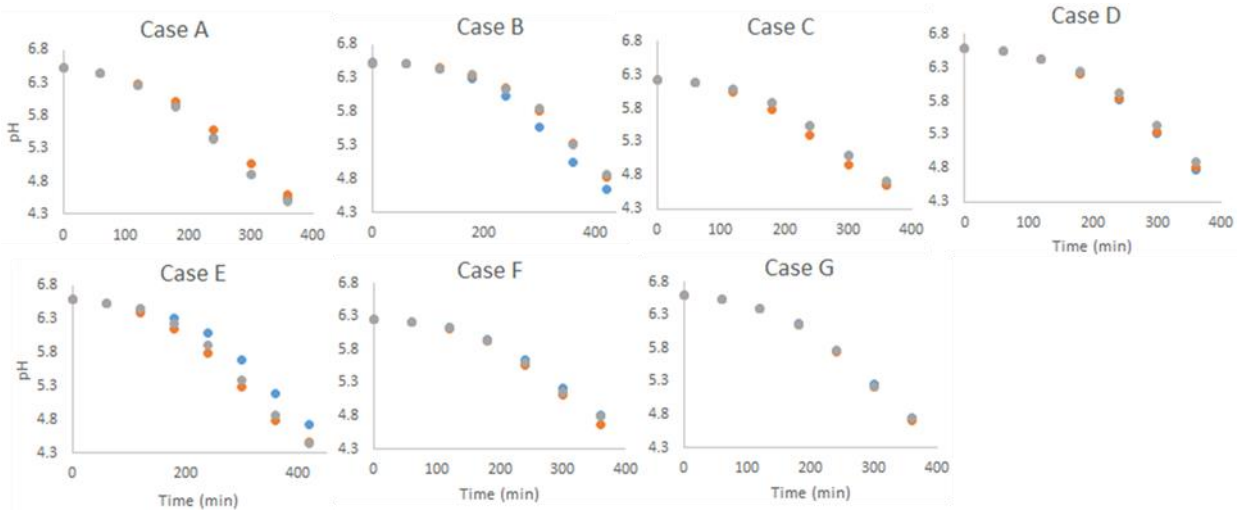

Fig. 2.5. pH versus time (min) for all cases. The blue, orange and grey lines represent the experimental data, prediction with feedback delay of sizes 2 and 3 respectively.

The network's pH prediction with a time step of 60 minutes was studied by applying feedback delay sizes, including 2 and 3 data points. Further increase of the feedback delay is equivalent to more time for providing the initial data points and running the model, which would make it impractical for batch scheduling. For feedback delay of size 2, the initial pH measurement and measurement at the first hour were given, and for the feedback of size 3, pH measurement at the second hour was also added. To have a consistent comparison, prediction errors were calculated at each hour from the third-hour data point until the end of fermentation

Table 2.8 summarizes the prediction error results. They show that the feedback delay of size 3 decreases the prediction error by approximately 4 percent.

Table 2.8 Percentage relative prediction errors using feedback delay of sizes 2 and 3 and time step of 60 minutes.

Feedback delay size	case A	case B	case C	case D	case E	case F	case G	summation
2	1.97	3.3	1.74	0.62	5.55	1.66	0.57	15.44
3	0.37	3.51	0.38	1.68	4.29	0.55	0.26	11.08

1.7.3.3. Time series start time

The fermentations' pH plots show that there are two primary behaviours in the dynamics—a slow dynamic in the first few hours, followed by a faster dynamic. To avoid the similarities of fermentation dynamics in the few first hours, the time series start time was shifted from time 0 to 60 minutes. The impact of this change was studied by a comparison between two architectures called I and II. These two architectures have 3 and 2 inputs, respectively, also different starting points. Architecture I is the feedback delay of size three, as used in the previous section. It includes data points at time 0, 60 minutes, and 120 minutes as the initial

data points. Architecture II has a feedback delay of size 2, starts from the 60 minutes data point, and its initial data points include 60 and 120 minutes data points. Table 2.9 shows the prediction error of both architectures. Architecture II reduced the prediction error, mainly due to the better predictions for cases B and E. Architecture I considers all the data from the fermentation start time where the dynamic is very slow, and the similarities between fermentations are very high. This affects the training and consequently, the prediction. Apart from data sets 3 and 6, the rest of the data sets have similar dynamics in the first hours. After that, differences between data sets 2 and 5 with the rest of fermentation increased. In architecture II, this part of the dynamics is used for prediction. Shifting or delaying the start time of the prediction helped to improve the result. For predicting data set 2 (case B), this led to the identification that data set 5 was the most similar dynamic case. The same happened for case E, where data set 2 used for training and data set 5 was predicted. This was not apparent when the prediction start time was not delayed. Lower prediction error was obtained which is shown in Fig. 2.6.

Table 2.9 Percentage relative prediction errors for architectures I and II.

Architecture	case A	case B	case C	case D	case E	case F	case G	summation
I	0.37	3.51	0.38	1.68	4.29	0.55	0.26	11.08
II	0.55	1.17	0.57	1.14	1.7	0.67	0.7	6.52

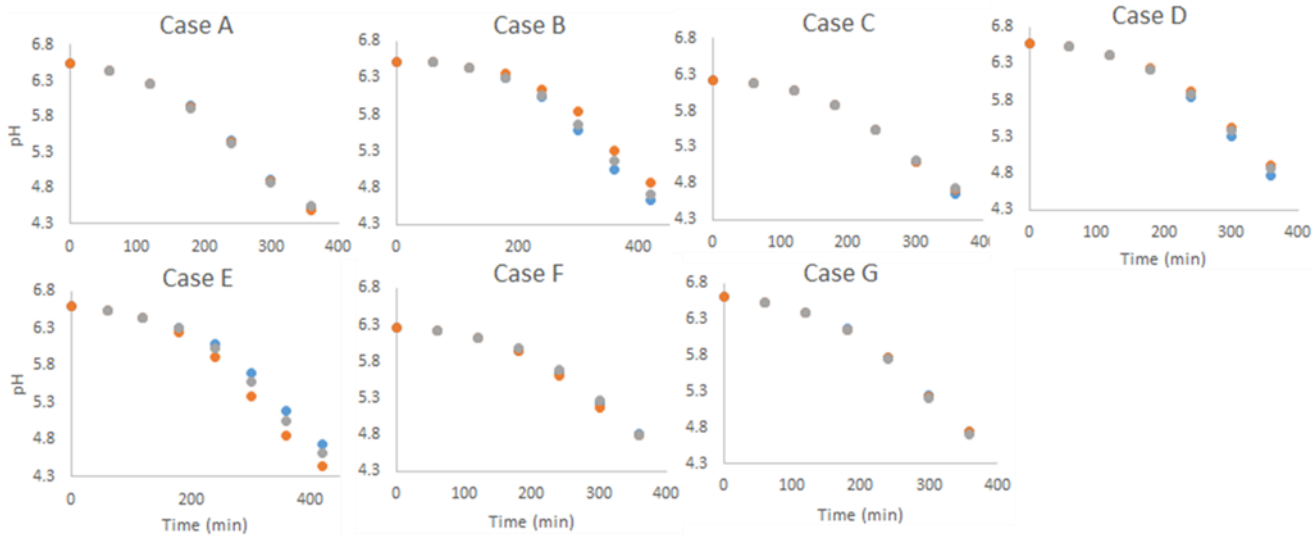

Fig. 2.6. pH versus time (min) for all cases. the blue, orange and grey lines represent the experimental data, architecture I and architecture II results respectively.

1.7.3.4. Industrial pH prediction

As discussed in sections 2.3.1 and 2.3.2, applying white and grey box models is challenging in industrial cases. However, pH is measured online and also can be manually sampled from vats. The accuracy of the network prediction in section 2.3.3 was high, and it was applied to industrial fermentations, as presented in this section. A set of 50 fermentations was selected from industrial data in which 70% of data used for training (35 fermentations), 15% for validating (8 fermentations) and 15% for testing (8 fermentations) the network performance. A network of 1 hidden layer with ten neurons was used. The feedback delay of size three and a time step of 60 minutes was chosen based on sections 2.3.3.1 and 2.3.3.2. It should be noted that all the numbers in this section were normalized due to confidentiality of industrial data. Fig. 2.7 shows the prediction of the network. Qualitatively, the models appear to predict the pH curves well, particularly their endpoints. Apart from fermentation run 4 the prediction model dynamics are slightly faster than those of the plant, especially for fermentation test run 2 and 1, 5, and 8. Quantitatively, Table 2.10 shows the relative prediction errors as percentages for all 8 fermentation test runs. The average of network percentage relative error is less than 14%, and only fermentation 2 has a large error of 34.09%. However, as the results show, the pH prediction at the final point matches the experimental data in all the test fermentations (Table 2.11) which can be due to the similarities between fermentations dynamic at the end of batches.

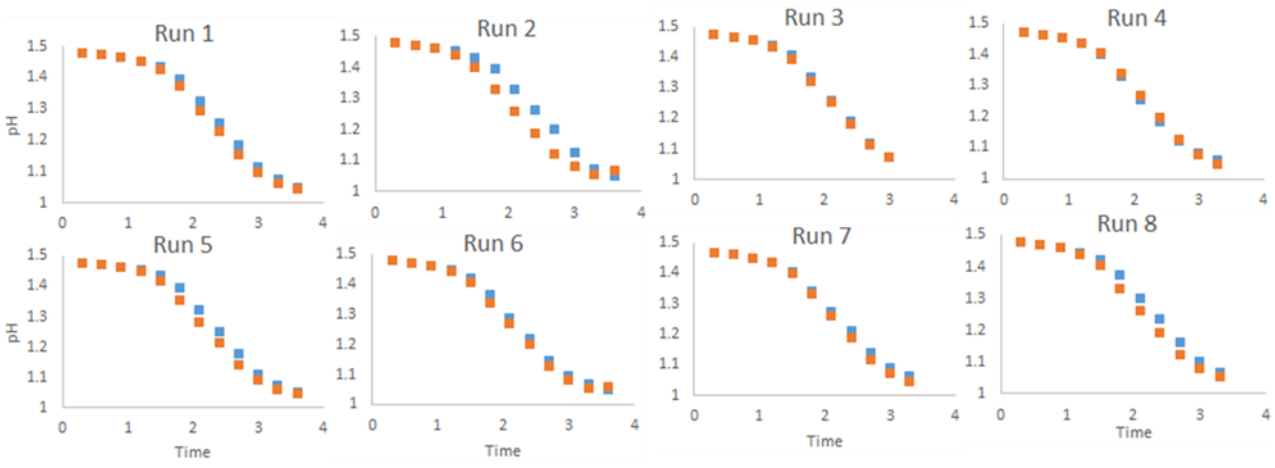

Fig. 2.7. pH versus time (hours) for all fermentations, blue and orange lines represent experimental and prediction data respectively.

Table 2.10 Percentage relative prediction errors for fermentations.

Fermentation test	1	2	3	4	5	6	7	8
Error (%)	12	34	5.4	3.7	17.3	11.5	8.8	18.1

Table 2.11 Percentage relative prediction error at the final data point for fermentations.

Fermentation test	1	2	3	4	5	6	7	8
Error (%)	0.5	1.8	0.2	1	0.2	0.9	1.5	1

This is important because it shows that the fermentation dynamics in the first hours can be linked to the pH at the end of fermentation, which strongly affects the quality of the final product. Therefore, applying such a model for scheduling purposes can increase the throughput and quality of the final product.

1.8. Conclusion

In this work, an investigation was carried out on developing a model for predicting the pH dynamics of cream cheese fermentations at both lab and industrial scales. To consider the effect of disturbances on the model performance, different concentrations of milk components and bacteria were added to the fermentation. The data was used for studying different types of models. A black box ANN model was developed and compared with white and grey box models. Results showed that applying white box model is challenging for cream cheese fermentation since the complex mechanisms involved in the cream cheese fermentation need many parameters, which could change along with the fermentation and also pH cannot be simply correlated to the model states such as lactic acid concentration. The grey box model solved the pH calculation issue by correlating the kinetic model states to the pH. However, as

both white and grey box models use kinetic models; they require a considerable amount of data not available online and challenging to measure. Unlike the white and grey box models, the black box model (an ANN model) was developed using the pH data measured online, which also can be measured manually by operators. Therefore, the large amount of data needed for training the ANN model can be found. Lab- scale data was also employed to help in determining the feedback delay size and proper time step for the ANN model. The configuration obtained was then applied to industrial cases, which illustrated the reliable performance of the model.

CHAPTER 3

Cream cheese fermentation scheduling

Foreword

Maintaining high throughput with consistent quality is challenging in industrial cream cheese plants since batch fermentation time varies. However, determining the batch duration right from the batch start time is challenging. This makes the scheduling of this plant difficult. The characteristics of the plant, the main process challenges, and the resulting framework, which included adaptive modelling and scheduling, are presented. This chapter has been accepted in the International Congress of *Process System Engineering* in Kyoto, Japan and has been included in the thesis.

1.9. Introduction

Fermentation batches are challenging to schedule due to the high inherent biological variability. Batch fermentations are common in various industries such as food, chemical, and pharmaceutical processing; therefore, much work has been carried out to schedule such systems. In [119], the authors worked on scheduling a copper plant. Raw materials variation affected the reaction time, which made the plant operation challenging. Reaction modelling with raw material changes was used in a mixed-integer formulation for scheduling of the overall production process. Scheduling of penicillin fermentation was studied in [52]. However, the authors did not consider the batch variation, and a nominal batch processing time was used in their scheduling formulation. A scheduling solution was presented for a beverage plant in the brewing industry in [53]. They use a constant fermentation time which is much longer than the mean values for the scheduling time, however the fermentation time variation was not addressed. Their schedule significantly reduced the process throughput. Additionally, the fermentation liquid product could be stored in tanks for several days.

In cream cheese plants the variation of batch duration affects the downstream continuous production rate and quality. Furthermore, the fermentation curds cannot be stored for a long time since over acidification degrades the quality. To avoid batch interferences during cooking, engineers in industry set up the fermentation scheduling with a long buffer time between two fermentation vats. This assures quality; however, the production rate is reduced significantly. Better scheduling of batches can decrease their variation by reducing possible interferences between batches due to variations of their duration. A new framework is presented in this work that provides a primary schedule with updating each batch durations predicted by a fermentation model at each time step. This schedule was updated in real-time by using an

adaptive model that predicted the batch duration along with the fermentation when enough measurements were available. A mixed-integer linear (MILP) programming optimization was formulated for real-time scheduling of the vats filling and draining. The constraints of the plant regarding the filling, draining, and cleaning of the vats were considered. The best configuration for scheduling was determined to minimize the cost and waste and improve the continuous operation of the plant.

1.10. Methodology

1.10.1. pH prediction model

In Chapter 2, the application of white, black, and grey box models for cream cheese pH prediction was studied. A reliable pH prediction model was achieved by applying neural networks to pH dynamics. Additionally, a grey box model developed by [116] was discussed. Further improvements of the grey box model prediction by introducing online measurements are introduced as follows.

An updated version of the model presented in [116] is presented in this work. The model maps the biomass, lactose and lactate concentration to pH.

The main drawback of the hybrid model is that biomass concentration measurements will be available only two days after the sampling. Unlike biomass concentration, lactose and lactate concentrations can be measured online during the fermentation process. Also, the lactate and lactose concentration measurements are more reliable than biomass concentration measurement. For these reasons, in the parameter estimation of the white box model, higher weights were considered for lactate and lactose measurements. As shown in Fig. 3.1, the initially measured biomass (X_0), lactate and lactose (P_0 and S_0) concentrations at initial point are used as inputs to the kinetic model. The simulated outputs are the inputs to the LSTM model. When new measurements of lactate and lactose are available (P_m and S_m), the kinetic model is simulated from that point, and the outputs of the kinetic model are used as the inputs to LSTM. This approach reconciles the states using the measured data and can reduce the deviations of the outputs coming from disturbances in the system.

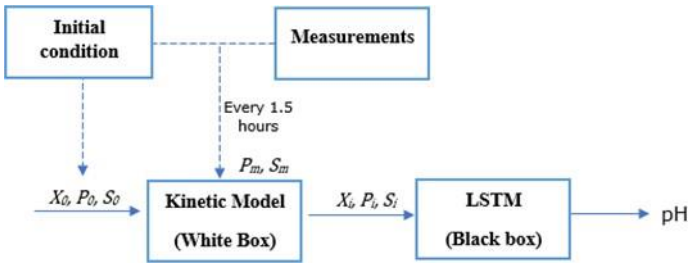

Fig. 3.1. Updating the grey model using the measurements.

1.10.1.1. Data sets

Cream cheese fermentation is affected by various disturbances. Milk composition is one of the significant disturbances which varies across different farms and seasons of the year. Additionally, bacteria's activity is an unpredictable and uncontrollable variable that affects the lactic acid production and, consequently, the pH dynamics. Details of the experiments can be found in Chapter 2. Table 3.1 shows the initial concentration of different components in g/L.

Table 3.1 Initial concentrations of components in the seven data sets. *X*, *S*, and *P* represent biomass, lactose and lactic acid respectively.

Component (g/L)	1 (X,S,P)	2 (2X,S,P)	3 (X,highS,P)	4 (X,S,highP)	5 (X,highS,highP)	6 (X,S,P)	7 (1.5X,S,P)
Biomass	0.035	0.123	0.038	0.053	0.042	0.034	0.06
Lactose	40.346	40.937	43.146	38.523	44.789	40.035	40.451
Lactate	0.012	0.024	0.026	0.472	0.45	0.027	0.072

Table 3.2 Datasets used for hybrid model training, validation and testing

Case	Datasets for hybrid model training and validation	Datasets for testing
A	(1,3,4,5,6,7)	2
B	(1,2,4,5,6,7)	3
C	(1,2,3,5,6,7)	4

Biomass, lactate and lactose concentrations were measured along with pH data for these seven. experiments. Table 3.2 shows the defined cases used for training and testing the hybrid

model. It should be noted that dataset 1 was used only for training as the pH dynamics was significantly different from other data sets.

1.10.2. Scheduling framework

As Fig. 3.2 shows, the downstream and upstream units connected to vats are ideally in continuous operation. The objective is to schedule vats to maintain continuous operation while considering filling, draining, and cleaning constraints, and varying batch duration. As shown in the figure, only one vat can be drained or filled at any time due to the draining and filling line architecture. Both filling and draining take 2 hours. After reaching the desired pH, batches should be cooked immediately to stop the fermentation. If one batch's pH reaches the desired value and the draining line is used by another vat, the batch can be cooled in the buffer tank and drained later. However, this will cause more energy consumption and extra cost for the plant. Therefore, interference between batches, as explained in the above example, should be avoided. These are two significant constraints that are considered in the optimization formulation. After the batch is drained, it should be cleaned for future usage. Dairy plants use the Cleaning in Place (CIP) term for cleaning. The CIP time also varies since it is monitored online and can be stopped based on CIP measurements. For this study we used a constant CIP value that was suggested by the plant.

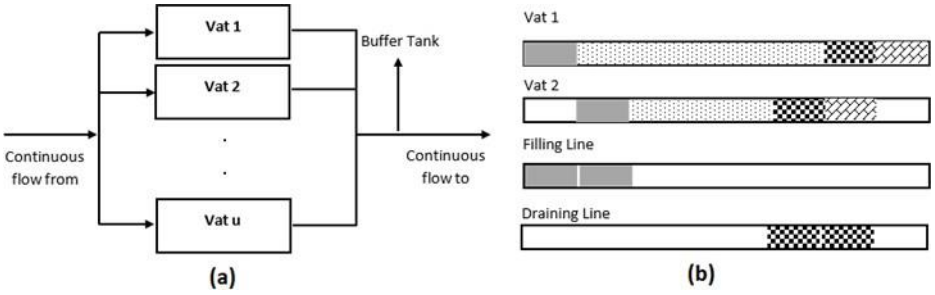

Fig. 3.2. Process flow diagram (a). Unit operation details (b). Vat filling is shown by ■. Vat draining is shown by patterns ▚. CIP is shown by ▨. This is the ideal scenario. Fermentation time in vats is shown by ▒.

The batch duration (the time required to reach the desired pH from the beginning of the batch) varies due to disturbances such as milk components changing from season to season due to cow nutrition and weather conditions. This makes the scheduling of vats a challenging task.

A mixed-integer optimization has been applied for solving this scheduling problem. The scheduling routine is shown in Fig. 3.3. When all vats are available, scheduling is carried out for all of them. The key problem is what batch duration time should we use? As mentioned before, batch duration varies. To deal with this problem, a default value is used first as the initial batch duration. The default value can be defined by engineers based on historical batch duration data. Different default values may impact the scheduling performance. Therefore, three default values, 12, 13 and 14 (hours), are investigated in this paper. After filling up the first batch, measurements from the batch beginning up to a specific time can be used in the pH prediction model to estimate the time for reaching the desired pH. This is important in the plant as the desired pH should be obtained at the end of batch draining, affecting the quality of the end-product. The updated batch duration will be used to reschedule the batches. Rescheduling will be repeated whenever enough data is available for determining the duration for each batch. The time needed to collect enough data for the pH prediction model and predict the actual batch duration can consequently affect the scheduling performance. The optimal estimate of the initial value of the batch duration is determined by evaluating the scheduling performance discussed in section 3.3.

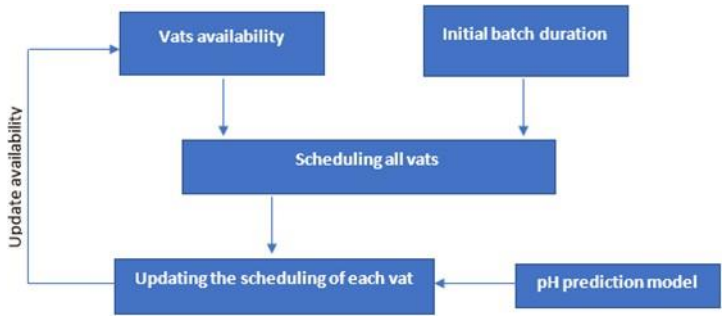

Fig. 3.3. Scheduling framework

1.10.2.1. Scheduling formulation

The operating conditions of the batch units were defined by two variables $W_{u,t}$ and $Y_{u,t}$ as shown in Table 3.3. The processing (fermentation) duration was defined between filling start time and the end of CIP. Variables $B_{u,t}$, $E_{u,t}$, $F_{u,t}$, $D_{u,t}$ and $G_{u,t}$ were used for distinguishing different occasions. The formulation and the details of the variables are given below.

$$C_{u,t} = C_{u,t-1} + W_{u,t} \qquad \forall u \in U, \forall t \in T : t > t_0 \tag{3.1}$$

$$C_{u,tt} - C_{u,t} \le (T_F - T_0)(1 - B_{u,t}) \qquad \forall u \in U, \forall t \in T, \forall tt \in (t+1)...\min(t + P_u - 1, T_F) \tag{3.2}$$

$$C_{u,t} - C_{u,t-P_u} \geq 1 \qquad \forall u \in U, \forall t \in T : \forall t \geq T_0 + P_u \qquad (3.3)$$

$$W_{u,t} + Y_{u,t} \geq 1 \qquad \forall u \in U, \forall t \in T \qquad (3.4)$$

$$Y_{u,t-1} - W_{u,t} \leq Y_{u,t} \leq Y_{u,t-1} + W_{u,t} \qquad \forall u \in U, \forall t \in T : t > t_0 \qquad (3.5)$$

$$W_{u,t} - Y_{u,t-1} \leq B_{u,t} \leq \frac{W_{u,t} + Y_{u,t}}{2} \qquad \forall u \in U, \forall t \in T \qquad (3.6)$$

$$F_{u,t+t_{FD}} = B_{u,t} \qquad \forall u \in U, \forall t \in T \qquad (3.7)$$

$$E_{u,t_{BD}} = B_{u,t} \qquad \forall u \in U, \forall t \in T \qquad (3.8)$$

$$D_{u,t_{DD}} = E_{u,t} \qquad \forall u \in U, \forall t \in T \qquad (3.9)$$

$$G_{u,t_{CIPD}} = D_{u,t} \qquad \forall u \in U, \forall t \in T \qquad (3.10)$$

$$\sum_{u=1}^{U} (B_{u,t} + F_{u,t}) = 1 \qquad \forall u \in U, \forall t \in T \qquad (3.11)$$

$$\sum_{u=1}^{U} (E_{u,t} + D_{u,t}) = 1 \qquad \forall u \in U, \forall t \in T \qquad (3.12)$$

T_0: start of the solution horizon

T_F: end of the solution horizon

u : batch unit number

t : time at any instant

P_u: batch duration for batch unit u in U

$B_{u,t}$ = 1: if batch unit starts filling a batch u at time t, 0 otherwise (Boolean variable)

U : domain of batch units 1…number of batch units

T : total time horizon from T_0 to T_F

$F_{u,t}$ = 1: if batch unit starts filling a batch u at time t, 0 otherwise (Boolean variable)

$E_{u,t}$ = 1: if batch unit starts filling a batch u at time t, 0 otherwise (Boolean variable)

$G_{u,t}$ = 1: if batch unit starts filling a batch u at time t, 0 otherwise (Boolean variable)

$C_{u,t}$ = 1: if batch unit starts filling a batch u at time t , 0 otherwise (Boolean variable)

$D_{u,t}$ = 1: if batch unit starts filling a batch u at time t, 0 otherwise (Boolean variable)

Equation's explanation:

Equation (3.1): At any time, *t*, if a batch starts on a batch unit, *u*, or the unit is idle, a counter is incremented

Equations (3.2)-(3.3): Batch cycles times must be longer than the specified value

Equations (3.4)-(3.6): Boolean relationships for ensuring the feasibility (Table 3.3 condition)

Equation (3.7): Batch filling time duration specification; t_{FD} is the filling duration

Equation (3.8): Batch complete time (from start time to reaching the desired pH)

Equation (3.9): Batch draining time duration specification; t_{DD} is the draining duration

Equation (3.10): Batch cleaning time duration specification; t_{CIPD} is the cleaning duration

Equation (3.11): Batches filling constraint; only one vat can be filled at any time

Equation (3.12): Batches draining constraint; only one vat can be drained at any time

The objective function maximizes the started vats which is equivalent to maximizing *Y* and *W* for all *u* vats at any time *t*.

$$MAX \qquad \sum_{u=1}^{U}\sum_{t=T_0}^{T_F} W_{u,t} + Y_{u,t} \tag{3.13}$$

Table 3.3 Operating condition of a batch unit

Variable	Start filling a batch	Processing a batch	Unit is idle	Infeasible
$W_{u,t}$	1	0	1	0
$Y_{u,t}$	1	1	0	0

1.11. Results

The batch duration varies in the industrial case due to disturbances such as milk composition variation and bacteria activity. Since the batch duration cannot be predicted at the

beginning of the batch, a default initial batch duration was assumed to schedule the vats. Three default batch durations (12, 13 and 14 hours) were selected for testing the impact of default batch duration on the scheduling performance. As soon as enough data was measured, the scheduling would be updated by the predicted fermentation time from the pH prediction model discussed in section 3.1.1. The effect of updating time on the scheduling was tested by considering the pH prediction model output availability 5 and 8 hours after the batch start time.

1.11.1. pH prediction model

A LSTM network in MATLAB was used. The network has two layers, and the inputs are biomass, lactose, and lactate concentrations which are the kinetic model outputs, with data frequency of ten minutes. The network training and hyper parameters values are provided in [116].

The initial biomass concentration and lactose and lactate initial concentrations were used as inputs to run the kinetic model. The lactose and lactate concentrations measurements at 1.5, 3, and 4.5 hours after the batch start time were used to reconcile the predicted states by the kinetic model. Fig. 3.4 (b,c) does not show a significant difference by using the measurements along the batch process. The end-point pH prediction error was -2.41% and -2.14 % for cases B and C. This is since almost similar initial conditions were seen during the training of network which helped the network extrapolation.

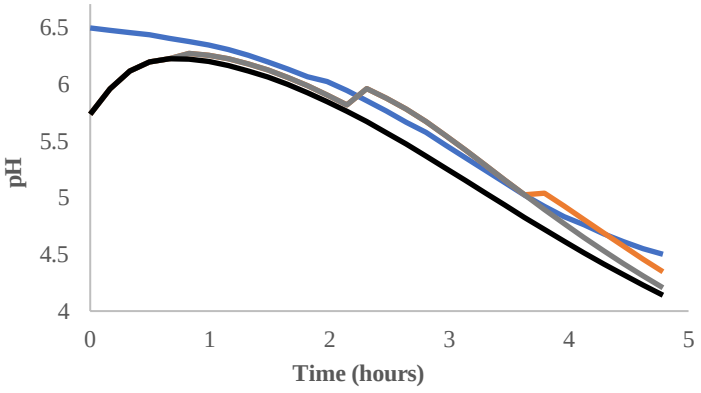

(a)

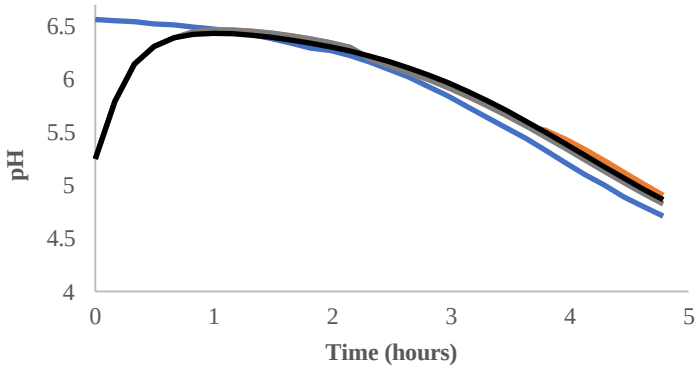

(b)

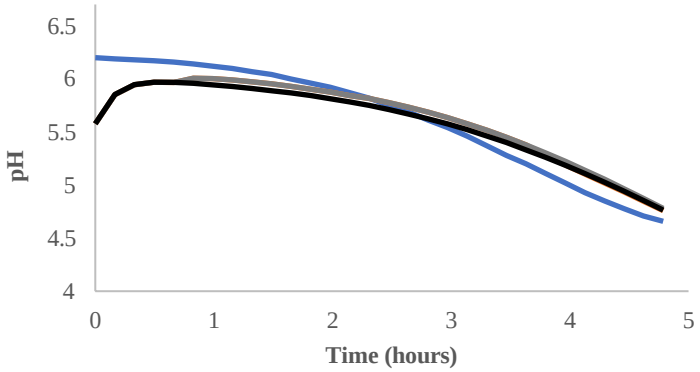

(c)

Fig. 3.4. pH prediction using the estimated initial biomass and measurements. The blue line represents the measured pH. Black represents the prediction only with the initial measurements. Grey is the prediction using the first and second online measurements, and orange is the prediction using the first, second and third online measurements

Fig. 3.4 (a) also shows the predictions for case A. The circles show the improvement in prediction by introducing the lactose and lactate measurements after the batch start time. Table 3.4 shows that by introducing more measurements, the end-point prediction improves. In case A, the testing data set has the highest amount of initial biomass, making the pH dynamics faster than the other data sets.

Table 3.4 pH prediction using measurements for case A

Number of online Measurements	Relative error (%)
1	8.01
2	6.55
3	3.42

This initial condition was different from other data sets. As similar pH dynamics were not seen during the parameter estimation and training of the network, initial biomass estimation and pH prediction were more challenging than the other cases.

1.11.2. Industrial scale scheduling

Batch duration data from a real cream cheese plant was used for testing the scheduling framework performance. The duration times of 20 batches in the sequence were used, which took approximately 70 operating hours in the plant. As shown Fig. 3.3, when all the vats are available, scheduling was carried out for all the vats.

As mentioned in previous sections, the batch duration cannot be determined before batches start. The initial batch duration in the scheduling algorithm was assumed to be a fixed value at the beginning of all batches run. For obtaining the best initial value, scheduling was applied to the industrial batch duration data. Scheduling was carried out by considering the default batch duration as 12, 13, and 14 hours. The initial batch duration was updated by the predictions from the pH prediction model. The pH model prediction output was assumed to be available 8 hours after the batch start time. The updated batch duration was used to update the scheduling of the vats.

Table 3.5 summarizes the scheduling results with different initial batch durations for five vats. The performance of the scheduling framework was studied by comparing three indicators - idle time, number of cooled batches, and number of waste batches. Idle time is the summation of hours in which the draining line is not in operation. This time should be minimized in the plant as continuous operation and consequently high throughput is desired. The number of cooled batches represents the draining interference of two batches when one is cooled and drained later. Wasted batches happen when more than two batches draining coincidence happens. One of the batches can be cooled at such a time, but the other one is wasted.

Table 3.5 Scheduling results with different initial default batch duration

Batch duration	Idle time (h)	Cooled batches	Wasted batches
12	22	3	1
13	20	4	1
14	24	4	2

Table 3.6 Scheduling results with different update availability

Update availability	Idle time	Cooled batches	Wasted batches
At 5 h	17	2	0
At 8 h	22	3	1

Table 3.5 shows that the 12 hours initial batch duration led to less cooled and wasted batches. This means that more energy and money are saved in the plant. However, the draining line idle time is more than 13 hours batch duration. The selection between the initial batch duration options should be made based on the plant's production, economic, and quality objectives. Without rescheduling, the idle time, number of cooled and wasted batches were 24 h, 4 and 3 respectively which shows the importance of rescheduling in improving the performance.

Fig. 3.5 shows an example of the scheduling framework performance for the five vats with an initial batch duration of 12 hours. The top part of the figure indicates the results for an initial batch duration of 12 hours for all vats at the batch start time. The scheduling update was carried out after determining the batch duration by pH prediction model. The bottom part of the figure shows the actual batch duration. The vat filling time was updated after time step 13 according to the actual batch duration determined by the pH prediction model.

Scheduling performance can be improved by providing the batch duration prediction earlier. This has been studied by providing the batch predictions 5 and 8 hours after the batches start scheduling with the initial batch duration estimate of 12 hours. Table 3.6 shows that the earlier update of the scheduling using the pH prediction model outputs can decrease the idle time, and the number of cooled and wasted batches. This will improve the scheduling performance in terms of energy, economy, and quality.

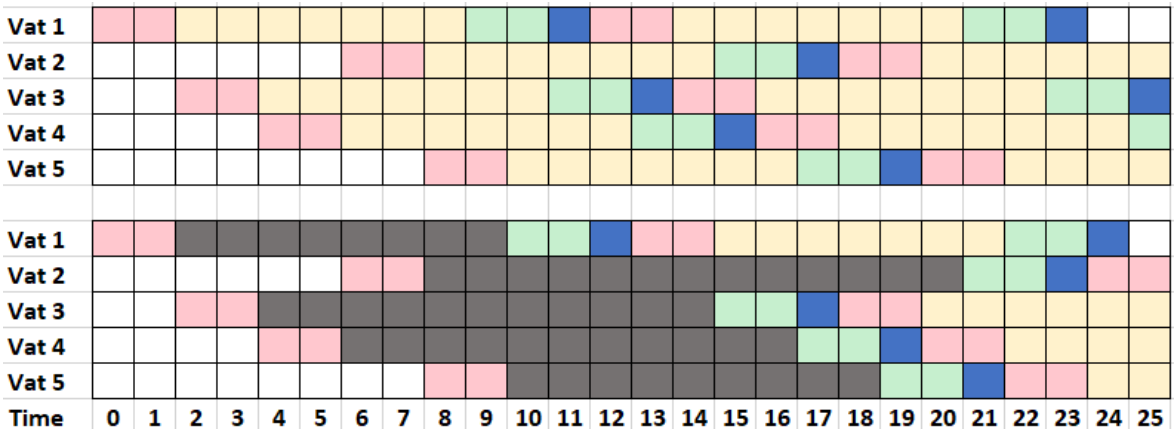

Fig. 3.5. Scheduling of vats before (top) and after (bottom) the update. Yellow colour is the initial batch duration, black colour is the actual batch duration, pink colour is the filling, green colour is draining, blue colour is CIP.

1.12. Conclusion

Scheduling cream cheese fermentation is challenging since batch duration varies. This work presented a scheduling framework that included an online pH prediction model along with MILP formulation. Online lactose and lactate measurements improved the pH prediction, which was achieved by reconciling the states. The formulation used the model output to reschedule the primary schedule, which was obtained by assuming a default initial batch duration. The framework performance was tested by scheduling 20 batches in sequence. Results showed that using 12 h as the default initial batch duration with batch prediction updating 5 hours after the fermentation started led to the minimum wasted and cooled batches.

CHAPTER 4

Economical design optimisation of a phase change material active system equipped with a solar collector

Foreword

Coupling solar air collectors and active systems of phase change materials is an efficient approach for improving building heating supply. Through design optimization, such a system can become economical and energy-efficient in different climates and for different types of buildings. However, previous works have not paid much attention to the economic feasibility of such systems during designing. In this paper, economical design optimization of a system including a solar collector and a PCM heat exchanger was explored. For this purpose, a model that integrated the solar collector, PCM storage, and hut dynamics was developed for the first time. The average mean square error between the measured and predicted hut temperatures over 11 days was 4 °C. The validated model was then used for the design optimization of the system for three different scenarios: office, domestic, and service, with different schedule times and comfort temperatures in the cold season of Auckland. Design optimization determined the optimum PCM amount and area of the solar collector while ensuring thermal comfort for each building by applying a corresponding control strategy. The results showed that the optimum surface area of the solar collector was the same at 1 square metre for all the scenarios; however, the optimum amounts of PCM mass for service, domestic, and office scenarios were 35 kg, 20 kg, and zero, respectively. This chapter has been submitted to *the Journal of Applied Thermal Engineering* and is under review.

1.13. Introduction

Buildings were responsible for almost 36% of energy consumption and nearly 40% of annual global greenhouse gas emissions in 2017 [120]. This is mainly due to the improvement of living standards and occupants' comfort demands, which has led to more cooling and heating in buildings [121]. Total energy consumption in the sector is expected to rise 3% annually in the foreseeable future [122].

Solar energy has been recognized as one of the reliable energy sources for supplying the global energy demand. However, solar energy is intermittent, which would cause a mismatch between the availability of the energy and the actual demand. Integrating thermal energy storage (TES) with the solar sources of heat could solve this issue. For decades, researchers have been interested in TES to reduce building energy consumption and improve thermal comfort [123]. TES can be used for storing energy in the storage medium, which can be released on demand, reducing the mismatch between supply and demand. TES can be applied

using four different methods: sensible heating, latent heat storage, thermo-chemical (reversible reactions), and physical absorption/adsorption. Latent heat storage using phase change materials (PCMs) can be applied easily and provides reasonable energy storage density at an almost constant temperature [124].

Design optimization of the systems, including solar collectors and PCM-based energy storage, can make them more economical and energy-efficient. Design optimization of such systems has been studied in different research. In [125], design optimization of heat pipe evacuated solar tube collectors with PCMs was carried out in two different modes of operation: normal and on-demand. Numerical models were used to simulate the system and determine the best design for improving the system's thermal performance. Heat pipe position in the glass tube and PCM were the design variables for enhancing the thermal energy storage of the system. An efficient and optimized PCM storage unit for a collector storage water heater system was explored in [126]. The storage unit was a multichannel flat tube and rectangular fins as heat exchanger elements. The theoretical analysis method was used for optimizing the storage unit by studying the influence of structural parameters of rectangular fins, as the design variable, on the charge/discharge process. The above research obtained the best design by analyzing the numerical models, which would not lead to the optimum solution.

Design optimization was also investigated by applying optimization algorithms for obtaining the optimum design variables. In [70] a multi-objective optimization was carried out for TES systems, including PCMs for solar air systems in a lab-scale test rig. Thermal storage design variables such as the number of the air channels and the number of PCM bricks were optimized. The optimum values increased the average heat transfer effectiveness and effective PCM charging time of the system. In [71], a two-level model-based strategy was used to optimize a system including a Photovoltaic/thermal (PVT) collector with a centralized PCM thermal energy storage. The electrical and thermal performance of the system were increased by obtaining the optimum air flow rate, and optimum slope and orientation of the PVT collector. The design of a PVT with a passive PCM was optimized in [72]. PCMs were embedded into the building envelopes, while the heated air from the PVT collector was used for heating the building. The Taguchi-Fibonacci search method was used for the optimization. The optimized variables were PCM air flow rate, PCM type, PCM layer thickness, and additional wall insulation. The objective function maximized the signal-to-noise ratio of the

coefficient of the thermal performance enhancement (CTPE) of the building simulated in TRNSYS.

In the above studies, the design optimization was focused only on improving the system's technical performance. However, ignoring the initial cost of solar collectors and PCM energy storage could lead to designing systems with long payback times, which could lead to infeasible economical systems. For instance, in [114], parametric analysis was used for designing a solar heating air system, including an air vacuum tube solar collector and a concentric-tube latent heat thermal energy storage. The design of the energy storage system was optimized regarding the air outlet temperature of the storage and peak shift of the heat supply. The results showed that the optimal mass of PCM was 150-200 kg/m^2. This amount of PCM introduces a high initial cost that leads to a very long payback time. The cost of implementing PCM is needed to be compared against the benefits of using such systems before making decisions [74]. The importance of economic factors was also mentioned in [75]. The optimal design of a solar collector integrating PCM thermal storage was carried out in this study. A front and back solar air collector (SAC) with a PCM-based absorber plate was considered. The objective function minimized the root mean square error between the solar air collector and the set temperature. The thickness of PCM in the absorber plate, the phase change temperature, and a parameter in the effective heat capacity curve were used as the optimization design variables. The objective function contained thermal performance parameters, but the authors concluded that the techno-economic constraints need to be added in future studies. The authors of [76] studied the optimal design of a renewable cooling and heating system that included a desiccant wheel, PVT, and a thermal storage unit. The objective function was a twenty-year life cycle cost which included PVT price, PCM price, electricity purchase price, and electricity sale price. The results showed that the optimized design decreased the system's life cycle cost by 32.4% and 31.2% compared to two other design cases. It was found the electricity sale price had a significant influence on the optimization results. However, the results cannot be helpful in designing solar air collectors without PV panels, which only generate heat. Economical design optimization of systems including the coupling of solar air collectors and PCM energy storage, which minimize the system cost could facilitate the deployment of such systems.

For design optimization purposes, a validated model that integrates the dynamics of the whole system, including solar collector, PCM storage, and the building, is needed. In [65], the authors numerically investigated a PCM-based cascaded energy storage unit with a solar air

collector. Three paraffin-based materials (RT50, RT65, and RT80) were used as PCM for the energy storage unit. The thermal energy storage unit and the solar collector were modeled. The model was validated by the experimental data with high accuracy (R-squared equal to 0.94). In another research, simulation of net-zero energy (NZE) was first developed using TRNSYS [66]. The authors investigated the energy flexibility and performance of NZE houses using a solar-assisted heating, ventilation, and air conditioning (HVAC) system with thermal energy storage (TES), PVT collector, and demand-side management (DSM) strategies. A simulation system of the NZE house was developed using TRNSYS to evaluate its performance under various conditions. The major components of the system, such as PVT collector and air-based PCM storage, were modeled and validated individually [67, 68]. In particular, the air-based PCM storage model was developed [68] to represent the thermal dynamics of the storage for cooling purposes in summer, using the free ambient cooling at night to solidify PCM. A novel solar thermal heater coupled with an active PCM heat storage wall was proposed in [69]. Hot water heated by the parabolic trough solar collectors was flown through the copper tube to discharge the cool load stored in the PCM wallboard. Also, the excess heat could be stored in the PCM wallboard to meet the indoor thermal demand when solar energy was insufficient. The transient model of the active PCM storage was combined with the TRNSYS model, which included the hut model. The indoor hut temperature was used to validate the accuracy of the model. The RSME during seven days of operation was 0.7^{o}C. Despite there being studies on modeling solar collectors with PCM storage, it appears that a model that integrates the solar air collector, and PCM storage, and building models has not been previously reported.

An economical design optimization was developed in this paper for the first time, for a heating system with a solar air collector and a PCM heat exchanger, supplying heat to an office-size hut. The optimization was carried out using an integrated model representing the whole system's dynamics and interactions. The model was validated by the experimental data of a winter season in Auckland, New Zealand. The validated model was controlled by applying an algorithm tested experimentally. Using the controlled virtual system, the optimum solar collector area and amount of PCM used were obtained by using the hut under different application scenarios such as office, domestic, and service. The objective function was defined by considering the energy cost saving of the system during the cold season of New Zealand, which was penalized by both the system capital and operating costs.

1.14. Methods

A hut heated by a solar collector and a PCM heat exchanger was considered in this work. The PCM heat exchanger could store diurnal solar energy for the later demand. The experimental setups and dynamic model are described in the next sections. Model validation was carried out by using two sets of experimental data from the winter of 2020.

1.14.1. Experimental set up

The setup includes an experimental hut equipped with a solar collector and a PCM heat exchanger, as shown in Fig. 4.1. It is located near Ardmore airport in Auckland (37.0314° S, 174.9724° E), New Zealand. The hut's external dimensions are 2.7 m x 2.7 m x 2.7m, and have a single-glazed window (0.8 m x 0.8 m) facing north. Polystyrene foam was used to insulate the floor, while glass wool was used to insulate the walls and ceiling.

Fig. 4.1. Experimental set up including a PCM heat exchanger (A) inside a hut equipped with a solar collector.

The hut includes fans, and control valves for directing the heated air, as shown in Fig. 4.2.

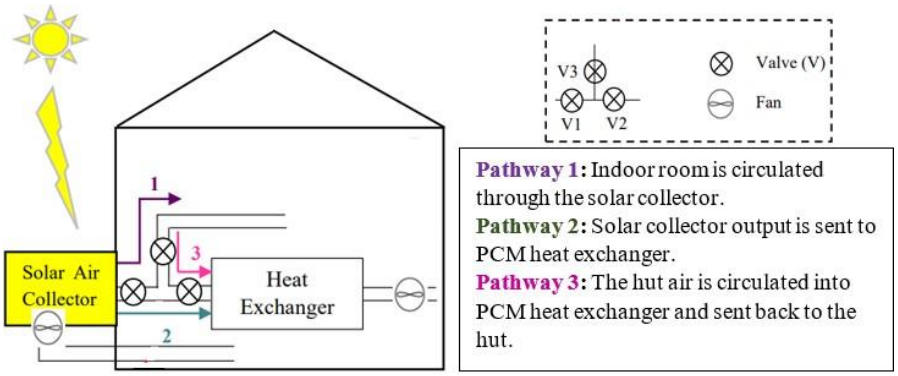

Fig. 4.2. Hut set up details. The arrows show different pathways. Air flow is adjusted by adjusting valves and fans.

The equipment's specifications can be found in Table 4.1.

Table 4.1 List of equipment used in the experimental hut.

Equipment	Description	Operating conditions	Electric power (W)
Solar air heater	1 m^2 flat plate	-	Maximum: 550
Fan	100 mm Plastic Duct Booster Inline Fan	Flowrate: 130 m^3/h	12
Valve	PVC	Fully open/fully closed	-

A PCM heat exchanger is also integrated with the solar collector in the hut. The PCM heat exchanger was made up of 19 sets of aluminum macro-encapsulated PCM panels (0.45 m x 0.30 m x 0.01 m) filled with 9.5 kg RT25HC (manufactured by Rubitherm GmbH). A side view of the heat exchanger unit is shown in Fig. 4.3. There was a 5 mm gap between the trays. Air enters the duct from one side and flows parallel to the trays, exchanging heat with the PCM in this configuration. To ensure a uniform flow, a distributor was made and installed in the pipe leading to the heat exchanger. A 20 mm layer of PVC/NBR black rubber foam was used to insulate the entire assembly from the environment (thermal conductivity of about 0.037 W/m·K). More details can be found in [127].

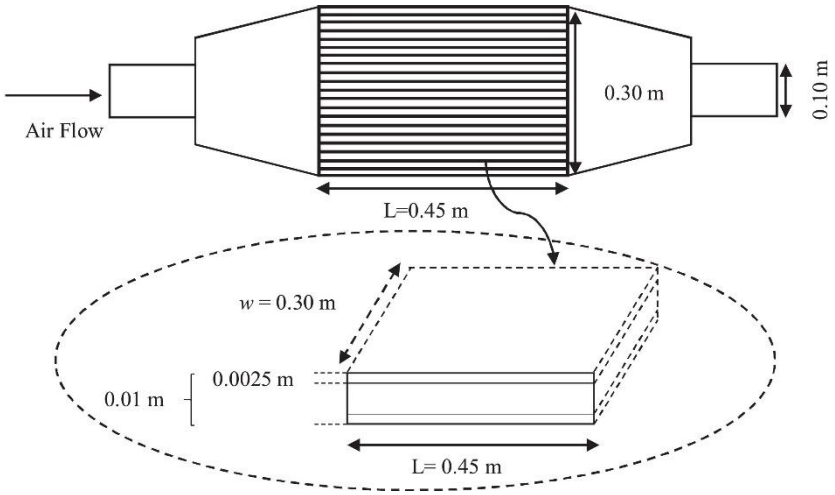

Fig. 4.3. Schematic side view of the heat exchanger unit with one magnified metal container [127].

Temperatures from the hut, solar collector, and PCM heat exchanger were fed into a temperature controller. The temperatures were measured using T-type thermocouples calibrated against a reference thermometer. The air velocity in pipes was measured using a digital anemometer. In pipes with a diameter of 10 cm, the air velocity was 3 m/s. A pyranometer was used to measure solar radiation. Table 4.2 shows the different types of measurement instruments and their accuracy.

Table 4.2 Measurement instrumentation.

Instrument	Accuracy range	Operating range	Model
Thermocouples	±0.45 ºC	0-50 ºC	T-type
Reference thermometer	0.02 ºC	0-50 ºC	Ebro TFX430
Digital anemometer	(± 2% + 0.2 m/s)	0.4-30 m/s	AM-4201
Pyranometer	<10 W/m^2	0-2000 W/m^2	VAEQ08E

The data was logged using a Compact Reconfigurable (CompactRIO) Data Acquisition System (NI Crio-9012, National Instruments, USA) and LabVIEW software. The system analog inputs received the temperatures and returned the decisions on the solar collector and PCM heat exchanger operation via analog outputs. These decisions were applied by manipulating valves and fans based on an ON/OFF control algorithm as described below.

There are three possible pathways for supplying heat, which are controlled through three valves (V1, V2, V3) shown in Fig. 4.4.

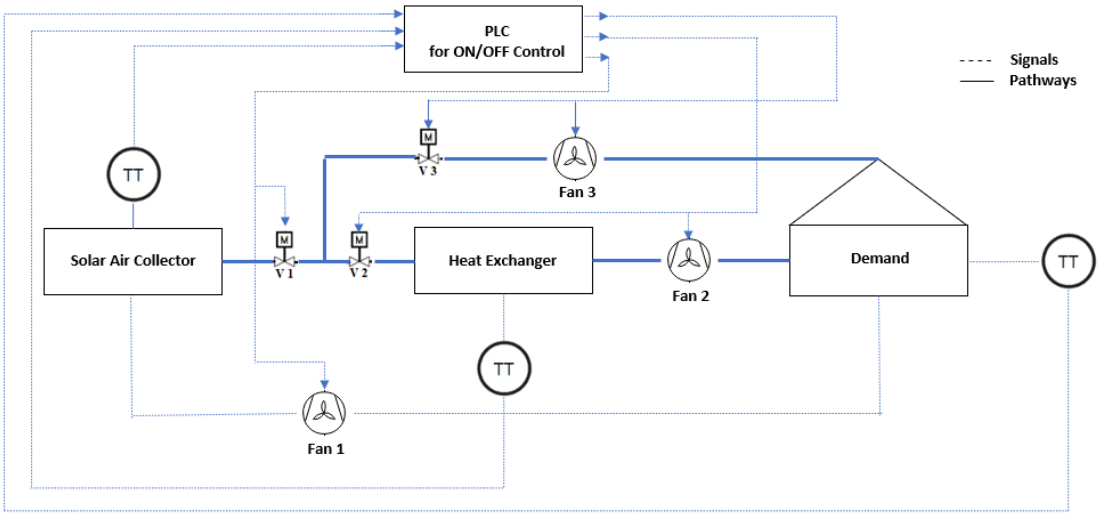

Fig. 4.4. Schematic view of the heating control. The temperatures of solar air collector, hut and heat exchanger are the inputs, and the three valves, and three fan settings are the outputs of programmable logic controller (PLC).

Pathway 1 (V1 and V3 open, V2 closed), heating the hut using solar energy: the solar collector sucks the hut air in and then sends the heated air back to the hut, using an electricity-driven fan (Fan 1 in Fig. 4.4).

Pathway 2 (V1 and V2 open, V3 closed), charging the PCM: the air heated by the solar collector is sent to the PCM heat exchanger before sending it back to the hut. This circulation was done by an electricity-driven fan, Fan 2, installed at the outlet of the PCM heat exchanger.

Pathway 3 (V2 and V3 open, V1 closed), heating the hut using PCM discharging: the hut air is circulated into the PCM heat exchanger and sent back to the hut, using the electricity-driven fan, Fan 3.

The desired lower and upper temperature bounds for the huts were set to be 19^{o}C and 25^{o}C, respectively. These desired bounds were maintained by adjusting air flow through the valve opening. If the temperature of hut was lower than the air coming from the solar collector, then the valve was opened, and the fan switched on to circulate the solar collector air to the hut and provide heating. The fan was switched off after reaching the desired upper bound (25^{o}C), and none of the pathways were used in this case. If after providing heating through Pathway 1, the hut temperature exceeded the desired upper bound, the air was circulated through Pathway 2

for melting PCM (charging). The stored heat was released later (discharging) during the cooler hours (hut temperature lower than 19^{o}C) through sucking the hut air via Pathway 3.

1.14.2. Dynamic model

Individual numerical sub-models describing system components make up the dynamic model, coded in either MATLAB or EnergyPlus software. In EnergyPlus, PCM can be defined as a layer on the building envelopes that is suitable for passive applications. Heat exchangers containing PCM materials, on the other hand, cannot be defined in EnergyPlus. To compensate for EnergyPlus's lack of flexibility in this case, the PCM heat exchanger was modelled in MATLAB and linked to EnergyPlus, via an EnergyPlus Co-simulation Toolbox interface that controlled data flow between the two software systems. The sub-models for the solar collector, heat exchanger, and hut interact together as shown in Fig. 4.5.

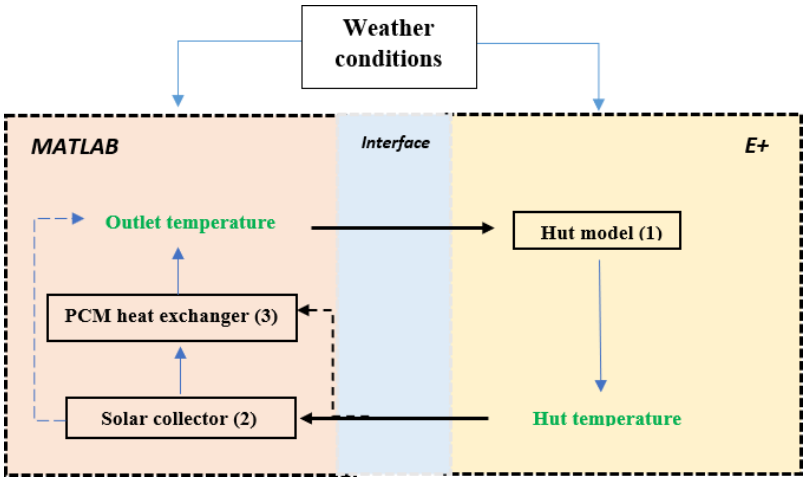

Fig. 4.5. Dynamic model structure. Dashed lines show the alternative heat supply pathways.

The models for hut, solar collector and PCM heat exchanger were named Sub-model 1, 2 and 3 respectively. The solar collector and PCM heat exchanger were modelled in MATLAB, while the hut was simulated using EnergyPlus (E+ in Fig. 4.5). Sub-model 1, 2 and 3 are fully interacted through an interface for exchanging the data between MATLAB and EnergyPlus software. In this case, the dynamic model operated under four different regimes as described below.

The first regime was when the PCM was charged, and the hut air was calculated in Sub-model 1 and passed from EnergyPlus to MATLAB via the interface. The hut temperature was introduced to Sub-model 2 along with the ambient temperature and solar radiation data. The calculated solar collector outlet temperature (blue dashed line) was sent back to the hut models in EnergyPlus through the interface code. This is the heat supply Pathway 1 described in Section 2.1.

The second regime (charging) was when the PCM was charged, and the hut air was calculated in Sub-model 1 and passed from EnergyPlus to MATLAB via the interface code. The hut temperature was introduced to Sub-model 2 along with the ambient temperature and solar radiation data. The calculated solar collector outlet temperature was the inlet to the heat exchanger. In Sub-model 3, the outlet temperature was the output which was sent back to EnergyPlus through the interface code. This cycle continued until the end of the charging phase. This is the heat supply Pathway 2 described in Section 2.1.

In the third regime (discharging), the hut air was circulated through the PCM heat exchanger to discharge the PCM without going through the solar collector. Therefore, the hut temperature determined from EnergyPlus was directly introduced to Sub-model 3 which is shown by the black dashed line in Fig. 4.5. The rest of the data flow was the same as for the charging regime. This is the heat supply Pathway 3 described in Section 2.1.

The fourth regime is when neither charging nor discharging happens. In this case, the heat supply was stopped, and the hut simulation was carried out using EnergyPlus.

The start and end times of the charging and discharging regime periods were determined from the experimental data and applied to the simulation. Due to the stability problems, the simulation time step was considered one minute.

1.14.2.1. Weather conditions

The ambient weather conditions were measured using the BRANZ [128] weather station. The measurements included dry bulb temperature, relative humidity, pressure, wind speed, solar radiation, and dew point temperature. The information was used in the weather file using the Elements software [129] which is an open source software tool for creating and editing custom weather files for building energy modeling.

Cloud cover data were recorded from the satellite information which was available on the Meteorological Service of New Zealand Ltd.'s weather forecast website [130]. As only global radiation was measured, the normal and diffuse solar radiation were calculated using cloud cover data for estimating the clearness index [131]. The sky condition was defined based on the cloud coverage data, which aimed to determine the clearness index as shown in Table 4.3. For every sky condition, a linear function correlated the opaque cloud coverage and clearness index ranges.

Table 4.3 Clearness index according to cloud cover.

Sky condition	Opaque cloud coverage	Clearness index (k_T)
Cloudy	88-100%	$k_T < 0.35$
Partially cloudy	6-87%	$k_T \geq 0.35$ and $k_T \leq 0.65$
Clear sky	0-5%	$k_T > 0.65$

Table 4.4 shows how the calculated clearness index was used to determine the fraction of the hourly radiation (I) on a horizontal plate which is diffuse (I_d) [132]. After introducing diffuse and global solar radiation, normal radiation was calculated in the Elements software.

Table 4.4 Fraction of diffuse radiation according to clearness index.

$\frac{I_d}{I}$	Clearness index (k_T)
$1 - 0.09k_T$	$k_T \leq 0.22$
$0.9511 - 0.16k_T + 4.388k_T^2 - 16.638\,k_T^3 + 12.336k_T^4$	$0.22 < k_T \leq 0.8$
0.165	$k_T > 0.8$

1.14.2.2. Solar collector model

The input to this model was the hut temperature, and the output either went to the hut (Pathway 1) or PCM heat exchanger (Pathway 2). The thermal dynamics of the collector were modeled in MATLAB using the following equation:

$$M_{SC}\frac{dh_{SC}}{dt} = F_{in}h_{in} - F_{out}h_{out} + Q_{sol} \quad (4.1)$$

Where *F* is the air mass flow rate in the collector and *M* is the solar collector mass. *h* is the enthalpy and subscripts *"sc", "in"*, and *"out"* refer to collector, collector inlet and outlet air streams respectively. These enthalpies were calculated based on the following equations:

$$h_{in} = T_{in}CP_{in} \quad (4.2)$$

$$h_{out} = T_{out}CP_{out} \quad (4.3)$$

$$h_{SC} = T_{SC}CP_{SC} \quad (4.4)$$

Where *T* is the temperature and *Cp* is the specific heat capacity. As an approximation, the collector temperature was assumed to be equal to the average inlet and outlet temperature. Q_{sol} is the heat gain from the solar radiation on the collector which was calculated by Equations (4.5) and (4.6).

$$\eta = \eta_o - p\frac{T_{in} - T_a}{G} \quad (4.5)$$

$$Q_{sol} = \eta GA \quad (4.6)$$

Where η is the efficiency of the collector and subscript *"a"* refers to the ambient temperature, *G* is the solar radiation and *A* is the collector surface area. η_0 is the intercept (maximum) efficiency and *lc* (W/m^2 ^{o}K) is the first order loss coefficient.

1.14.2.3. PCM heat exchanger

The model inputs came from the hut (Pathway 3) or the solar collector (Pathway 2). The output passed to the hut model.

A two-dimensional explicit finite difference model was used to model the heat exchanger in MATLAB [127]. Non-linear algebraic equations describing the heat transfer medias, which include PCM, metal container, and air, were solved using the finite differences method. Nodal distribution of the model is shown in Fig. 4.6. The nodal counts in the *x* and *y* directions are denoted by *i* and *j*, respectively. Δx refers to nodal discretization in *x* direction and Δy in *y* direction. *dp* and *dc* show half of PCM thickness and metal container thickness,

respectively. L is the length of the metal container in the flow direction. $T_{p,centre}$ represents PCM temperature in the center of the PCM layer in x and y directions. PCM behaviour was studied using the enthalpy method, which simplifies the heat transfer process during the phase change [133]. The enthalpy information was provided by Rubitherm GmbH [134].

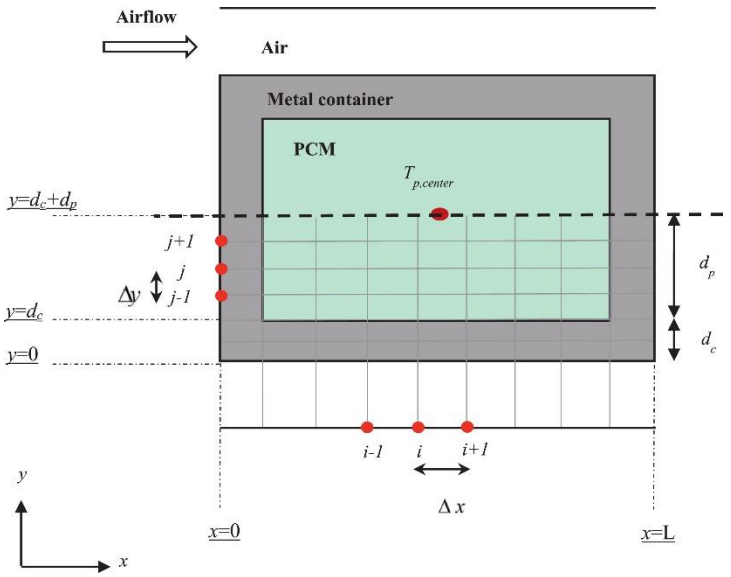

Fig. 4.6. Nodal distribution in the 2-D system of current study [127].

During the model's development, a number of assumptions were taken into account. The air between the metal containers was assumed to be distributed evenly. The heat transfer between the air and the containers was modeled in two dimensions in PCM and containers, but the airflow direction was taken into account for the heat transfer between the air and the containers. Additionally, the air density was assumed to be unchanged during the air flow in the ducts.

The advantage of this comprehensive model over previous models is the inclusion of natural convection in the melted PCM, the thermal mass of the PCM container's wall, and the effect of PCM volume expansion. The model was validated at the lab scale with a good agreement of less than 8% average deviation between the model, and experimental temperature measurements of PCM and air [127].

The inlet air flow rate and temperature were introduced to the heat exchanger model. The PCM initial temperature was measured prior to charging. In the discharging phase, the PCM initial temperature was set to be the same as the temperature reached at the end of the charging

phase.

1.14.2.4. Hut model

The model input either came from the solar collector model (Pathway 2) or the PCM heat exchanger model (Pathway 3). EnergyPlus was used to model the huts. More details about the model equations can be found in the software documentation [135]. The details of hut envelope materials and their properties were similar to the hut used in [136].

To consider the heat supply from the PCM heat exchanger, a "ZoneHVAC:IdealLoadsAirSystem" object was defined in EnergyPlus. This object's air flow rate and temperature were introduced from the PCM heat exchanger model in MATLAB to EnergyPlus via the MATLAB-E+ interface code.

Inside the hut was a heat exchanger and its connections to the solar collector, which could store heat during the day and release it during the cooler hours. This would have an impact on the hut's temperature dynamics. As a result, the mass of the equipment inside the hut was defined using EnergyPlus' "InternalMass" object.

A curtain was draped across the north side of the hut's window. This had a significant impact on heat gain from solar radiation. The "WindowMaterial:Shade" object was used to define the window shade materials' properties, which represented the radiation transmission and reflection through the curtain.

The hut is near other structures that provide shade to the outside walls. This is particularly important on the hut's east external wall, which impacts the heat gained through radiation. The sun exposure of the east external wall was defined using the "BuildingSurface:Detailed" object.

The air infiltration through the door was also added as a "ZoneInflitration:EffectiveLeakageArea" object. This model is based on Sherman and Grimsrud's work [137] which needs the effective air leakage area. The other parameters were set based on the default values in EnergyPlus.

1.14.2.5. Interface model interface

The interface exchanged data between MATLAB and EnergyPlus. On one side of the interface, the hut temperature came from the hut model in EnergyPlus, and on the other side of the interface, either the solar collector or PCM heat exchanger outlet temperature was fed to

the hut model in EnergyPlus. The interface employed between MATLAB and EnergyPlus was the EnergyPlus Co-simulation Toolbox [138]. The air temperature and air mass flow rate of the "ZoneHVAC: IdealLoadsAirSystem" object was defined as three variables exchanged between MATLAB and EnergyPlus. The exchange of these variables was built by defining "EnergyManagementSystem: Actuator" and "ExternalInterface: Actuator" objects in EnergyPlus. These two objects were linked together by programming using the "EnergyManagementSystem: program" object.

4.3. Modelling results and discussion

Two sets of data were considered for validating the model performance. The first set of data was collected from the 5th to the 10th of July 2020. During this period, the integrated model components, and individual models of the solar collector, PCM heat exchanger, and hut were compared with experimental data. To further analyse the system integrated model, validation was carried out from 13th to 17th of July 2020 by comparing the measured temperatures with those predicted by the hut models. The outside temperature and solar radiation for the first and second data sets are shown in Fig. 4.7, respectively. Solar radiation varied from early morning to late afternoon and reached a maximum of 700 (W/m^2). The lowest temperature was close to 2 ^{o}C, in data set 2, and the maximum temperature was around 18 ^{o}C.

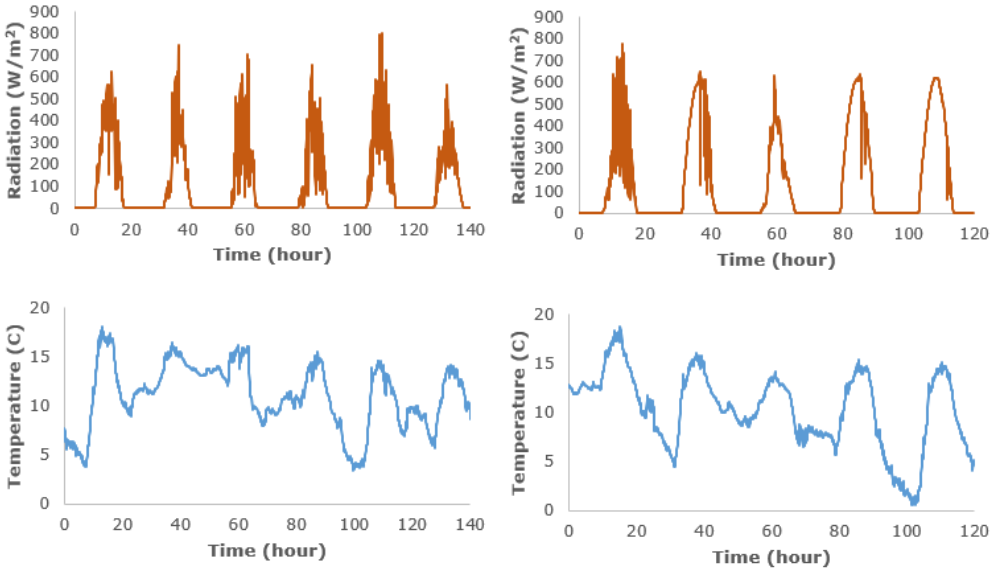

Fig. 4.7. Solar radiation and ambient temperature from the 5th to the 10th (first row) and from the 13th to the 17th (second raw) of July 2020.

4.3.1. Solar collector model

For simulating the solar collector outlet temperature, the air inlet flow rate and temperature along with solar radiation were introduced to the solar collector model. The air inlet temperature was generated from the hut simulation in EnergyPlus. The values of parameters η_0 and *lc* in Equation (4.5) were estimated as 0.42 and 2.3, respectively. These values were obtained by fitting a line to Equation (4.5), where the solar collector supplied heat was calculated by the heat transferred to the air. The solar collector validation was carried out by comparing simulation results and experimental data, which are presented for the 7th and 9th of July when the solar collector provided heat from early morning to late afternoon. Fig. 4.8 shows the comparison for the 9th of July. In fact, the collector efficiency was expected to be higher since the heat loss was not considered in the model. The heat loss was mainly in the pipeline between the hut and the collector inlet that was exposed to the ambient temperature, which could decrease the inlet temperature to the collector. The root mean square errors between the model output and the solar collector outlet temperature for the 7th and 9th of July were 2.89 ^{o}C and 2.75 ^{o}C, respectively.

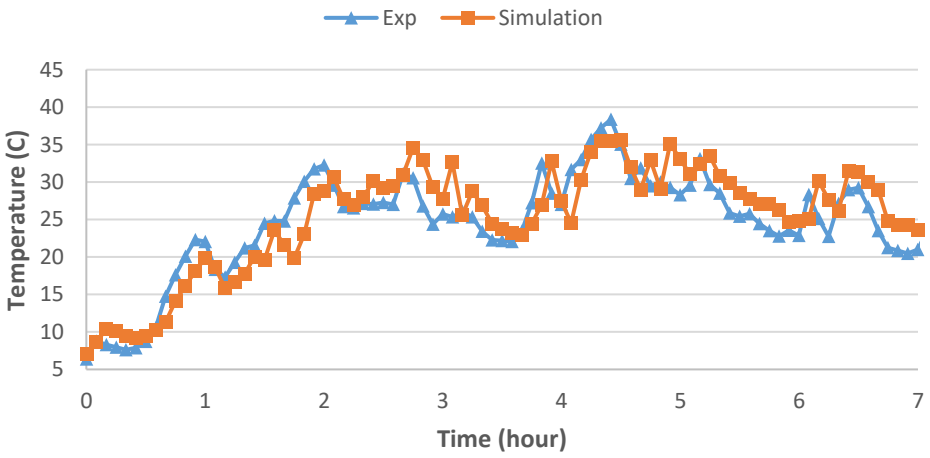

Fig. 4.8. Solar collector outlet temperature for 9th of July 2020. The root mean square errors is 2.75^{o}C.

The results show that the model can simulate the gross dynamic behaviour of the solar collector. The difference between experimental measurements and simulation results may be firstly due to the mismatch between the specified inlet air temperature obtained from EnergyPlus and the experimentally measured hut air temperature. Secondly, the solar collector was composed of different materials with different heat capacities. Considering the imprecise

thermal mass of these individual components in the model could affect the overall heat capacity of the collector and consequently its thermal dynamics, leading to the observed mismatches. This also caused a slight time lag between the measurements and simulation in Fig. 4.8. This time lag is of the order of 5-10 minutes.

4.3.2. PCM heat exchanger model

The heat exchanger model was simulated during both charging and discharging phases for hut 2. During charging, the inlet air temperature to the heat exchanger was set equal to the outlet temperature of the solar air collector, while discharging, the hut air was circulated through the exchanger. Heat exchanger simulation was carried out for 4 days from the 5th to the 8th of July. PCM was not charged for the 9th and the 10th of July since the solar heat was not enough to melt the PCM. The solar collector outlet was only introduced to the hut during these two days. Fig. 4.9 shows the simulation results for day 1.

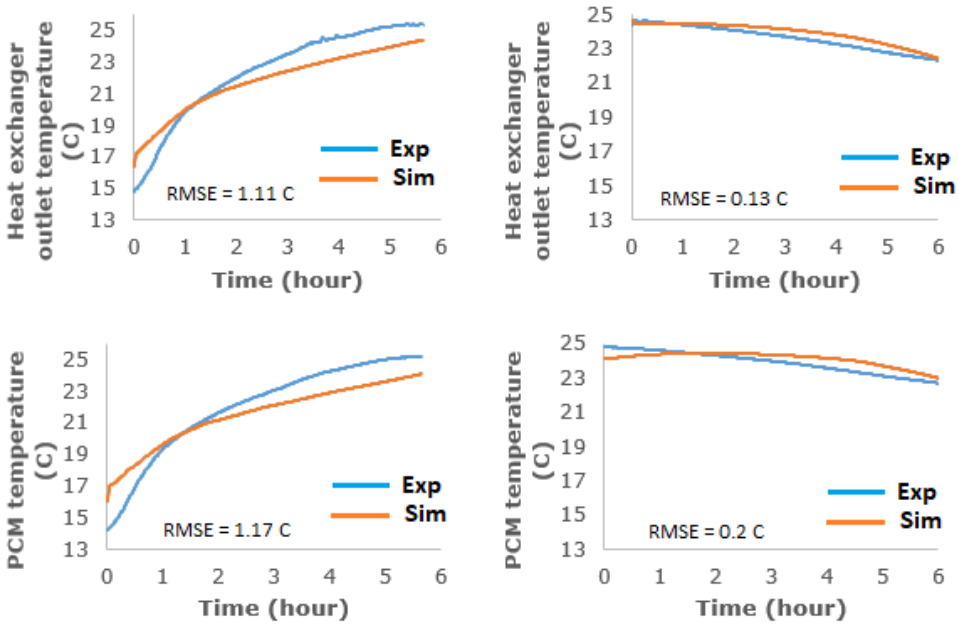

Fig. 4.9. PCM temperature and heat exchanger outlet temperature during charging (left column) and discharging (right column) phases for day 1.

Fig. 4.9 illustrates the non-linear evolution of the PCM temperature, which is mainly due to the absorbing and releasing of the latent heat during the charging and discharging phases. Fig. 4.9 shows a good agreement between the simulated and measured PCM temperature during both charging and discharging phases. The heat exchanger outlet temperature was very similar

to PCM temperature since the PCM temperature was measured at the end of the plate which was close to the heat exchanger outlet.

During the charging phase, the highest error is less than 1.5 ^{o}C, which happened in the charging phase of day 1. The root mean square error between the measured PCM temperature and the model output was 1.17 ^{o}C, the highest error (Table 4.3). Although there was a mismatch between simulation and experimental PCM temperature during charging, the PCM temperature at the end of the charging phase on day 1 was less than 1 ^{o}C. The PCM temperature at the end of the charging phase is important because it determines the amount of stored heat available during the discharging phase.

During the discharging phase, the hut air was the inlet to the heat exchanger. The highest mean square error was 1.2 ^{o}C which occurred during day 2 (Table 4.5). The difference between simulated hut temperature and the experimental data was the main reason for the mismatch between the simulated and experimental heat exchanger temperatures.

Table 4.5 Simulation root mean square error (^{o}C) for four days.

Day	PCM during charging	Heat exchanger during charging	PCM during discharging	Heat exchanger during discharging
1	1.17	1.11	0.2	0.13
2	0.18	0.13	1.21	1.17
3	0.13	0.1	0.23	0.31
4	0.008	0.85	0.013	0.12

The simulated hut temperature during days 1 and 3 was higher than the experimental temperature right from the beginning of the discharging phase (as shown in Fig. 4.9), which led to a higher inlet air temperature to the heat exchanger and consequently higher outlet temperature. During day 2, the heat exchanger outlet temperature was lower than the experimentally measured temperature since the inlet air temperature from hut 2 was lower than that measured experimentally. During day 4, however, hut air temperature was very close to the measured value which resulted in a good match between the simulated and experimental heat exchanger temperatures.

Furthermore, it should be noted that the non-uniform distribution of the air inside the exchanger could lead to non-uniform heat transfer between the exchanger surface and the air. Moreover, the PCM temperature was only measured from a plate at the end of the exchanger

which was considered the initial temperature for all plates that could have led to observed simulation errors.

4.3.3. Hut model

As described in the methodology section, the above models were coupled with the hut model of EnergyPlus through the E+ Co-simulation toolbox interface.

4.3.3.1. First data set

Fig. 4.10 shows the capability of the dynamic model in simulating the huts' temperature dynamics. The root mean square error between the huts' temperatures and the models' outputs was 1.53 ^{o}C. The maximum mismatch is around 2 ^{o}C, which happened at noon and early morning, as shown by the rectangular and circle shapes in Fig. 4.10.

4.3.3.2. Second data set

For further validation, a comparison was made between the dynamic model hut temperatures and the measured data using the second data set. Fig. 4.11 shows these results. As Fig. 4.9 shows, the hut temperature reached below the melting point of PCM (22 ^{o}C), which indicates that PCM was fully melted to provide the required heat to the hut.

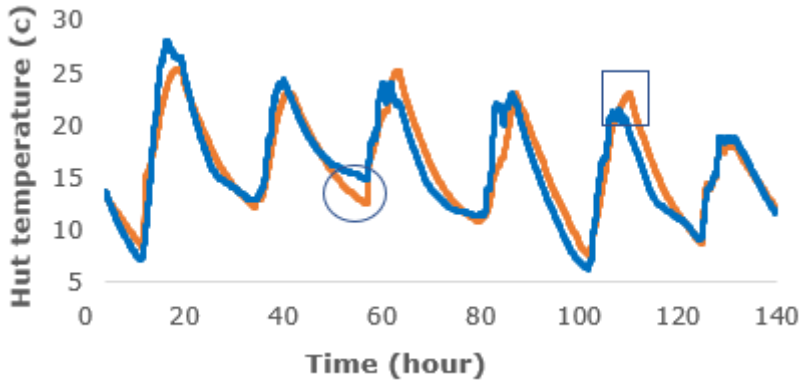

Fig. 4.10. Hut temperature from 5th to 10th of July 2020.

The root mean square error between the hut temperatures and the model outputs was 2 ^{o}C. The rectangular shapes in Fig. 4.11 show the maximum temperature difference between the simulation and experimental data, which happened at noon.

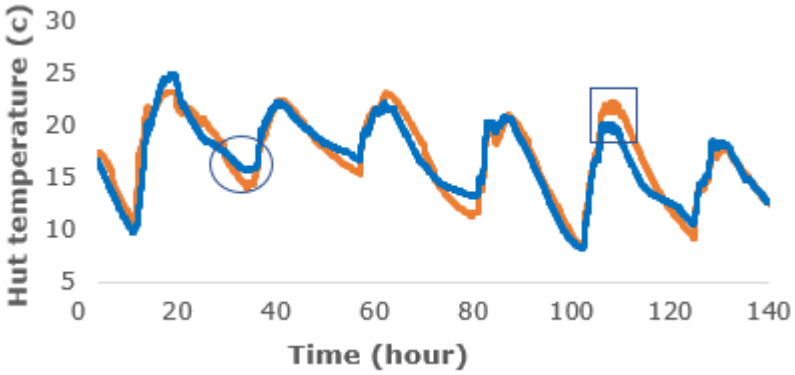

Fig. 4.11. Hut temperature from 13th to 17th of July 2020.

4.3.3.3. Discussion

In both data sets, the maximum mismatch happened during the midday and early morning. The mismatch may be due to the solar radiation and sky temperature data which are related to the cloud cover. However, the cloud cover data are not measured online but are predicted based on the satellite information, which is not updated online. Additionally, the cloud cover was used for clearness index calculation which determined the diffuse fraction of hourly radiation. The correlation between the fraction of hourly radiation, which was diffuse, and the clearness index is well established but approximate, which can be another source of mismatch.

Moreover, another reason for mismatches was the way solar radiation data are defined in EnergyPlus. This data is provided via a weather file every hour, and solar radiation is interpolated at each simulation time step. This causes differences between real and interpolated solar radiation, which is expected to contribute to the hut's error in the solar heat gain. The higher difference between the real and interpolated solar radiation happens on partially cloudy days when solar radiation changes considerably. For instance, Fig. 4.12 shows the solar radiation variation on days 13th to 15th of July. The solar radiation variation for July 15th is smoother than July 13th, which was a partially cloudy day. On July 14th, a significant change in solar radiation happened between 12 pm and 1 pm, as indicated by the orange circle in Fig. 4.12, which interpolated data cannot be represented.

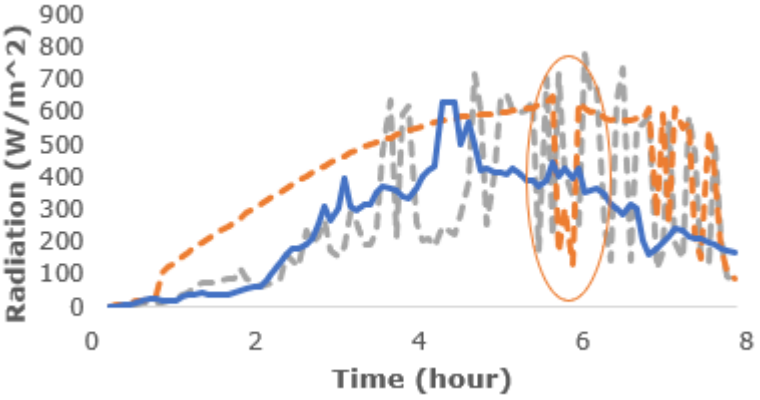

Fig. 4.12. Solar radiation variation for three days.

4.4. Design optimization

The validated model was applied for the design optimization of the system. Three types of scenarios were considered to simulate office, domestic, and service buildings. The control strategy was defined to maintain the temperature at comfort ranges. The design optimization was formulated to minimize the cost of the system while a control strategy was applied. The optimal design was obtained for the weather conditions of the cold season in Auckland, which was averaged over four years. The data flow between the optimization and simulation environments can be found in Fig. 4.13.

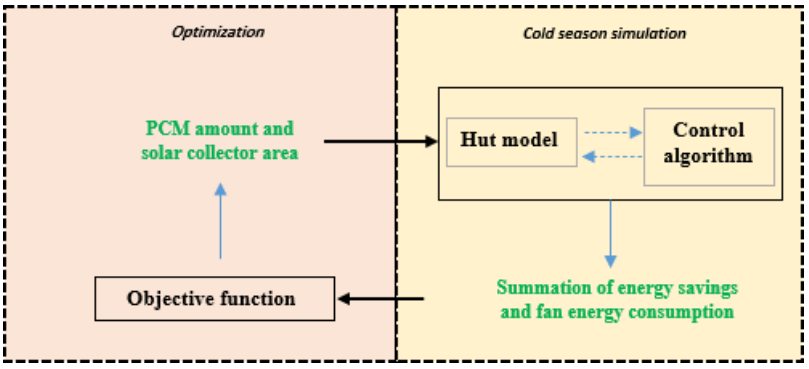

Fig. 4.13. Data flow for design optimization.

4.4.1. Control system

The schedules for the three types of buildings are different. The schedule represented the time of day that HVAC system needed to operate to maintain the space temperature at a comfort range. Table 4.6 depicts the details of the schedules applied in the simulation.

Table 4.6 Buildings schedule times and comfort temperatures [97].

Building	Comfort temperature range (°C)	Schedule time
Service	20-25	24 h
Office	20-24	8 am – 4 pm
Domestic	20-24	6 pm – 12 am

The upper and lower temperatures were set for the control system. According to the PCM, hut, and solar collector temperatures, the control logic forced air flow in different pathways to keep the hut temperature in a specific range. The control logic is different from the control strategy in Section 2.1 since the backup heater is also added to the system. Fig. 4.14 shows the control algorithm. For each scenario, the control was applied considering the period shown in Table 4.6.

A solar air collector, an electric heater, and a PCM heat exchanger unit supplied heat to the hut. The air was circulated from the solar collector to the hut so long as the hut temperature was within the comfort level and stopped once it reached the upper bound of thermal comfort. On the other hand, the backup heater would be started when the hut temperature dropped below the lower bound of the thermal comfort range. Hut received energy from the solar collector and stored it in PCM so long as the hut temperature was within comfort level.

The energy stored in PCM was supplied the heat to the hut in the following cooler hours. The backup heater would be used when the hut temperature dropped below the comfort level. Once the hut temperature reached the upper bound of the thermal comfort, all energy sources were stopped. If the hut temperature exceeded the upper bound of comfort temperature and the PCM temperature was lower than the hut temperature, then the PCM heat exchanger units collected the extra heat from the hut through Pathway 3. Fig. 4.14 shows the flowchart of the control strategy used in the hut.

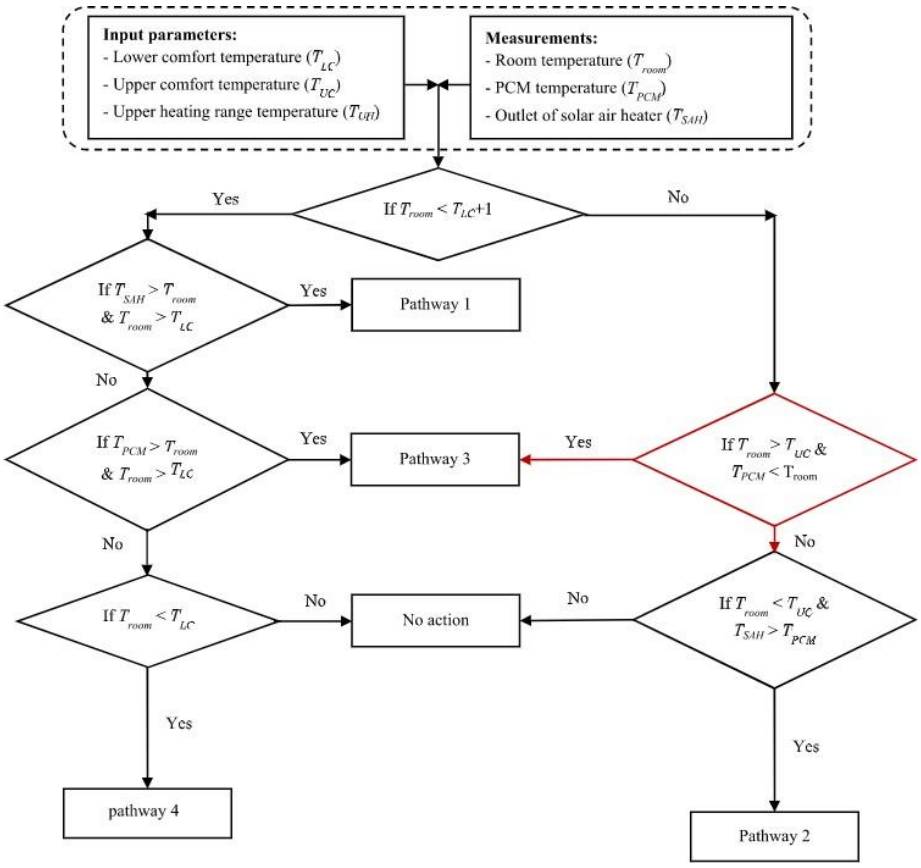

Fig. 4.14. Control algorithm for heating the hut [93].

4.4.2. Objective function

The optimization problem minimizes the objective function in Equation (4.7), which is the summation of the minimized cost over the New Zealand cold season from May until the end of August.

The first two terms in Equation (4.7) are PCM and solar collector capital costs. The third term is the fan usage cost which is the cost of circulating the air in the PCM heat exchanger.

$$OF = \sum_{k=o}^{n} \frac{M_{pcm} P_{pcm}}{Lf_{pcm}} + \frac{A_{SC} P_{SC}}{Lf_{SC}} + E_{fan} P_{ele} - E_{save} P_{ele} \tag{4.7}$$

The last term is the saved energy cost through using the PCM heat exchanger and solar collection. The saved energy was calculated by summating the heat energy supplied by the solar collector and the PCM heat exchange.

The weight parameters were considered for obtaining the objective function value annually. The last two terms were calculated for one cold season which leads to an annual amount. To consider the annual amount for the first two terms, the capital cost of PCM and solar collectors was divided by their lifetimes.

The design variables are the amount of PCM, M_{pcm}, and the area of the collector, A_{SC}, which are presented in detail in Table 4.7. The upper and lower bounds for the constraints were specified based on our knowledge from the hut's experimental data. The lower bound for solar collector area is one, by assuming that solar collector is certainly a component of the system. Details of the parameters in the objective function are given in Table 4.8. E_{save} is the total energy supplied by the solar collector and PCM heat exchanger.

Table 4.7 Optimization design variables details.

Symbol	Design variable	Type	Domain	Unit
M_{PCM}	Amount of PCM	Continuous	[0, 100]	Kg
A_{SC}	Area of collector	Continuous	[1,5]	m^2

The values were obtained from quotes of prices requested from commercial vendors. Based on some of these large values, one may be skeptical, however, they were quoted from the manufacturers, and it is out of the scope of this study to challenge them. It should be noted that P_{PCM} is the cost of the PCM material plus the heat exchanger body, which was estimated per kilogram of PCM material on a commercial production scale basis. The wholesale price of a PCM with a melting point of 23°C was asked from a PCM manufacturing company in the USA. The freight cost to New Zealand was also included in the price. The heat exchanger wholesale price was estimated by asking the heat exchanger containers and body price from manufacturers. It should be mentioned that the plastic containers were considered in the design that is more economical than the aluminum containers used in the experiments.

E_{fan} is the electricity consumed for circulating the air through the solar collector and PCM heat exchanger. It is calculated by equation:

$$\dot{Q}_{fan} = \frac{\Delta p}{\eta_{fan}} \dot{Q}_{air} \tag{4.8}$$

$\dot{Q}_{air}$ is the air volume flow rate and is system overall pressure drop which is calculated using Darcy's Law for parallel plates in the PCM heat exchanger and the pressure drop equation as follows:

Table 4.8 Objective function parameter details.

Symbol	Parameter	Value	Unit
P_{PCM}	PCM storage price	15	USD/kg
P_{SC}	Solar collector price	800	USD/m^2
Lf_{PCM}	PCM lifetime	100	Years
Lf_{SC}	Solar collector lifetime	30	Years
P_{ele}	Electricity price	0.22	USD/kwh

$$\Delta p = \frac{fL\rho v_t^2}{dH} \tag{4.9}$$

Where f is the Darcy friction factor, L is the length of the plate containg the PCM, ρ is the air density, v_t is the air velocity and dH is the hydraulic diameter. Δp changes by the amount of PCM (M_{pcm}) as the number of plates changes accordingly to fit the PCM amount, as per Equation (4.10).

$$N = \frac{M_{pcm}}{M_{pl}} \tag{4.10}$$

In which N is the number of plates and M_{pl} is the mass of the PCM in each plate.

4.4.3. Optimization method

The objective function was minimized using fminsearch, in MATLAB. This free derivative method was chosen as the hut model equations in EnenrgyPlus were not explicitly available. The objective function was calculated by applying the control system to the simulation environment given in Fig. 4.14. The simulation was carried out for the cold season which begins in May and finishes at the end of August in Auckland. The ambient condition for this period was obtained by averaging four years of weather data.

4.4.4. Results and discussion

The computational time needed for finding the optimum points was 3 hours using a Corei5-7600 CPU computer with 16GB RAM. The optimum values of design variables for different scenarios are given in Table 4.9.

Table 4.9 Optimum value of the design variables.

Building type	M_{PCM} (kg)	A_{SC}(m^2)
Service	35	1
Office	0	1
Domestic	20	1

The optimum mass of PCM for service type building is higher than the other types of building use, since the bigger saved energy during the day can be used at any time during the day. However, a lower amount of PCM is needed in the domestic building type as the stored energy is only required from 6 pm to 12 am. In the office scenario, the PCM heat exchanger is not needed as the scheduled time is from 8 am to 4 pm, when the solar collector can provide the heat directly to the hut. The solar collector area was one square meter (variable lower limit) for all types of building use, which is due to the high capital cost of the solar collector. This shows that the solar collector capital cost is one of the barriers toward increasing the deployment of such systems.

Aside from schedule differences, the number of people in the hut for various scenarios would vary. This may affect the internal load and the ventilation rate, which would consequently change the optimum design variables. The hut occupancy in the EnergyPlus model was not taken into account because the validation data was gathered in an unoccupied

situation. Additionally, including occupancy by adding the different numbers of people for the small hut of this study would not be realistic. EnergyPlus, on the other hand, allows users to specify the number of people and their activities for the hut model.

Furthermore, the optimum values of the variables were obtained considering a fixed price for electricity all day long. These values can change for regions where the on-peak and off-peak electricity prices can be different. In that case, heaters can be used to charge the PCM heat exchanger with a lower price and release that in cold on-peak hours with a higher price.

Although the price of sole air collectors is unlikely to change, the price of PCM is likely to fall as more commercial production is anticipated in the future. This would have an impact on the objective function's weight parameters as well as the optimum design values.

4.5. Conclusion

This paper presents the dynamic modeling and economical design of a system, including an active PCM storage system and a solar collector in an office-sized hut. An integrated model was obtained by coupling EnergyPlus with MATLAB via an EnergyPlus Co-simulation Toolbox interface. Experimental validation of the integrated model proved the reliability of the model in representing the dynamics of the systems. The importance of accurate measurements of influencing variables such as solar radiation on the mismatch between the model and experimental data was discussed. The validated model was used for economical design optimization of the system equipment. The highest amount of PCM mass (35 kg) was obtained for a service type building use and the lowest (zero) for office building use. This was due to the higher heating demand for service building use (24 hours) compared to office building use where heat is needed only during the daytime (8 am - 4 pm). However, the optimum value of the solar collector area was the same at one square meter for all the building types due to the high price of solar collectors. This demonstrates that the capital cost of solar collectors is one of the barriers to the deployment of more of these systems. The results also indicate that an economic analysis based on the building application is essential for designing solar collector systems with PCM storage. The results were obtained by considering a fixed electricity price, however PCM potential for peak load shifting could increase the system cost saving for varying electricity prices during the day. In future research, design optimization will be investigated for a system controlled by a price-based control to add the potential of PCM for peak load shifting.

CHAPTER 5

Optimal control of an active PCM system using reinforcement learning

Foreword

Optimal control of systems, including solar collector and phase change material (PCM), can increase thermal comfort and cost savings. This work presents an optimal control solution for a system including a PCM heat exchanger, a solar air collector, and a backup heater. The rigorous models involved make it difficult to achieve optimal control of buildings equipped with such systems. Aside from nonlinear models, the problem is complicated by binary variables such as PCM heat capacity calculations and fixed airflow rates through pathways. First, a model predictive control formulation was created, and the challenges of implementing this system control strategy were discussed. The results showed that MPC was unable to fully utilise the PCM heat exchanger's storage and release capabilities. For the first time, a deep Q-learning network (DQN) reinforcement learning was used to address the complexity of the optimal control formulation for the studied system. DQN includes deep neural networks and can map binary actions to continuous states. Simulating a validated model of the entire system was used to train and test DQN. A novel formulation was proposed, which allowed prioritizing thermal comfort and energy cost savings by adjusting a reward. By prioritizing the cost-savings, 97% more cost was saved than in the thermal comfort case; however, the offset from the desired temperature was 54% less. By adjusting the reward, a balance between energy cost savings and thermal comfort was achieved. A part of this chapter has been submitted in *the 7th International Symposium on Advanced Control of Industrial Processes*, Vancouver, Canada and has been included in the thesis.

1.14.3. Introduction

The building sector accounts for 30% of greenhouse gas emissions and 40% of total energy consumption [59]. The energy demand in this sector increases at an annual rate of 2.3% [139]. These two facts highlight the need for energy-saving strategies in the building sector.

Phase change materials (PCMs) have been considered energy storage in buildings to reduce or shift the profile of energy demand by changing the thermal inertia of the system. PCM systems can be classified into active or passive systems according to how thermal energy is delivered to PCM. Heat is exchanged using fluid, circulated, or electric heaters in active systems, but mechanical equipment is not required in passive systems.

The full potential of PCM benefits in buildings can be realized with more effective control of active systems. A comparison was made between an active and a passive system with the same energy storage capacity [93]. The results showed that active systems have greater energy-saving (22% less energy consumption) and more efficient peak load shifting (32% less electricity cost) than the passive approach. These conclusions were achieved by applying ON/OFF control for a system including a solar thermal heater, PCM heat exchanger, and backup heater.

The authors of [97] demonstrated that applying model predictive control to the same active system can result in further improvements. Simulation-based optimization was applied by considering the heating demand of the building and low-cost night-time electricity. Diurnal solar thermal energy was stored in the active PCM system and released on demand to reduce energy cost and consumption. The energy demand of the building was simulated in EnergyPlus and provided offline via Excel for optimization. The rationale behind this approach is that rigorous models such as those using EnergyPlus lead to complex nonlinear systems [140]. Therefore, the optimization problem takes much computational effort and time, possibly making them impractical for real-time applications.

However, it is essential to consider the building condition stated in the MPC formulation. This is because implementing MPC relies on the readily available states from the system measurements [141]. A requisite of implementing MPC is for the controller to exchange data with the building. This communication is required because the building's feedback measures can aid in reconciling the model states to the actual building states and compensating for the model mismatch.

Although the offline calculation of demand aimed at lowering the computational effort, the problem in [97] was a mixed-integer non-linear problem due to the PCM heat capacity calculation. Solving this complex problem in real-time is challenging and needs specific solvers [81].

As an alternative, machine learning-based approaches such as Reinforcement Learning (RL) can be applied as an optimal control approach. Pre-computing the optimal solutions through offline RL training overcomes the high online computational effort of MPC [82].

Although RL has been applied to energy management in buildings [142, 143], there have not been many studies related to energy storage control in buildings using RL [144]. In [145],

the authors applied the SARSA algorithm of reinforcement learning for controlling a ventilated façade with PCM. The façade was used for cooling purposes in summer by solidifying the PCM placed in the chamber during the night and absorbing the heat during peak hours. RL controlled the charging and discharging of PCM, considering a simple isothermal model for PCM and weather conditions. The authors extended their work in [146], where three different objective functions were considered based on cost-savings, energy reduction, and CO2 mitigation. The energy-saving, cost-saving, and CO2 mitigation averages were 4.3%, 7.8%, and 16.7%, respectively.

The classical RL, which was applied in the early works, included tables and simple functions for representing the state-action pairs. The more powerful version of RL is called Deep reinforcement learning (DRL), which has raised attention due to including deep neural networks (DNN). DNN has added the power of increasing the dimension of action-state pairs, which can describe the dynamics of complex systems with high nonlinearity.

Deep reinforcement learning was used for controlling a HVAC system in a building with PCM on the walls [147]. The authors adopted a model-free actor-critic on-policy reinforcement learning method based on deep deterministic policy gradient (DDPG) which did not have access to the full dynamics of the building. DDPG could learn from interacting with the building using the actor-critic feature. DDGP was compared with approximate dynamic programming (ADP) approach which used a simple RC model for representing the system thermal dynamics. For this passive system, the authors concluded that ADP had slightly better performance than DDPG. In another work [148], an innovative complex hybrid energy storage was operated using DRL as a high-level control. The system integrated different subsystems such as photovoltaic (PV) panels, Fresnel solar thermal collector, a sorption chiller connected with a reversible heat pump, and energy storage in electrical and thermal forms. The objective was to reduce the energy demand for heating, cooling, and domestic hot water (DHW) of a standard single-family residential building. The thermal dynamics of the building was not included in DRL and the building demand profile for cooling, heating and DHW were specified. The results showed that DRL can reduce the operating cost up to 50% compared to rule-based control.

This work considered an active system including PCM storage, solar collector, and a backup heater that supplied heating for an office-sized hut. The problem of finding an optimal control solution for the system was investigated. The system included ON/OFF valves and

fixed airflow rate, which led to a representation of the system in terms of binary variables in the optimal control formulation. The challenges of using MPC, such as the difficulty of online computation and the problem of local optimum, were investigated. Deep Q-learning (DQN) reinforcement learning, which can deal with problems with binary actions and continuous states, was used to solve these problems. Unlike previous research, hut dynamics such as temperature were considered as states in RL, allowing for the use of hut feedback measurements. In addition, a new method for defining the control system's objectives was presented. Using this method, the controller can be set to prioritise either energy savings or thermal comfort.

1.15. Methodology

A hut heated by a solar collector, a PCM heat exchanger and a backup heater was studied in this work. The PCM heat exchanger can store diurnal solar energy for later use. Below are descriptions of the experimental setups and control strategies. In terms of energy cost savings and providing thermal comfort, a new control method based on reinforcement learning was developed, and the results were compared to a traditional optimal control strategy, model predictive control.

1.15.1. Experimental set up

The setup includes a hut located near Ardmore airport in Auckland (37.0314° S, 174.9724° E), New Zealand. The huts' external dimensions are 2.7 m x 2.7 m x 2.7m, and it has a single-glazed window (0.8 m x 0.8 m) facing north. As shown Fig. 5.1, the hut was equipped with a solar collector, fans, and control valves for directing the heated air. In addition, the hut contains a PCM heat exchanger, integrated with the solar collector. The PCM heat exchanger was composed of 19 sets of macro-encapsulated PCM panels made of aluminium and filled with 9.5 kg RT25HC (manufactured by Rubitherm GmbH). The design of the PCM heat exchanger is explained in detail in [127].

The hut temperature was controlled using measured temperatures from the hut, solar collector, and PCM heat exchanger. The manipulated variable was the air flow and the final control elements were valves and fans. There were four possible pathways for supplying heat, which were controlled through three valves (V1, V2, V3) and fans as shown in Fig. 5.1.

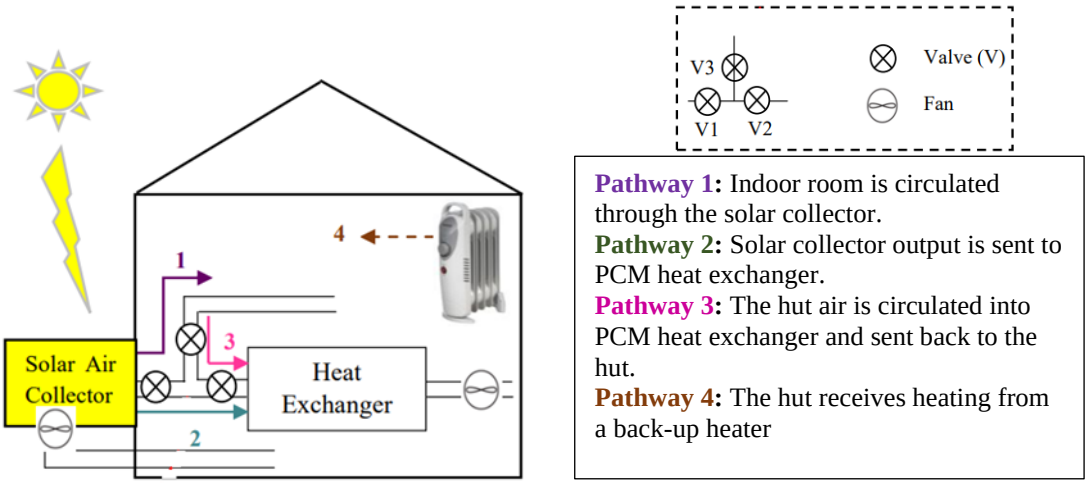

Fig. 5.1. Hut set up details. The arrows show different pathways. Air flow is adjusted by adjusting valves and fans.

Table 5.1 shows the valves and fans operating conditions for each pathway.

Table 5.1 Valves and fans operating conditions.

Pathway	V1	V2	V3	Fan (solar collector)	Fan (PCM heat exchanger)	Back-up heater
1	ON	OFF	ON	ON	OFF	OFF
2	ON	ON	OFF	OFF	ON	OFF
3	OFF	ON	ON	OFF	ON	OFF
4	OFF	OFF	OFF	OFF	OFF	ON
No heating	OFF	OFF	OFF	OFF	OFF	OFF

1.15.2. Model predictive control (MPC)

MPC is an optimization-based strategy for control decisions based on model predictions over a specified receding horizon. The key element for an MPC application is a dynamic model of the system, allowing the calculation of future states from the values of manipulated variables and disturbances. Several types of constraints may be added to the optimization problem, such as bounds on manipulated or process variables, physical limitations, and of course the system model itself. An objective function must be chosen to define what is the goal of the control system, for instance the distance to a given set point or an economic cost. The solution of this optimization problem is a vector of control actions. Only the first element of the control vector, corresponding to the current time step, is applied as the system input, and the remainder are discarded. The entire process is repeated in the next time step. The following equations describe a general formulation of MPC.

$$\min_{u_0,\ldots,u_{N-1}} \sum_{k=0}^{N-1} l_k(x_k, u_k)$$

Subject to

$$x_{k=0} = x_0 \tag{5.1}$$

$$x_{k+1} = f(x_k, u_k)$$

$$(x_k, u_k) \in X_k \times U_k$$

Where l is the objective function, N is the prediction horizon and control horizon, $x_k \in \mathbb{R}^n$ is the state and $u_k \in \mathbb{R}^m$ is the control input. X_k and U_k define the state and input constraints respectively.

System model, physical limitations, manipulated and controlled variables range are the constraints. The objective function can be defined based on power consumption, energy cost, demand cost, for example.

An MPC formulation was developed for a similar system in [97] which was used here with modifications. The authors in [97] considered a system with variable airflow rates, which led to continuous variables in the optimization formulation. However, the valves are either fully open or closed in the actual design, and fan flow air was at a fixed rate. This configuration added binary variables to the optimization problem, resulting in a case of Mixed-Integer Nonlinear Programming (MINLP). Although this class of problems is much harder to solve than the continuous problems often used in MPC, it is applied to a system with slow dynamics and large sampling time, which allows its online solution without further issues.

The objective function used in this study is the energy cost of heating (NZD), which includes the electricity cost of back-up heater $(\dot{Q}_{BH})$ and fans $(\dot{Q}_f)$.

$$\min_{\substack{Q_{BH},\ldots,Q_{BH}(N-1) \\ Q_f,\ldots,Q_f(N-1)}} (\sum_{k=0}^{N-1} (\dot{Q}_{BH(k)} + \dot{Q}_{f(k)}) \Delta t.Electrcity\,\mathrm{Pr}\,ice \tag{5.2}$$

Subject to:

$$T_{PCM|k=0} = T_{PCM(0)} \tag{5.3}$$

$$T_{PCM(k+1)} = T_{PCM(k)} + \frac{\dot{Q}_{SAC-HE(k)} - \dot{Q}_{HE-Room(k)}}{M_{PCM} C_{p,PCM}} \Delta t \tag{5.4}$$

$$Demand_{(k)} = \dot{Q}_{SAC-Room(k)} + \dot{Q}_{HE-Room(k)} + \dot{Q}_{BH(k)} \tag{5.5}$$

$$d_{SAC-HE(k)} + d_{SAC-Room(k)} + d_{HE-Room(k)} \leq 1 \tag{5.6}$$

$$Active_{(k)} \geq d_{SAC-HE(k)} + d_{SAC-Room(k)} \tag{5.7}$$

$$\dot{Q}_{SAC-Room(k)} = \dot{m} d_{SAC-Room(k)} (T_{out,SAC(k)} - T_{Room(k)}) \tag{5.8}$$

$$\dot{Q}_{SAC-HE(k)} = \dot{m} d_{SAC-Room(k)} (T_{out,SAC(k)} - T_{out,HE(k)}) \tag{5.9}$$

$$\dot{Q}_{HE-Room(k)} = \dot{m} d_{HE-Room(k)} (T_{out,HE(k)} - T_{Room(k)}) \tag{5.10}$$

$$20^{\circ}C \leq T_{PCM} \leq 60^{\circ}C \tag{5.11}$$

$$0 \leq \dot{Q}_{HE(k)} \ \& \ \dot{Q}_{BH(k)} \leq demand \tag{5.12}$$

$T_{PCM(0)}$ is the initial temperature of the PCM. In Equation (5.5), *Demand* is the hut's heating demand calculated offline using EnergyPlus. $\dot{Q}_{SAC-HE(k)}$ is the heat amount and subscripts *SAC* and *HE* represent solar collector and heat exchanger, respectively.

Equations (5.6) and (5.7) describe the physical limitations of the system. In the experimental set-up, airflow can be driven in one pathway at any time which is described in Equation (5.6). Variables *d* are used to show the binary variables. They show the airflow in pathways 1, 2, and 3. In Equation (5.7), *Active* is a binary parameter that shows the availability of solar collector airflow at any time. The *Active* parameter and solar collector output temperature ($T_{out,SAC(k)}$) values were specified at any time.

Equations (5.8)-(5.10) describe the heat flow through pathways 1-3, where $\dot{m}$ is the air mass flow rate, which is a fixed value. Equations (5.11) and (5.12) are the operating range of variables. In [97] authors expressed $C_{p.PCM}$ for different temperature ranges.

The mathematical representation of $C_{p.PCM}$ is modified here to facilitate the numerical calculation. $C_{p.PCM}$ was defined in [97] using the following equation:

$$C_{p,PCM} = \begin{cases} C_{p,s} & T_{PCM} < T_m - \frac{\Delta T_m}{2} \\ C_{p,s} + \frac{LH_{PCM}}{\Delta T_m} & T_m - \frac{\Delta T_m}{2} < T_{PCM} < T_m + \frac{\Delta T_m}{2} \\ C_{p,l} & T_{PCM} > T_m + \frac{\Delta T_m}{2} \end{cases} \quad (5.13)$$

where $C_{p,PCM}$ is specific heat capacity, LH is heat of fusion, and ΔT_m is an arbitrary small value representing the range of phase change temperature. Subscripts *s*, *l*, and *m* represent the solid phase, liquid phase, and melting conditions of PCM. $C_{p,l}$ and $C_{p,s}$ are 2 $(\frac{kJ}{kg.K})$ and LH_{PCM} is 230 $(\frac{kJ}{kg})$.

The authors of [97] defined Equation (5.13) in the optimisation formulation using if-conditional statements. However, this slows down the real-time computational process of finding solutions. The Big-m formulation was used to define $C_{p,PCM}$ values according to the PCM temperature in order to reduce computational time. Appendix A contains more information on the new formulation.

1.15.3. Reinforcement learning

Reinforcement learning is a framework for the learning of an agent to perform actions, in a sequential decision-making process [84]. A Markov decision process is generally used as a mathematical formalization of the process, where the environment is modelled as a set of states' *S*, which can be continuous or discrete, and the agent can decide to execute one of a set of actions *A* at each state. Once the agent executes an action, the environment changes into a new state value and produces a scalar reward *r* to the agent, which the agent can use for feedback and learning. After the agent has been trained, it can be used in new instances of the environment without the reward signal.

MATLAB and Python software was used in this work. A deep Q-network (DQN) was trained in Python, utilizing TensorFlow, and the system dynamics simulation was carried out in MATLAB using EnergyPlus. The data flow between Python and MATLAB is shown in Fig. 5.2.

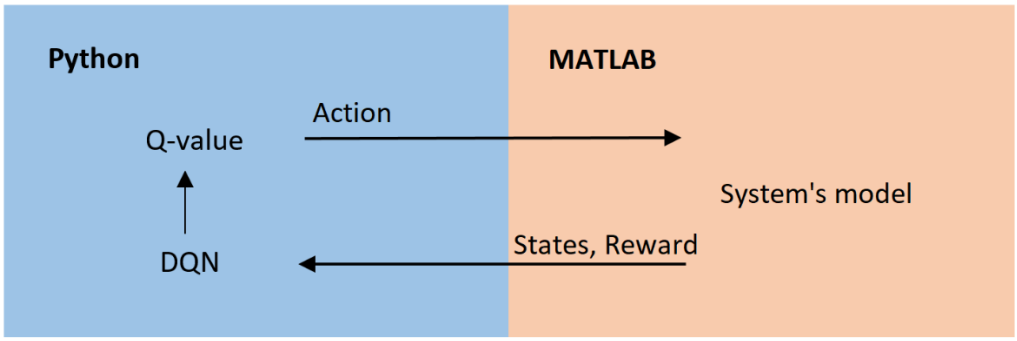

Fig. 5.2. Data flow between MATLAB and Python for building RL

1.15.3.1. States

Sets of states, actions, and rewards must be defined for the DQN algorithm. In this application, thirteen elements were considered in the state vector. They include temperatures and electricity prices, which can be used to describe the system's status from the comfort and economic viewpoints, as can be seen in Table 5.2.

The first five elements of the state vector are hut, PCM, ambient temperature, solar collector output temperatures, and electricity price. The next four state vector elements are predictions of ambient temperature in the next 12 hours, with each value corresponding the average of a period of 3 hours. Finally, the same procedure was applied for summarizing the electricity price in the next 12 hours.

Table 5.2 State vector elements

State	Size	Normalization factor
Hut temperature	1	40
PCM temperature	1	40
Ambient temperature	1	20
Solar collector output temperature	1	50
Electricity price	1	1
Future ambient temperature	4	20
Future electricity price	4	1

State elements were normalized by dividing the original values by the corresponding factor given in Table 5.2. The normalization procedure keeps the states between 0 and 1, conveying

an optimization problem with better numerical properties, which is essential for the training problem.

1.15.3.2. Actions

Five discrete actions, including no air flow, Pathway 1, Pathway 2, Pathway 3 and Pathway 4, were considered (details given in Table 5.1). The details of the actions and their corresponding pathways are given in Table 5.3. The actions were introduced to the hut model at every 15 minutes.

Table 5.3 Action's description

Action	Air flow condition
0	No air flow
1	Pathway 1
2	Pathway 2
3	Pathway 3
4	Pathway 4

1.15.3.3. Rewards

Rewards were defined based on the state and action pairs. They were used to balance between thermal comfort and energy saving by defining when to charge or discharge PCM and use the back-up heater. Rewards were defined as per the following equations:

$$If\ \ T_{PCM} < T_{Room}\ \&\ Action = 3\ then\ Reward = -1 \tag{5.14}$$

$$If\ T_{out,SAC} < T_{Room}\ \&\ Action = 1\ then\ Reward = -1 \tag{5.15}$$

$$If\ T_{out,SAC} < T_{PCM}\ \&\ Action = 2\ then\ Reward = -1 \tag{5.16}$$

$$If\ T_{Room} < 22^{o}C\ \&\ Action = 0\ then\ Reward = -1 \tag{5.17}$$

$$If\ T_{Room} \geq 22^{o}C\ \&\ (Action = 1\ \text{or}\ Action = 3\ \text{or}\ Action = 4\ )\ then\ Reward = -1 \tag{5.18}$$

$$If\ T_{Room} < 22^{o}C \,\&\, T_{out,SAC} > T_{Room} \,\&\, Action = 1\ then\ Reward = ES \tag{5.19}$$

$$If\ T_{Room} < 22^{o}C \,\&\, T_{PCM} > T_{Room} \,\&\, Action = 3\ then\ Reward = ES - K(20 - T_{Room}) \tag{5.20}$$

Equations (5.14) and (5.15) ensure that the PCM and solar collector output temperatures are greater than the hut temperature when Pathways 1 and 3 are taken. Equation (5.16) shows that PCM charging starts once the solar collector output temperature is higher than PCM temperature.

Equations (5.17) and (5.18) indicate that Pathways 1, 2 and 3 would not supply heat if hut temperature exceeds 22°C. Otherwise, heating is required.

Equations (5.19) and (5.20) are used to determine how to manage solar energy. Solar energy can either heat the hut or charge the PCM used to heat the hut later during the night. Reward values were chosen between -1 and 1 in equations (5.14)-(5.18). Additionally, reward values in Equations (5.19) and (5.20) is the saved energy cost that is for a 15-minute time step is between 0 and 1. The reward values in combination with states normalization helps with the numerical conditioning of the training problem. If the solar collector output is used directly for heating the hut, the reward is calculated by the amount of saved energy cost (*ES*) using the following equation:

$$ES = Q \times E_p \tag{5.21}$$

In which Q is the amount of supplied heat *(KJ)* and E_p $(\frac{NZD}{KJ})$ is the electricity price.

If solar energy is stored in PCM and discharged later through pathway3, the reward is calculated based on energy saving (*ES*) and the offset of hut temperature from 20 ^{o}C. $K(\frac{NZD}{^{o}C})$ is the parameter used for trading-off between economic saving and reaching the comfort temperature. If the hut temperature drops below 20 ^{o}C, *ES* would be penalized. The high value of *K* would make the reward negative for discharging the PCM heat exchanger. In this case, the back-up heater would be used rather than PCM discharge to reach the comfort temperature.

If the state and action pair condition was not in any of the previous condition the reward was set to zero.

1.15.3.4. System model

The solar air collector and PCM storage were modelled in MATLAB, while the hut was modelled in EnergyPlus. The model's configuration is shown in Fig 5.3. The models were integrated together to represent the system described in Fig. 5.1. Experimental data from Auckland's winter season was used to validate the integrated model. The results showed that it can represent the hut and system dynamics reliably. Chapter 4 contains more information about the model. The model was used as a virtual plant in this study to train and validate the RL performance.

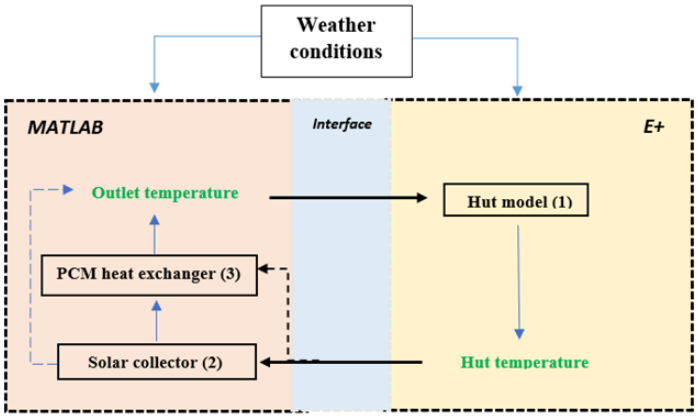

Fig 5.3. Dynamic model structure. The Orange, yellow, and blue colours show MATLAB, EnergyPlus (E+) and the E+ Co-simulation Toolbox interface code, respectively. Dashed lines show the alternative heat supply pathways.

1.15.3.5. Deep Q-Learning

DQN [149] is one of the first Deep Reinforcement Learning algorithms, and it was initially used to play ATARI games at super-human performance. It is an extension of Q-Learning with a neural network function approximator for Q-values. These values are defined as the reward obtained on state *s* and taking action *a* and then behaving optimally until the end state. Q-values can be estimated by solving the Bellman equation:

$$Q(s,a) - R(s,a) + \gamma \sum_{s' \in S} T(s,a,s') \max_{a'} Q(s',a') \tag{5.22}$$

Selection of actions during training is made through an ε -greedy exploration policy, where the action that maximizes the Q-value is selected, but with probability ε a random action is chosen.

DQN uses the following loss, which performs regression of the Q-values, enabling simultaneous learning of the Q-function with only partial information obtained by interacting with EnergyPlus.

$$L_i(\theta_i) - E\left[(y_i - Q(s,a;\theta_i))^2\right] \tag{5.23}$$

$$y_i - r + \gamma \max_{a'} Q(s',a';\theta_{i-1}^{-}) \tag{5.24}$$

Where (s',a',r) is the experience tuple obtained from interacting with EnergyPlus via MATLAB at each timestep during training. An experience replay buffer is used that includes the last *M* experience tuples collected, and a mini-batch of size *B* is sampled to train the network during each step.

θ_{i-1}^{-} denotes the target network weights, which define the values used to compute the target during training. The target network weights are kept fixed and only copied from the training network θ_i every C steps. This technique is used to stabilize the convergence of Q-values.

The network is trained using the Adam optimizer with a learning rate α = 0.001 for 10000 episodes using a batch size *B* = 440 and replay buffer of *M* = 10000 experience tuples.

Once the network that estimates the Q-values is trained, at inference time, a forward pass is made giving a state as input, and a vector of Q-values is produced as output, one value for each possible action. An action is selected by taking the one with maximum Q-value. The process is repeated with the new state after the action is executed in MATLAB, until the end state is reached.

1.16. Results and discussion

The system was controlled using the two strategies described in the Methodology section. Control strategies performance was determined with respect to cost and thermal comfort in four days of winter. For training RL, twelve winter days were considered when variation of disturbances such as ambient conditions happened. Four consecutive typical winter days were chosen for testing the control strategies and their performance is reported in the following sections. The ambient temperature and solar radiation during these days are shown in Fig. 5.4.

During these consecutive four days, ambient temperature experienced a reasonable change that happens during winter in Auckland. The lowest ambient temperature was 7 ^{o}C which

happened in the early hours of the last day and the highest temperature was 16 ºC which happened at the midday of the second day. The solar radiation is the lowest in the first day and almost similar in the rest of the days.

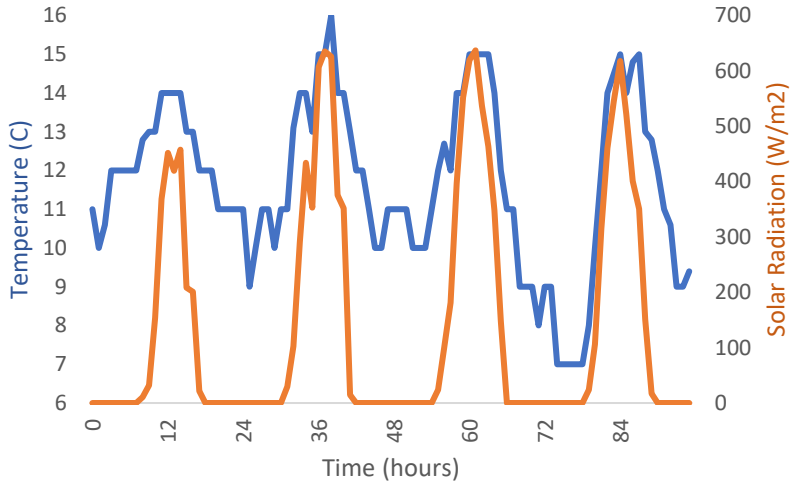

Fig. 5.4. Ambient conditions for the test days. Orange and blue lines represent ambient temperature and solar radiation respectively.

The electricity price profile for a typical day in winter in shown in Fig. 5.5. The electricity price profile indicates two main peaks: morning and evening. The desired control system can manipulate the pathways to store the solar energy during the day and use it during the early evening peak hours for heating the hut.

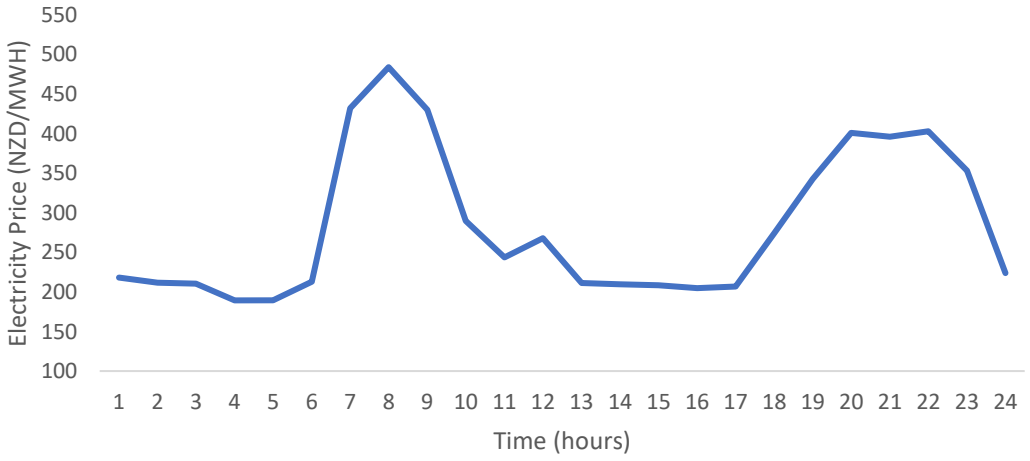

Fig. 5.5. Electricity price for a typical day.

1.1.1. MPC

MPC formulation was applied for the same period. The decision time step and number of prediction horizon were 15 minutes and 90 respectively. As explained in the Methodology section, the heating requirement of the hut was calculated offline. The calculated demand was saved and used in the MPC. The demand was the heating required to keep the hut temperature above 20 °C.

As explained in Equation (5.5), the required demand could be provided by back-up heater, solar energy or PCM heat exchanger. The back-up heater in the MPC formulation did not have any limit constraint in providing heat. However, the objective function tried to minimize the back-up heater power consumption cost.

The total cost of heating was 10 NZD. The heating demand was mainly provided by the back-up heater. Fig. 5.6 shows the amount of heating energy that the back-up heater supplied.

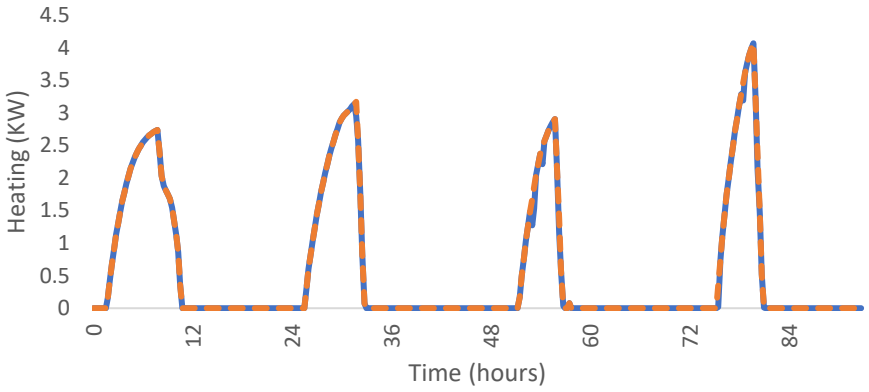

Fig. 5.6. Hut demand (blue) and back-up heater supplied energy (orange)

As Fig. 5.6 shows, almost all the demand was supplied by the back-up heater. However, this happened when the PCM heat exchanger could supply a part of the heating demand. Fig. 5.7 shows the PCM temperature during the simulation.

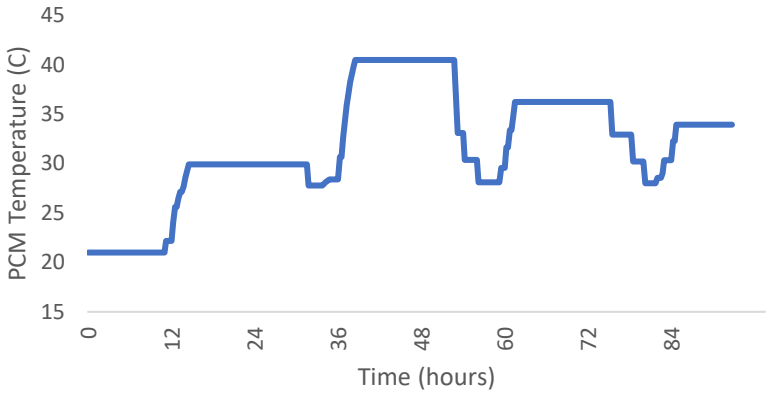

Fig. 5.7. PCM temperature during the test days.

The PCM temperature decline shows that it was discharged for supplying the demand. However, the large amount of energy was stored as the latent heat between 23 ^{o}C and 27 ^{o}C which was not used.

MPC formulation is a nonlinear optimization problem with binary variables. There are many local optimal solutions to this problem. Although there could be better solutions to the problem, finding the global optimum for such a problem is very difficult.

Furthermore, heating demand is calculated offline and provided to the MPC formulation. Using this approach, the computational effort of the optimization decreases as hut model is not included in the optimization. However, this formulation would not work in practice since perfect model of the hut would not be available. In MPC feedback of the plant plays very important role in reconciling the states and decreasing the drawbacks of the mismatch between the model and the real plant.

Additionally, the formulation assumed that the back-up heater has unlimited capacity to supply the required demand. This assumption was necessary for respecting the equality constraint in Equation (5.5). However, in practice, the back-up heater has a specified capacity that would not supply the required demand.

Performance of MPC was compared with an ON/OFF control strategy described in [93]. Fig. 5.8 shows the hut temperature simulation.

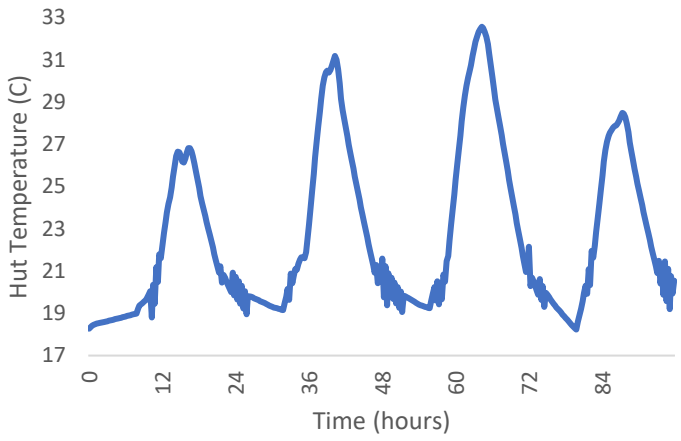

Fig. 5.8. Hut temperature using an ON/OFF control strategy.

Fig. 5.8 shows that the hut temperature fell below 20 ^{o}C in some periods. This is because the back-up heater could not supply enough heat, and the controller did not consider models for controlling the temperature. PCM temperature is shown in the Fig. 5.9. Like MPC, the full capacity of PCM was not used. PCM was charged however the stored energy was not used for heating which would add extra operating cost for running fans. This is because PCM was used in the control algorithm when the temperature was higher than 20 ^{o}C. By decreasing this threshold, PCM would be used more for supplying heat but in expense of more offset from 20 ^{o}C since the back-up heater supplies more heat than PCM storage. It should be mentioned that the ON/OFF control decisions were only based on the thermal comfort, since the energy cost dynamics could not be calculated in the algorithm.

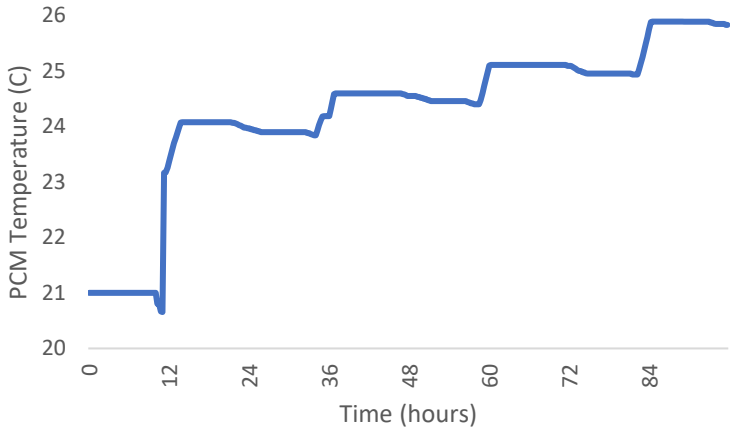

Fig. 5.9. PCM temperature using ON/OFF control.

5.3.2. RL

Reinforcement learning was trained and tested using data of 16 days in winter. To train the networks, a simulation of the first 12 days was considered. RL performance was as tested using same four days that used for testing MPC. Fig. 5.10 shows the learning curve of the RL networks.

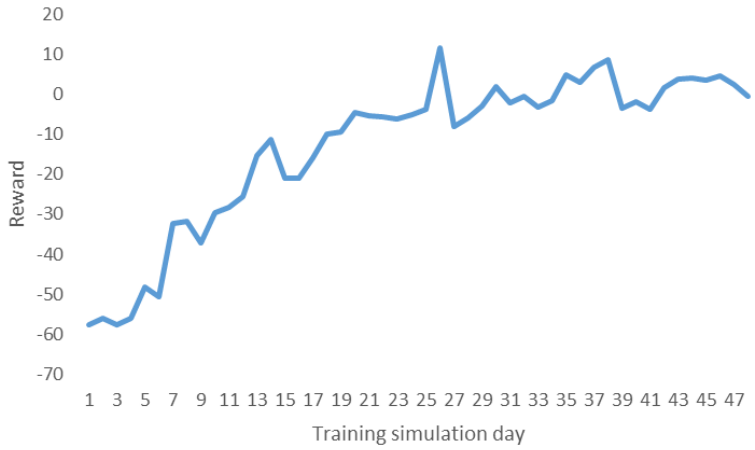

Fig. 5.10. Reward improvement during the training process.

After four epochs, the training was stopped to avoid overfitting the training data. The RL performance was validated using four days of simulations, and reward values were monitored. Each epoch included 12 simulation days. The reward is the summation of rewards during a whole day of simulation and is shown in Fig. 5.10. The timestep in the simulation was 15 minutes, so the total number of rewards in each day was 96. As explained in section 1.5.5, the selection of actions during training was made through an ε-greedy exploration policy. Using this policy, the number of random actions at the beginning of training is high and it decreases as training proceeds while networks learn by training. Fig. 5.10 indicates that the reward value was low at the beginning of training. Over time, it increased as the networks' parameters were adjusted during the training and the agent took more actions using the networks rather than merely random actions.

The RL performance was tested on the same days used for testing MPC control scheme. The trained networks were tested using the 4 days. Fig. 5.11 shows the simulation results for the testing period.

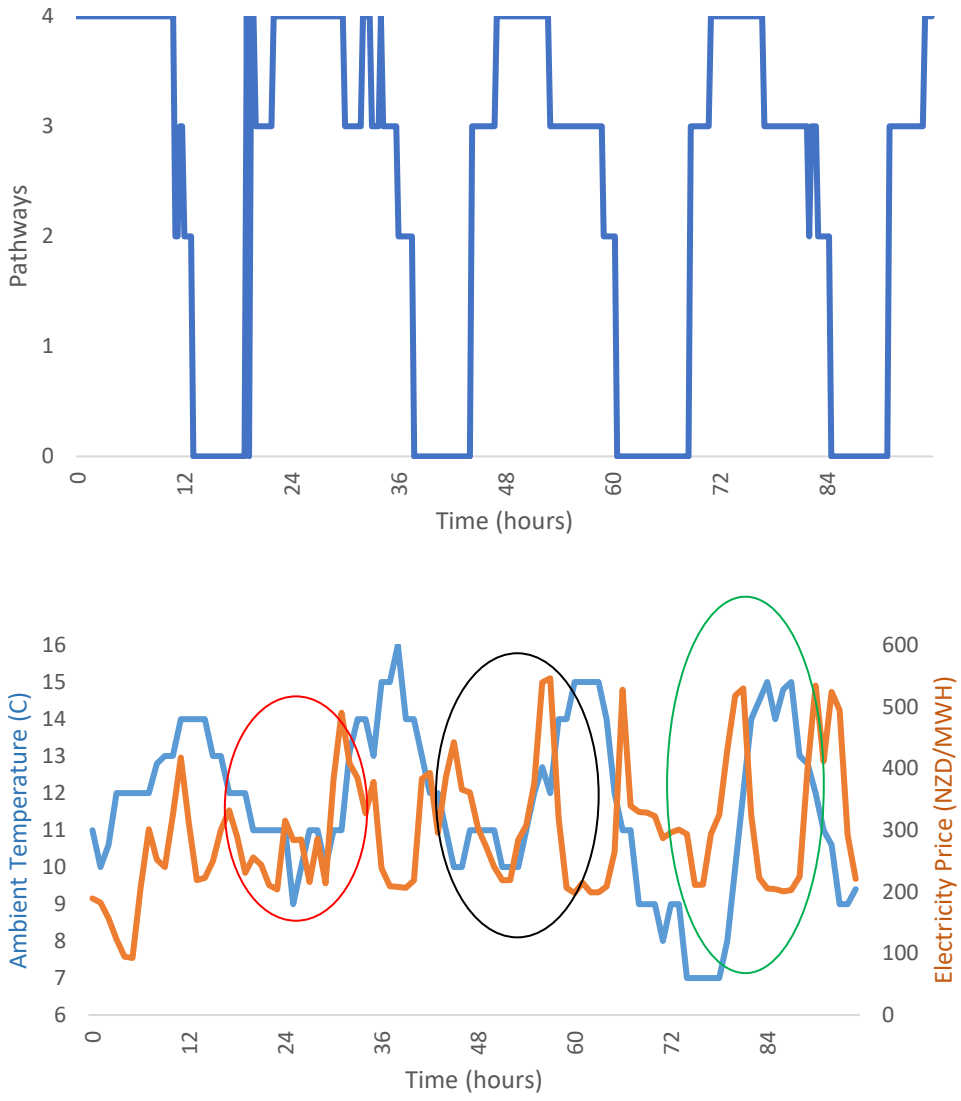

Fig. 5.11. RL performance with K = 0.25 during the test days. The circles show the heating time during the same 4 test days. Taken actions (above). Blue colour shows the ambient temperature and orange shows electricity price (below).

In Fig. 5.11, circles show the periods after the midnight when heating was started. The *K* value which determines the balance between thermal comfort and cost saving in Equation (5.20) was considered to be 0.25 in this case. The higher the value of *K*, the more cost saving will be penalized by the offset from the desired temperature. It can be seen that Pathways 3 and 4 were applied during this period. Whenever electricity price and ambient temperatures were low, the back-up heater supplied heat. This is since with the low electricity price cost saving through pathway 3 was low. At the same time the ambient tempearture decreased which means

more heat was required to make up the offset from the desired temperature. The back-up heater was used since electricity price was low, also the back-up heater could provide more heating eenergy comparing to the PCM heat exchanger.

The PCM temperarture during the test days is shown in Fig. 5.12. It shows that the PCM heat exchanger was charged during the day and discharged during the night time for supplying the required heating.

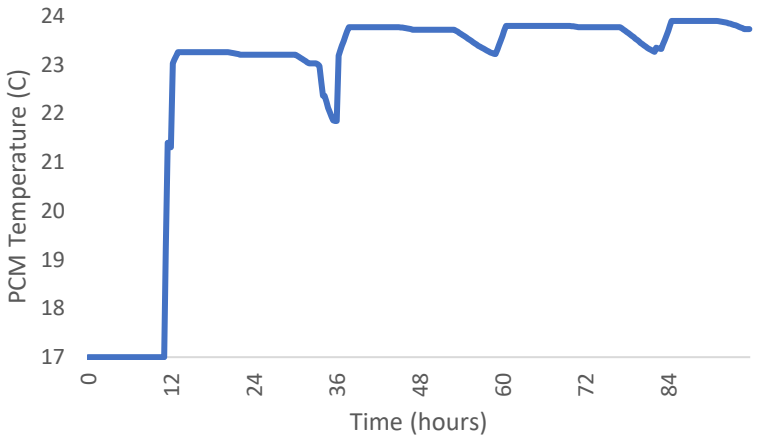

Fig. 5.12. PCM temperature during the test days.

The value of *K* can be used for prioritizing either cost saving or thermal comfort. If low values of *K* chosen, the reward from action 3 would increase as costs are saved by using the stored solar energy. In contrast, if *K* increases, the offset from the comfort temperature would penalize the pathway 3 reward and action 4 would be taken. This is shown in Fig. 5.13.

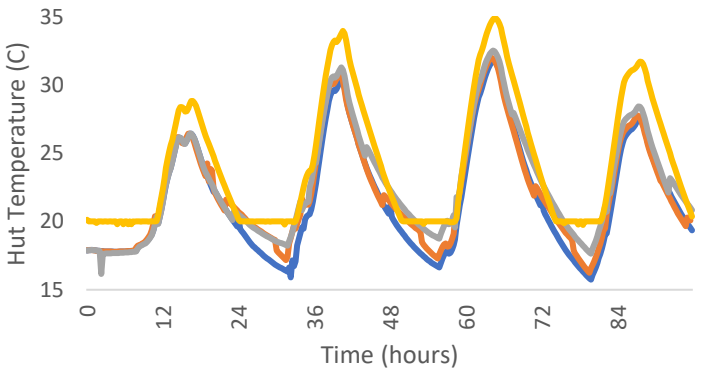

Fig. 5.13. Hut temperature for different K values. Blue, orange, and grey colours show the results for K values of 0, 0.25, and 1 respectively. Yellow line shows the MPC result.

As Fig. 5.13 shows, hut temperature during the heating period (midnight to early morning) for $K = 1$ was higher than the other cases since the back-up heater was used for heating the hut. For $K = 0$, the PCM heat exchanger was dischared for supplying heat since cost saving was not penalized with thermal comfort. As Fig. 5.13 showed, with $K = 0.25$ both pathways were used for heating since both cost saving and thermal comfort played important roles in calculating the rewards of pathway 3. Fig. 5.13 also includes the MPC result. As stated in the previous section, MPC provided the required demand for keeping the hut temperature above 20 °C. This led to minimun offset, however more energy was consumed which was mostly supplied by the back-up heater.

Table 5.4 shows the cost saving and offset from 20°C which is the root square mean error for different values of *K*. The highest cost saving is for $K = 0$ since PCM was discharged in this case more than the other values. However, the correspoding thermal comfort is the worst. In contrast, $K = 1$ led to the least offset, which means the highest thermal comfort. A balance between these two factors was achieved by using $K = 0.25$.

Table 5.4 Summary of cost saving and thermal comfort for different values of K

K value	Cost saving (NZD)	Offest (C)
0	0.97	2.38
0.25	0.52	1.64
1	0.03	1.1

Fig. 5.14 summarizes the effect of *K* value on the control performance. Lower values of *K* leads to more cost saving however it is obtained in expense of more offset from the desired temperature.

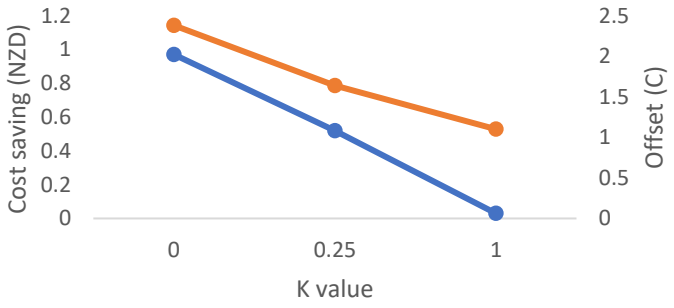

Fig. 5.14. Effect of K value on cost saving and offset from the desired temperature.

1.17. Conclusion

A study was conducted to determine the best control strategy for energy management in a system that included a solar collector, PCM heat exchanger, and backup heater. The challenges of implementing MPC as an optimal control strategy were discussed by developing a formulation for the studied system, which resulted in a nonlinear mixed-integer problem. Although the MPC optimisation problem could be solved, the results showed that local optimum solutions did not fully utilise the PCM heat exchanger storage and release capabilities. The DQN reinforcement learning technique was shown to be capable of dealing with the problem's complexity. We were able to include hut dynamics, current and future ambient conditions, and electricity price as states using deep neural networks. The results showed that DQN could solve the optimal control problem in real time. By adjusting a parameter in the reward definition, a trade-off between thermal comfort and energy cost savings could be achieved.

CHAPTER 6

Conclusions and recommendations

6.1. Conclusion

Two of the four priority areas in New Zealand's energy strategy toward Zero Carbon Act are the development of renewable energies and the efficient use of energy [25]. In this thesis, these two areas were targeted by studying the digitalization opportunities in the dairy and renewable energy industries. The literature review showed that the DT entity for the processes studied in this research has not been developed. Combinations of data-driven and mechanistic methods were used to develop virtual entities for improving online operation.

The remarkable conclusions and findings and possible future work are discussed in this chapter.

In the first process, mechanistic models include many parameters and could not provide reliable online predictions of the fermentation pH dynamics. Data-driven models were used in combination of optimization formulation to build a virtual entity.

- Data-driven based models were able to represent the pH dynamics of cream cheese fermentation. ANN reliably predicted the pH dynamics using the pH data as inputs on both lab and industrial scales. Additionally, the hybrid model prediction was improved using the in-line measurements along with the fermentation. Both models performed well in predicting the batch duration of cream cheese fermentation using the available measurements.
- A DT virtual entity was developed by using optimization formulation for online scheduling of the fermentation vats, considering the unit constraints. It used the developed data-driven model's outputs. The results showed that using the models to update the batch duration prediction improved the unit operation by saving energy, reducing waste, and reducing the idle time of the fermentation vats.

- Although mechanistic models could represent the system dynamics in the second process, the online optimization was not achievable due to its high computational cost. A virtual entity for optimal control was achieved by using the mechanistic models for offline training of a data-driven method.

- Dynamic modelling and economical design optimization of an active PCM system equipped with a solar air collector in Auckland were investigated. The experimental data were used to validate a model coupling the sub-models representing the dynamics

of the system's components. Results revealed the reliability of the model. The economical design optimisation for three scenarios using the dynamics model revealed different amounts of PCM for each scenario. The solar collector surface area, on the other hand, was 1 metre at its lowest point, indicating that the capital cost of solar collectors is one of the barriers to the cost-effective design of such systems.

- A DT virtual entity was developed for optimal control of the active PCM system using the developed dynamic model. As a classical optimal control approach, MPC was not able to provide an online solution and use the full potential of the system to save energy and cost. Reinforcement learning was trained offline using the dynamic model. It showed better performance by providing an online solution that could be prioritized for temperature comfort or cost-saving.

6.2. Recommendations for future work

The developed DT entities showed reliable solutions for both processes. However, more research is necessary for implementing the DT tools.

- Data-driven models for predicting cream cheese fermentation pH dynamics can be improved using more industrial pH data, measured manually in the plant. These measurements can be used to verify the sensor's data which could be unreliable. Furthermore, lactose and lactate measurements in the plant can be taken more frequently in order to test the hybrid model using industrial data.
- The DT for scheduling the fermentation vats can be used as a digital model or shadow to test its performance. This could show the challenges of using the developed tool before using that as a DT tool interacting with the plant.
- Economical design optimization can be extended to bigger buildings. Additionally, some details, such as occupancy data, can be added to the building model to account for internal gain in various building application scenarios. This additional information would have an impact on the building's optimal design.
- DT tools for optimal control of the active PCM system can be implemented in the facilities of Ardmore Campus. The Data Acquisition system is already available, which can receive the optimal control actions for manipulating the valves and fans.

Appendices

Appendix A

Two binary variables ($E_{1(k)}$ and $E_{2(k)}$) with the if-conditional function were used to determine the $C_{p,PCM}$ value based on the PCM temperature as follows:

If $E_{1(k)} = 1,\ T_{PCM(k)} \le 27$. Else, $T_{PCM(k)} \ge 27 + \varepsilon$ (A.1)

If $E_{2(k)} = 1,\ T_{PCM(k)} \ge 23$. Else, $T_{PCM(k)} \le 23 - \varepsilon$ (A.2)

is an arbitrary small value.

Therefore, there are three possible situations in terms of temperature:

If $T_{PCM(k)} \le 23 - \varepsilon \Rightarrow E_{1(k)} = 1, E_{2(k)} = 0$ (A.3)

If $23 \le T_{PCM(k)} \le 27 \Rightarrow E_{1(k)} = 1, E_{2(k)} = 1$ (A.4)

If $T_{PCM(k)} \ge 27 + \varepsilon \Rightarrow E_{1(k)} = 0, E_{2(k)} = 1$ (A.5)

Replacing the values of $E_{1(k)}$ and $E_{2(k)}$ the equation to calculate C_p for each of these situations,

$$C_{p,PCM(k)} = (E_{1(k)} + E_{2(k)} - 2E_{1(k)}E_{2(k)}) / C_{p,\min} + (E_{1(k)}E_{2(k)}) / C_{p,\max} \quad \text{(A.6)}$$

If $T_{PCM(k)} \le 23 - \varepsilon \Rightarrow \dfrac{1}{C_{p,PCM(k)}} = \dfrac{1}{C_{p,\min}}$ (A.7)

If $23 \le T_{PCM(k)} \le 27 \Rightarrow \dfrac{1}{C_{p,PCM(k)}} = \dfrac{1}{C_{p,\max}}$ (A.8)

If $T_{PCM(k)} \ge 27 + \varepsilon \Rightarrow \dfrac{1}{C_{p,PCM(k)}} = \dfrac{1}{C_{p,\min}}$ (A.9)

The above approach for calculating $C_{p,PCM}$ includes if else statements and multiplication of binary variables which makes the computational effort very heavy.

In this work, the above approach was replaced by Big-M formulation to facilitate the optimization problem. Three possible temperature zones (i = 1,2,3) and three binary variables, $Y_{i(k)}$ were defined. $Y_{i(k)}$ is 1 if temperature is at zone i and 0 otherwise. In other words, the PCM temperature zone separation will be:

Temperature zone 1: If $T_{PCM(k)} \le 23-\varepsilon \Rightarrow Y_{1(k)} = 1$ (and 0 for others) (A.10)

Temperature zone 2: If $23 \le T_{PCM(k)} \le 27 \Rightarrow Y_{2(k)} = 1$ (and 0 for others) (A.11)

Temperature zone 3: If $T_{PCM(k)} \ge 27+\varepsilon \Rightarrow Y_{3(k)} = 1$ (and 0 for others) (A.12)

The if statements of the original formulation were replaced by the following equations in the optimization formulation:

$$Y_{1(k)} + Y_{2(k)} + Y_{3(k)} = 1 \tag{A.13}$$

$$\frac{1}{C_{p,PCM(k)}} = \frac{1}{C_{p,\min}} Y_{1(k)} + \frac{1}{C_{p,\max}} Y_{2(k)} + \frac{1}{C_{p,\min}} Y_{3(k)} \tag{A.14}$$

$$T_{PCM(k)} - 23 + \varepsilon \le M(1 - Y_{1(k)}) \tag{A.15}$$

$$23 - T_{PCM(k)} \le M(1 - Y_{2(k)}) \tag{A.16}$$

$$T_{PCM(k)} - 27 \le M(1 - Y_{2(k)}) \tag{A.17}$$

Equation A.13 is a logic constraint which ensures that the PCM temperature is at only one temperature zone defined in equations A.10-A.12 at any time. $C_{p,PCM}$ is calculated as a function of current temperature zone using Equation A.14. Since Equation A.13 forces only one Y_i to be non-zero at any given time, this value is the one assigning the value to $C_{p,PCM}$. In Equation A.15, for values under $23-\varepsilon$, $Y_{1(k)} = 1$ and M is taken as a large value in this case $M = 20^{o}C$ was chosen. The last two constraints (Equations A.16 and A.17) are used to detect when the PCM temperature is at the second temperature zone (equation A.11). There is no need for a zone constraint regarding $Y_{3(k)}$, since it will be the default case when $Y_{1(k)}$ and $Y_{2(k)}$ are zero.

References

1. Tao, Fei, et al. "Digital twin-driven product design framework." *International Journal of Production Research* 57.12 (2019): 3935-3953.
2. Rosen, Roland, et al. "About the importance of autonomy and digital twins for the future of manufacturing." *Ifac-papersonline* 48.3 (2015): 567-572.
3. Glaessgen, Edward, and David Stargel. "The digital twin paradigm for future NASA and US Air Force vehicles." *53rd AIAA/ASME/ASCE/AHS/ASC structures, structural dynamics and materials conference 20th AIAA/ASME/AHS adaptive structures conference 14th AIAA*. 2012.
4. Tao, Fei, and Meng Zhang. "Digital twin shop-floor: a new shop-floor paradigm towards smart manufacturing." *Ieee Access* 5 (2017): 20418-20427.
5. Hermann, Mario, Tobias Pentek, and Boris Otto. "Design principles for industrie 4.0 scenarios." *2016 49th Hawaii international conference on system sciences (HICSS)*. IEEE, 2016.
6. Panetto, Hervé, et al. "Challenges for the cyber-physical manufacturing enterprises of the future." *Annual Reviews in Control* 47 (2019): 200-213.
7. Tammaro, Antonio, et al. "Extending Industrial Digital Twins with Optical Object Tracking." *CEIG*. 2017.
8. Kunath, Martin, and Herwig Winkler. "Integrating the Digital Twin of the manufacturing system into a decision support system for improving the order management process." *Procedia Cirp* 72 (2018): 225-231.
9. Grieves, Michael. "Digital twin: manufacturing excellence through virtual factory replication." *White paper* 1 (2014): 1-7.
10. Kritzinger, Werner, et al. "Digital Twin in manufacturing: A categorical literature review and classification." *IFAC-PapersOnLine* 51.11 (2018): 1016-1022.
11. Liu, Mengnan, et al. "Review of digital twin about concepts, technologies, and industrial applications." *Journal of Manufacturing Systems* 58 (2021): 346-361.
12. Liu, Jinfeng, et al. "Dynamic evaluation method of machining process planning based on digital twin." *IEEE Access* 7 (2019): 19312-19323.
13. Sun, Heqing, et al. "Optimized throughput improvement of assembly flow line with digital twin online analytics." *2017 IEEE International Conference on Robotics and Biomimetics (ROBIO)*. IEEE, 2017.
14. Jones, David, et al. "Characterising the Digital Twin: A systematic literature review." *CIRP Journal of Manufacturing Science and Technology* 29 (2020): 36-52.
15. Cutler, Charles R., and Brian L. Ramaker. "Dynamic matrix control?? a computer control algorithm." *joint automatic control conference*. No. 17. 1980.
16. Qin, S. Joe, and Thomas A. Badgwell. "A survey of industrial model predictive control technology." *Control engineering practice* 11.7 (2003): 733-764.
17. Garcia, Carlos E., David M. Prett, and Manfred Morari. "Model predictive control: Theory and practice—A survey." *Automatica* 25.3 (1989): 335-348.
18. Shokri, Saeid, et al. "Real time optimization as a tool for increasing petroleum refineries profits." *Petroleum & coal* 51.2 (2009): 110-114.
19. Bonvin, Dominique. *Real-time optimization*. MDPI (Multidisciplinary Digital Publishing Institute), 2017.
20. Joly, Marcel, et al. "Refinery production scheduling toward Industry 4.0." *Frontiers of Engineering Management* 5.2 (2018): 202-213.

21. Dassisti, Michele, et al. "Industry 4.0 paradigm: The viewpoint of the small and medium enterprises." *7th International Conference on Information Society and Technology, ICIST 2017*. Vol. 1. 2017.
22. Semeraro, Concetta, et al. "Digital twin paradigm: A systematic literature review." *Computers in Industry* 130 (2021): 103469.
23. Sadati, Najibesadat, Ratna Babu Chinnam, and Milad Zafar Nezhad. "Observational data-driven modeling and optimization of manufacturing processes." *Expert Systems with Applications 93* (2018): 456-464.
24. Wright, Louise, and Stuart Davidson. "How to tell the difference between a model and a digital twin." *Advanced Modeling and Simulation in Engineering Sciences* 7.1 (2020): 1-13.
25. Koulouris, Alexandros, Nikiforos Misailidis, and Demetri Petrides. "Applications of process and digital twin models for production simulation and scheduling in the manufacturing of food ingredients and products." *Food and Bioproducts Processing* 126 (2021): 317-333.
26. https://www.mbie.govt.nz/building-and-energy/energy-and-natural- resources/energy-strategies-for-new-zealand/
27. Teixeira, Arthur A., and Charles F. Shoemaker. *Computerized food processing operations*. *Springer Science & Business Media*, 2012.
28. McFarlane, Ian. Automatic control of food manufacturing processes. *Springer Science & Business Media*, 1995.
29. https://www.dcanz.com/about-the-nz-dairy-industry/
30. https://www.mbie.govt.nz/have-your-say/process-heat-in-new-zealand- opportunities-and-barriers-to-lowering-emissions/
31. Hoare, P. (1978) "Automation in the dairy industry". J. Soc. Dairy Technol., 32 (4), 217-219.
32. Freund, Judit Nagy–Zsófia Jámbor–Anna. "Digitalization in the food industry– opportunities and impedimental factors." *The Challenges of Analyzing Social and Economic Processes in the 21 st Century*: 10.
33. García-Burgos, María, et al. "New perspectives in fermented dairy products and their health relevance." *Journal of Functional Foods* 72 (2020): 104059.
34. Doran, Pauline M. Bioprocess engineering principles. Elsevier, 1995.
35. Nielsen, Jens, Karin Nikolajsen, and John Villadsen. "Structured modeling of a microbial system: I. A theoretical study of lactic acid fermentation." *Biotechnology and Bioengineering* 38.1 (1991): 1-10.
36. Nielsen, Jens, Karin Nikolajsen, and John Villadsen. "Structured modeling of a microbial system: II. Experimental verification of a structured lactic acid fermentation model." *Biotechnology and bioengineering* 38.1 (1991): 11-23.
37. Cachon, R., and C. Divies. "Generalized model of the effect of pH on lactate fermentation and citrate bioconversion in Lactococcus lactis ssp. lactis biovar. diacetylactis." *Applied microbiology and biotechnology* 41.6 (1994): 694-699.
38. Solomatine, D., Linda M. See, and R. J. Abrahart. "Data-driven modelling: concepts, approaches and experiences." *Practical hydroinformatics* (2009): 17-30.
39. Luo, Shuai, et al. "A review of modeling bioelectrochemical systems: engineering and statistical aspects." *Energies* 9.2 (2016): 111.
40. Fisher, Oliver J., et al. "Considerations, challenges and opportunities when developing data-driven models for process manufacturing systems." *Computers & Chemical Engineering* 140 (2020): 106881.
41. Shetty, K. Vidya, Santosh Nandennavar, and G. Srinikethan. "Artificial neural networks model for the prediction of steady state phenol biodegradation in a pulsed plate bioreactor." *Journal of Chemical Technology & Biotechnology: International Research in Process, Environmental & Clean Technology* 83.9 (2008): 1181-1189.

42. Cui, Lei, et al. "Data-driven prediction of the product formation in industrial 2-keto- L-gulonic acid fermentation." *Computers & chemical engineering* 36 (2012): 386- 391.
43. Becker, T., T. Enders, and A. Delgado. "Dynamic neural networks as a tool for the online optimization of industrial fermentation." *Bioprocess and Biosystems Engineering* 24.6 (2002): 347-354.
44. Horiuchi, Jun-ichi, et al. "Artificial neural network model with a culture database for prediction of acidification step in cheese production." *Journal of food engineering* 63.4 (2004): 459-465.
45. Laursen, Siris Ö., Daniel Webb, and W. Fred Ramirez. "Dynamic hybrid neural network model of an industrial fed-batch fermentation process to produce foreign protein." *Computers & chemical engineering* 31.3 (2007): 163-170.
46. Psichogios, Dimitris C., and Lyle H. Ungar. "A hybrid neural network-first principles approach to process modeling." *AIChE Journal* 38.10 (1992): 1499-1511.
47. James, Scott, Raymond Legge, and Hector Budman. "Comparative study of black- box and hybrid estimation methods in fed-batch fermentation." *Journal of process control* 12.1 (2002): 113-121.
48. Gellert, Torsten, Wiebke Höhn, and Rolf H. Möhring. "Sequencing and scheduling for filling lines in dairy production." *Optimization Letters* 5.3 (2011): 491-504.
49. Escobet, Teresa, et al. "Optimal batch scheduling of a multiproduct dairy process using a combined optimization/constraint programming approach." *Computers & Chemical Engineering* 124 (2019): 228-237.
50. Kopanos, Georgios M., Luis Puigjaner, and Michael C. Georgiadis. "Efficient mathematical frameworks for detailed production scheduling in food processing industries." *Computers & chemical engineering* 42 (2012): 206-216.
51. Doganis, Philip, and Haralambos Sarimveis. "Optimal production scheduling for the dairy industry." *Annals of Operations Research* 159.1 (2008): 315-331.
52. Lau, S., et al. "Predictive scheduling of a penicillin bioprocess plant." *IFAC Proceedings Volumes* 37.1 (2004): 463-468.
53. Baldo, Tamara A., et al. "An optimization approach for the lot sizing and scheduling problem in the brewery industry." *Computers & Industrial Engineering* 72 (2014): 58-71.
54. Sainani, M. R., H. K. Vyas, and P. S. Tong. "Characterization of particles in cream cheese." *Journal of dairy science* 87.9 (2004): 2854-2863.
55. Pombo, Alan F. Wolfschoon. "Cream cheese: Historical, manufacturing, and physico-chemical aspects." *International Dairy Journal* 117 (2021): 104948.
56. Coutouly, Aliénor, et al. "Effect of heat treatment, final pH of acidification, and homogenization pressure on the texture properties of cream cheese." *Dairy Science & Technology* 94.2 (2014): 125-144.
57. https://www.mbie.govt.nz/building-and-energy/energy-and-natural- resources/energy-statistics-and-modelling/energy-publications-and-technical- papers/energy-in-new-zealand/
58. https://environment.govt.nz/acts-and-regulations/acts/climate-change-response- amendment-act-2019/
59. Geng, Yang, et al. "A review of operating performance in green buildings: Energy use, indoor environmental quality and occupant satisfaction." *Energy and Buildings* 183 (2019): 500-514.
60. Sarbu, Ioan, and Calin Sebarchievici. "A comprehensive review of thermal energy storage." *Sustainability* 10.1 (2018): 191.
61. da Cunha, Sandra Raquel Leite, and José Luís Barroso de Aguiar. "Phase change materials and energy efficiency of buildings: A review of knowledge." *Journal of Energy Storage* 27 (2020): 101083.
62. Anisur, M. R., et al. "Curbing global warming with phase change materials for energy storage." *Renewable and Sustainable Energy Reviews* 18 (2013): 23-30.
63. Faraj, Khaireldin, et al. "A review on phase change materials for thermal energy storage in

buildings: Heating and hybrid applications." *Journal of Energy Storage* 33 (2021): 101913.
64. Navarro, Lidia, et al. "Thermal energy storage in building integrated thermal systems: A review. Part 1. active storage systems." *Renewable Energy* 88 (2016): 526-547.
65. Nekoonam, Saeed, and Ramin Roshandel. "Modeling and optimization of a multiple (cascading) phase change material solar storage system." *Thermal Science and Engineering Progress* 23 (2021): 100873.
66. Ren, Haoshan, et al. "Improving energy flexibility of a net-zero energy house using a solar-assisted air conditioning system with thermal energy storage and demand- side management." *Applied Energy* 285 (2021): 116433.
67. Fiorentini, Massimo, Paul Cooper, and Zhenjun Ma. "Development and optimization of an innovative HVAC system with integrated PVT and PCM thermal storage for a net-zero energy retrofitted house." *Energy and Buildings* 94 (2015): 21-32.
68. Lopez, Juan Pablo Arzamendia, et al. "Numerical modeling and experimental validation of a PCM to air heat exchanger." *Energy and Buildings* 64 (2013): 415- 422.
69. Li, Han, et al. "A novel solar thermal system combining with active phase-change material heat storage wall (STS-APHSW): Dynamic model, validation and thermal performance." *Energy* 201 (2020): 117610.
70. Lin, Wenye, et al. "Multi-objective optimisation of thermal energy storage using phase change materials for solar air systems." *Renewable energy* 130 (2019): 1116- 1129.
71. Lin, Wenye, et al. "Experimental investigation and two-level model-based optimisation of a solar photovoltaic thermal collector coupled with phase change material thermal energy storage." *Applied Thermal Engineering* 182 (2021): 116098.
72. Lin, Wenye, and Zhenjun Ma. "Using Taguchi-Fibonacci search method to optimize phase change materials enhanced buildings with integrated solar photovoltaic thermal collectors." *Energy* 106 (2016): 23-37.
73. Arkar, Ciril, and Sašo Medved. "Optimization of latent heat storage in solar air heating system with vacuum tube air solar collector." *Solar energy* 111 (2015): 10- 20.
74. Markarian, Elin, and Farivar Fazelpour. "Multi-objective optimization of energy performance of a building considering different configurations and types of PCM." *Solar Energy* 191 (2019): 481-496.
75. Zálešák, Martin, Lubomír Klimeš, and Pavel Charvát. "Design optimization of a solar air collector integrating a phase change material." *Chemical Engineering Transactions* 81 (2020): 211-216.
76. Ren, Haoshan, et al. "Optimisation of a renewable cooling and heating system using an integer-based genetic algorithm, response surface method and life cycle analysis." *Energy Conversion and Management* 230 (2021): 113797.
77. Fiorentini, Massimo, et al. "Hybrid model predictive control of a residential HVAC system with on-site thermal energy generation and storage." *Applied Energy* 187 (2017): 465-479.
78. Serale, Gianluca, et al. "Formulation of a model predictive control algorithm to enhance the performance of a latent heat solar thermal system." *Energy conversion and management* 173 (2018): 438-449.
79. Touretzky, Cara R., and Michael Baldea. "A hierarchical scheduling and control strategy for thermal energy storage systems." *Energy and Buildings* 110 (2016): 94- 107.
80. Papachristou, Anastasios C., et al. "A numerical and experimental study of a simple model-based predictive control strategy in a perimeter zone with phase change material." *Science and Technology for the Built Environment* 24.9 (2018): 933-944.
81. Achterberg, T. SCIP: Solving constraint integer programs. Math. Program. Comput. 2009, 1, 1–41s.
82. Nian, Rui, Jinfeng Liu, and Biao Huang. "A review on reinforcement learning: Introduction and applications in industrial process control." *Computers & Chemical Engineering* 139 (2020):

106886.
83. Russell, Stuart, and Peter Norvig. "Artificial intelligence: a modern approach." (2002).
84. Sutton, Richard S., and Andrew G. Barto. Reinforcement learning: An introduction. MIT press, 2018.
85. Maravelias, Christos T., and Charles Sung. "Integration of production planning and scheduling: Overview, challenges and opportunities." *Computers & Chemical Engineering* 33.12 (2009): 1919-1930.
86. Shin, Joohyun, et al. "Reinforcement learning–overview of recent progress and implications for process control." *Computers & Chemical Engineering* 127 (2019): 282-294.
87. Rawlik, Konrad, Marc Toussaint, and Sethu Vijayakumar. "On stochastic optimal control and reinforcement learning by approximate inference." *Proceedings of Robotics: Science and Systems* VIII (2012).
88. Nian, Rui, Jinfeng Liu, and Biao Huang. "A review on reinforcement learning: Introduction and applications in industrial process control." *Computers & Chemical Engineering* 139 (2020): 106886.
89. Brujeni, Lena Abbasi, Jong Min Lee, and Sirish L. Shah. Dynamic tuning of PI- controllers based on model-free reinforcement learning methods. IEEE, 2010.
90. Moriyama, Takao, et al. "Reinforcement learning testbed for power-consumption optimization." *Asian Simulation Conference*. Springer, Singapore, 2018.
91. Joy, Midhun, and Niket S. Kaisare. "Approximate dynamic programming-based control of distributed parameter systems." *Asia-Pacific Journal of Chemical Engineering* 6.3 (2011): 452-459.
92. Oh, Dong-Hoon, et al. "Actor-critic reinforcement learning to estimate the optimal operating conditions of the hydrocracking process." *Computers & Chemical Engineering* 149 (2021): 107280.
93. Zhang, Yinping, et al. "Application of latent heat thermal energy storage in buildings: State-of-the-art and outlook." *Building and environment* 42.6 (2007): 2197-2209.
94. Gholamibozanjani, Gohar, and Mohammed Farid. "A comparison between passive and active PCM systems applied to buildings." *Renewable Energy* 162 (2020): 112- 123.
95. Finck, Christian, et al. "Review of applied and tested control possibilities for energy flexibility in buildings." Review of applied and tested control possibilities for energy flexibility in buildings (2018).
96. Gholamibozanjani, Gohar, and Mohammed Farid. "A critical review on the control strategies applied to PCM-enhanced buildings." *Energies* 14.7 (2021): 1929.
97. Gholamibozanjani, Gohar, et al. "Model predictive control strategy applied to different types of building for space heating." *Applied energy* 231 (2018): 959-971.
98. Phadungath, Chanokphat. "Cream cheese products: A review." Songklanakarin *Journal of Science and Technology* 27.1 (2005): 191-199.
99. Fox, Patrick F., et al. Fundamentals of cheese science. New York: Springer US, 2017.
100. Gadgil, Chetan J., and K. V. Venkatesh. "Structured model for batch culture growth of Lactobacillus bulgaricus." *Journal of Chemical Technology & Biotechnology: International Research in Process, Environmental AND Clean Technology* 68.1 (1997): 89-93.
101. Bouguettoucha, Abdallah, Béatrice Balannec, and Abdeltif Amrane. "Unstructured models for lactic acid fermentation-a review." *Food Technology and Biotechnology* 49.1 (2011): 3.
102. Fu, Wenge, and A. P. Mathews. "Lactic acid production from lactose by Lactobacillus plantarum: kinetic model and effects of pH, substrate, and oxygen." *Biochemical engineering journal* 3.3 (1999): 163-170.
103. Ohara, Hitomi, Keiichiro Hiyama, and Toshiomi Yoshida. "Kinetic study on pH dependence of growth and death of Streptococcus faecalis." *Applied microbiology and biotechnology* 38.3 (1992): 403-407.

104. Roupas, Peter. "Predictive modelling of dairy manufacturing processes." *International Dairy Journal* 18.7 (2008): 741-753.
105. Ganguly, Somenath. "Prediction of VLE data using radial basis function network." *Computers & chemical engineering* 27.10 (2003): 1445-1454.
106. Valeh-e-Sheyda, Peyvand, et al. "Application of artificial neural networks for estimation of the reaction rate in methanol dehydration." *Industrial & Engineering Chemistry Research* 49.10 (2010): 4620-4626.
107. Elmolla, Emad S., Malay Chaudhuri, and Mohamed Meselhy Eltoukhy. "The use of artificial neural network (ANN) for modeling of COD removal from antibiotic aqueous solution by the Fenton process." *Journal of hazardous materials* 179.1-3 (2010): 127-134.
108. Jimenez-Marquez, S. A., J. Thibault, and C. Lacroix. "Prediction of moisture in cheese of commercial production using neural networks." *International dairy journal* 15.11 (2005): 1156-1174.
109. Jimenez-Marquez, S. A., C. Lacroix, and J. Thibault. "Impact of modeling parameters on the prediction of cheese moisture using neural networks." *Computers & chemical engineering* 27.5 (2003): 631-646.
110. Yet-Pole, I., Wu Wen-Tengu, and Liu Yung-Chuan. "Neural network modelling for on-line state estimation in fed-batch culture of L-lysine production." *The Chemical Engineering Journal and the Biochemical Engineering Journal* 61.1 (1996): 35-40.
111. Latrille, Eric, Georges Corrieu, and J. Thibault. "Neural network models for final process time determination in fermented milk production." *Computers & chemical engineering* 18.11-12 (1994): 1171-1181.
112. Thompson, Michael L., and Mark A. Kramer. "Modeling chemical processes using prior knowledge and neural networks." *AIChE Journal* 40.8 (1994): 1328-1340.
113. Saraceno, Alessandra, et al. "A hybrid neural approach to model batch fermentation of "ricotta cheese whey" to ethanol." *Computers & Chemical Engineering* 34.10 (2010): 1590-1596.
114. Lin Y. Cream cheese fermentation pH prediction. Master's thesis; University of Auckland, New Zealand; 2018.
115. Boonmee, Mallika, et al. "Batch and continuous culture of Lactococcus lactis NZ133: experimental data and model development." *Biochemical engineering journal* 14.2 (2003): 127-135.
116. Li, Bing, et al. "Application of mechanistic modelling and machine learning for cream cheese fermentation pH prediction." *Journal of Chemical Technology & Biotechnology* 96.1 (2021): 125-133.
117. Kriesel, David. "A brief introduction to neural networks, 2007." URL http://www. dkriesel. com (2015).
118. Lucey, J. A. "Acid and Acid/Heat Coagulated Cheese, Encyclopedia of dairy science." (2002): 350-356.
119. Harjunkoski, Iiro, Hans Werner Borchers, and Marco Fahl. "Simultaneous scheduling and optimization of a copper plant." *Computer Aided Chemical Engineering*. Vol. 21. Elsevier, 2006. 1197-1202.
120. International Energy Agency, Statistics, 2017.
121. Soares, Nelson, et al. "Review of passive PCM latent heat thermal energy storage systems towards buildings' energy efficiency." *Energy and buildings* 59 (2013): 82- 103.
122. Energy Technology Perspectives – Executive Summary, 2017.
123. Dincer, Ibrahim, and Marc A. Rosen. Thermal energy storage systems and applications. John Wiley & Sons, 2021.

124. Mewes, D., and F. Mayinger. "Heat and cold storage with PCM: An up to date introduction into basics and applications." (2008).
125. Pawar, Vivek R., and Sarvenaz Sobhansarbandi. "Design optimization and heat transfer enhancement of energy storage based solar thermal collector." *Sustainable Energy Technologies and Assessments* 46 (2021): 101260.
126. Chen, C. Q., et al. "Optimization of phase change thermal storage units/devices with multichannel flat tubes: A theoretical study." *Renewable Energy* 167 (2021): 700- 717.
127. Gholamibozanjani, Gohar, and Mohammed Farid. "Experimental and mathematical modeling of an air-PCM heat exchanger operating under static and dynamic loads." *Energy and Buildings* 202 (2019): 109354.
128. BRANZ, https://www.branz.co.nz/, (accessed March 28, 2022).
129. Elements, https://bigladdersoftware.com/projects/elements/, (accessed March 28, 2022).
130. MetServices, https://www.metservice.com/, (accessed March 28, 2022).
131. Kotti, M. C., A. A. Argiriou, and A. Kazantzidis. "Estimation of direct normal irradiance from measured global and corrected diffuse horizontal irradiance." *Energy* 70 (2014): 382-392.
132. Duffie, John A., and William A. Beckman. "Solar Radiation." Solar engineering of thermal processes 4 (2013): 3-42.
133. Zalba, Belen, et al. "Review on thermal energy storage with phase change: materials, heat transfer analysis and applications." *Applied thermal engineering* 23.3 (2003): 251-283.
134. Rubitherm Technologies GmbH, Macroencapsulation - CSM, (n.d.). https://www.rubitherm.eu/en/index.php/productcategory/organische-pcm-rt (accessed march 28, 2022).
135. U.S. department of Energy, EnergyPlus documnetation, https://energyplus.net/documentation (accessed March 28, 2022)
136. Devaux, Paul, and Mohammed Mehdi Farid. "Benefits of PCM underfloor heating with PCM wallboards for space heating in winter." *Applied energy* 191 (2017): 593- 602.
137. Ashrae, Ashrae Handbook Fundamentals, and Ga Atlanta. "American society of Heating." *Refrigerating and Air-Conditioning Engineers* 1 (2009).
138. Dostal, Jiri, and Tomas Baumelt. "Model predictive control for buildings with active one-pipe hydronic heating." *E3S web of conferences*. Vol. 111. EDP Sciences, 2019.
139. U.S. Energy Information Administration (EIA). International Energy Statistics n.d. Available online: https://www.eia.gov/international/data/world (accessed on 14 June 2019).
140. Thieblemont, Hélène, et al. "Predictive control strategies based on weather forecast in buildings with energy storage system: A review of the state-of-the art." *Energy and Buildings* 153 (2017): 485-500.
141. JBJ, B. Rawlings, and D. Q. Mayne. "Model Predictive Control Theory and Design." (1999).
142. Mason, Karl, and Santiago Grijalva. "A review of reinforcement learning for autonomous building energy management." *Computers & Electrical Engineering* 78 (2019): 300-312.
143. Yu, Liang, et al. "Deep reinforcement learning for smart building energy management: A survey." *arXiv e-prints* (2020): arXiv-2008.
144. Wang, Zhe, and Tianzhen Hong. "Reinforcement learning for building controls: The opportunities and challenges." *Applied Energy* 269 (2020): 115036.
145. de Gracia, Alvaro, et al. "Control of a PCM ventilated facade using reinforcement learning techniques." *Energy and Buildings* 106 (2015): 234-242.
146. de Gracia, Alvaro, et al. "Control strategies comparison of a ventilated facade with PCM–energy savings, cost reduction and CO2 mitigation." *Energy and Buildings* 130 (2016): 821-828.
147. Rahimpour, Zahra, Gregor Verbič, and Archie C. Chapman. "Actor-critic learning for optimal building energy management with phase change materials." *Electric Power Systems Research* 188 (2020): 106543.

148. Zsembinszki, Gabriel, et al. "Deep learning optimal control for a complex hybrid energy storage system." *Buildings* 11.5 (2021): 194.
149. Mnih, Volodymyr, et al. "Human-level control through deep reinforcement learning." *nature* 518.7540 (2015): 529-533.